The Influence of the Surface Humidity Flux on the Snow Isotopic Composition

---

Revisiting the Formation of the Climate Signal
Stored in Ice Core Water Isotope Records

Sonja Wahl

Dissertation for the degree of Philosophiae Doctor (PhD)
Geophysical Institute, University of Bergen

Supervisor: Dr. Hans Christian Steen-Larsen
Co-Supervisor: Prof. Joachim Reuder

2021

Scientific Environment

This thesis was conducted at the Geophysical Institute of the University of Bergen in Norway. Additionally, I was affiliated with the Bjerknes Centre for Climate Research (BCCR) and therein part of the Hazards research group. I was engaged with the BCCR leader group through my role as head of the BCCR PhD Forum leader board in 2020 and 2021. This study is part of the ERC starting grant "SNOWISO - Signals from the Surface Snow: Post-Depositional Processes Controlling the Ice Core Isotopic Fingerprint" (Grant ID: 759526) led by my supervisor Hans Christian Steen-Larsen. During my Ph.D. period, I participated in two field campaigns on the Greenland Ice Sheet where I was hosted by the EastGRIP community headed by PICE (Physics of Ice, Climate and Earth) of the University of Copenhagen, Denmark. I also joined in the 2018/2019 field campaign ASTI at Kohnen Station in Dronning-Maud-Land, Antarctica organized by the Alfred-Wegener-Institute, Helmholtz-Center for Polar and Marine Research (AWI), Bremerhaven, Germany. The campaign leader Maria Hörhold likewise was a strong collaborator throughout the time of this thesis and hosted me for several shorter research stays at AWI in Bremerhaven. At the AWI stable water isotope laboratory, I performed stable water isotope analysis on the snow samples collected during the field campaigns. In the beginning of 2020, I was able to attend a field course in boundary layer meteorology at the University Centre in Svalbard (UNIS). My stay there was supported by the Meteorology group of the Geophysical Institute. Throughout my time as PhD student, I was enrolled in the Norwegian Research School on Changing Climates in the Coupled Earth System (CHESS) which provided me with the opportunity to join courses on scientific and soft skill development.

European Research Council
Established by the European Commission

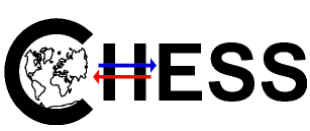

Acknowledgements

It seems like yesterday that I was sitting on a plane to Bergen, writing down my expectations, not knowing what awaited me, when in fact, it was 3.5 years ago that I started my thesis work. Reading my notes now, I have to smile about the unnecessary things that I worried about and the actually troublesome situations, that never even crossed my mind back then. But one thing I knew for sure and it has turned out to be true;
I would learn a lot: About isotopes, about remote places, about snow and ice and climate and I learned a lot about myself. I am proud to have made it until the end but there are others that have contributed to this work by being themselves and supporting me:
First, I would like to thank you, **HC**, for being a demanding but supportive, sometimes oblivious but focused, critical but enthusiastic supervisor and fun group leader. Especially your responsiveness to any question that I had - and I had many - makes you a great supervisor and I will gladly remember (almost) all discussions we had. Thank you also **Jochen**, my co-supervisor, for the honest second opinions, the open door and the right words at the right time. I could always count on your constructive feedback.
I also want to thank you, **Maria**, for being a mentor for me. Your support and encouragement definitely helped me through difficult situations. I remember so many long and honest conversations, be it am Deich, in Kangerlussuaq, in Capetown, Kohnen or EastGRIP that continue to have an effect on me. This thesis would not have been possible without you. I am also extremely grateful to you, **Melanie**, for your calmness in stressful situations and the time you repeatedly spent for explaining me to work with Picarro, Swagelok and co.
Thanks to the ever-growing research group that I was lucky to be part of; **AK**, for an always open ear, useful advice and so many happy hours in our sunny office; **Daniele**, for your patience and open door no matter what detail needed clarification; **Sandro & Ines**, for the good vibes in the final phase of this thesis and specifically **Laura** - my academic sister who I dreaded a bit before I met her and now never want to have missed - thank you for always joining-in on any kind of Gedankenexperiment.
Thank you also **Stephan** for help in understanding turbulence and turbulence software.
I am grateful to the EastGRIP community for the opportunity to join and be part of a bigger picture and unforgettable memories on the ice.
I am extremely happy that I could experience EastGRIP together with you, **Nico**. Thank you for all the times you were there to encourage, criticize, distract, discuss, calm me down and most of all listen to me. I am excited to see where life takes us next.
And of course, thanks to all my friends who helped in making Bergen my home. Specifically **Morven, Karita, Lisa and Niklas** and the climbing gang **Anaïs, Xabier, Nadine, Jakob, Anne-Kari, Augustin, Danielle, Alexios, Kristine, Lander, Vår, Etienne, Zoé & Francesca**. I also want to mention the friends I made in Svalbard in the beginning of 2020. The liberty and joy that I experienced with you during that time made life afterwards so much easier.
Last but not least I want to thank my extended family and friends at home who were only a phone or video call away. Thank you for being supportive in the decision to go abroad and always welcoming me with open arms when I visit. Ihr habt nie an mir gezweifelt und das bedeutet mir viel.

Sonja Wahl
Bergen, 29 October 2021

Abstract

Accurate projections of future climate rely on knowledge of natural climate variability on different time scales. Climate proxies, such as stable water isotope records recovered from ice cores, provide insights into the climate variability of the past. A prerequisite for an accurate proxy-interpretation, however, is an in-depth understanding of the signal formation process capturing the climate signal in the isotopic composition of surface snow, which is buried and archived in the ice.

This thesis improves the understanding of how the climate imprints a signal on the snow isotopic composition. Specifically, the surface humidity flux, and the associated exchange of water isotopes between atmospheric water vapor and snow pack, is investigated as a potential process composing the isotope signal in the snow after deposition. First, in Paper I, we explore the vapor-snow exchange of stable water isotopes through in-situ isotope flux measurements taken in the interior of the Greenland Ice Sheet. For this, we developed a method that permits direct observations of the isotopic composition of the humidity flux. We find that the isotopic composition of the humidity flux is dependent on the snow and vapor isotopic composition during sublimation and deposition times, respectively. Additionally, we document isotopic fractionation during snow sublimation - a process that has been a subject of debate in the past and which is currently not implemented in isotope-enabled climate models.

Secondly, Paper II investigates the effect of sublimation on the isotopic composition of the snow. Based on laboratory experiments, we show that sublimation leads to an isotopic enrichment and an accompanying decrease in the d-excess value in the snow. The same is observed in field experiments, albeit less extreme, due to weaker sublimation fluxes. The study demonstrates that the snow surface isotopic composition is modulated on sub-daily timescales, documented through several high-temporal-resolution (3h) in-situ snow sampling experiments.

Paper III investigates the role of vapor-snow exchange on the temporal evolution of the isotope signal in the snow. For this, we set up a mass balance model of the snow surface system, forced with observations from two summers on the Greenland Ice Sheet. Three model simulations were performed with changing parameterizations for the sublimation process from kinetic and equilibrium fractionation to no fractionation. The isotopic composition of the deposition flux was parameterized with empirical functions of Paper I. We discover that the model can explain 35 % and 52 % of observed δ^{18}O and δD variability in the simulation, including kinetic fractionation, whereas it fails when no fractionation is included. Furthermore, we find that the importance of vapor-snow exchange for the snow isotope signal is not constant throughout the observation period, with days with higher net sublimation having a greater impact on the snow isotope signal. The results motivate the realization of fractionation during snow sublimation in isotope-enabled climate models.

The three papers together form a holistic picture of a vapor-snow exchange that has the potential to imprint a climate signal in the snow. The relative importance of this process for the ice core isotope signal is variable in space and time, depending on the humidity flux magnitude within precipitation-free periods. Hence ice core isotope records might contain a continuous climate signal rather than a precipitation signal only.

Zusammenfassung

Um genaue Vorhersagen über die zukünftige Entwicklung des Klimas machen zu können, muss man die natürliche Variabilität, die natürlichen Schwankungen des Klimas über verschiedene Zeitskalen hinweg kennen. Eiskerne aus Grönland und der Antarktis stellen Klimaarchive dar, anhand derer Veränderungen des Klimas in der Vergangenheit rekonstruiert werden können. Dafür benutzt man unter anderem die Konzentration der stabilen Wasserisotope welche als Stellvertreter (Proxy) für Änderungen des Klimas interpretiert werden kann. Um stabile Wasserisotope als Klimaproxy richtig zu interpretieren braucht es jedoch ein grundlegendes Verständnis über die Bildung des Isotopensignals im Oberflächenschnee, welches bei der Umwandlung von Schnee zu Eis archiviert wird.
Diese Dissertation trägt essentiell zum Verständnis über die Bildung des Klimasignals im Schnee bei, also wie sich die atmosphärischen Bedingungen (d.h. das Klima) auf die Isotopenzusammensetzung des Schnees einprägen. Der Schwerpunkt dieser Arbeit befasst sich mit der Auswirkungen des turbulenten Flusses von Luftfeuchte an der Schneeoberfläche auf die Isotopenzusammensetzung des bereits abgelagerten Schnees, und dem damit zusammenhängenden Austausch von Wasserisotopen zwischen Schnee und Wasserdampf in der Atmosphäre.
In Artikel I wird der Isotopenaustausch zwischen Schneeoberfläche und Wasserdampf in der darüber liegenden Luftschicht auf dem Grönländischen Eisschildes mittels Feldbeobachtungen untersucht. Dafür habe ich eine Methode entwickelt, die erstmalig eine direkte Messung des Isotopengehaltes des Feuchteflusses auf einem Eisschild ermöglicht. Die Schneeoberfläche erfährt Sublimation und Resublimation von Schneekristiallen Prozesse die die Isotopie des Feuchteflusses bestimmen. Während der Sublimation (Verdampfung) von Schnee, hängt die Isotopie des Flusses von der Isotopie des sublimierten Schnees ab und während der Resublimation (Kondensation) von der Isotopie des Wasserdampfes. Außerdem zeigen unsere Messungen eindeutig, dass Sublimation eine Fraktionierung (d.h. eine Veränderung der Zusammensetzung) von Wasserisotopen hervorruft. Durch Sublimation hervorgerufene Fraktionierung war lange umstritten und ist deshalb bisher auch nicht Teil von Klimamodellen.
In Artikel II wird die Auswirkungen von Sublimation auf den Schneeisotopengehalt im Detail untersucht. Die Ergebnisse unserer Laborexperimente zeigen dabei deutlich, dass Sublimation zu einer Anreicherung von schweren Wasserisotopen und gleichzeitiger Abnahme des d-excess Wertes im Schnee führt. Wir beobachten ähnliche Entwicklungen im Schnee während unserer Feldarbeit in Grönland. Dabei sind die Auswirkungen geringer da die Sublimation schwächer als im Labor ist. Die Studie beweist, dass sich das Isotopen Signal im Schnee im Verlauf des Tages ändert, was wir durch Ergebnisse einer engmaschigen Schneeprobennahme (3H) belegen.
In Artikel III untersuchen wir die Rolle des Austausches zwischen Schnee und Wasserdampf für die relativ schnell ablaufenden Veränderungen des Schneeisotopengehaltes. Dafür setzen wir ein Massenbilanz Modell auf, das die Schneeoberfläche und den Austausch mit der Atmosphäre simuliert. Das Modell wird von Daten der Messungen aus dem Feld von 2 Kampagnen angetrieben. In der Studie werden drei Szenarien untersucht, in denen die Art der Fraktionierung variiert wird. Szenario eins bezieht kinetis-

che Fraktionierung mit ein, Szenario zwei Gleichgewichtsfraktionierung während in Szenario drei gar keine Fraktionierung während der Sublimation enthält. Allein durch die die Simulation mit kinetischer Fraktionierung ist das Modell in der Lage, die beobachtete Variabilität des Schneeisotopensignals zu 35 % für δ^{18}O und 52 % für δD zu erklären. Außerdem wird ersichtlich, dass die Auswirkungen des Wasserdampf-Schnee Austausches über den Beobachtungszeitraum nicht konstant sind. Der Einfluss ist an Tagen mit höherer netto Sublimation größer. Die Ergebnisse dieses Artikels verdeutlichen die Notwendigkeit nach der Einbindung von Isotopenfraktionierung während des Sublimationsprozesses in Klimamodellen.
Die drei Artikel zusammen ergeben ein ganzheitliches Bild eines Wasserdampf-Schnee Austausches, der das Potential hat, sich auf die Isotopenzusammensetzung des Schnees auszuwirken. Wie wichtig dieser Prozess für das letztendlich im Eiskern gemessene Klimaproxy Wasserisotopen-Signal ist, scheint zeitlich und räumlich variabel, und abhängig von der Stärke des Feuchtefluss in Niederschlags-freien Perioden zu sein. Zusammenfassend deuten die Ergebnisse meiner Dissertation darauf hin, dass Eiskerne nicht nur ein Archiv für das Klimasignal während Schneefall Ereignissen sind, sondern Eiskerne vielmehr ein kontinuierliches Klimasignal archivieren.

Thesis Outline

This PhD thesis consists of three scientific papers that are embedded in an introductory part and a concluding discussion. In Chapter 1, the motivation behind this thesis is given and the objectives are outlined. Further, an introduction to the field of stable water isotopes with a focus on their use as climate proxy is given. Data and methods used throughout the thesis are presented in Chapter 2. The individual papers are summarized briefly in Chapter 3. In Chapter 4, the synergy of the presented papers is outlined and my work is discussed in the context of climate proxy interpretation.

The papers included in this thesis (Chapter 5) are:

I **Wahl, S.**, Steen-Larsen, H. C., Reuder, J., and Hörhold, M. (2021)
Quantifying the Stable Water Isotopologue Exchange Between Snow Surface and Lower Atmosphere by Direct Flux Measurements
Journal of Geophysical Research: Atmospheres **126/13**
(doi:10.1029/2020JD034400)

II Hughes, A. G., **Wahl, S.**, Jones, T. R., Zuhr A., Hörhold, M., White, J. W. C. and Steen-Larsen, H. C. (2021)
The Role of Sublimation as a Driver of Climate Signals in the Water Isotope Content of Surface Snow: Laboratory and Field Experimental Results
The Cryosphere **15** (doi:10.5194/tc-15-4949-2021)

III **Wahl, S.**, Steen-Larsen, H. C., Hughes, A., Dietrich, L. J., Zuhr, A., Behrens, M., Faber, A.-K. and Hörhold, M.
Challenging Old Axioms: Interpretations of Water Isotopes in Ice Cores
(submitted to *Nature Geoscience*)

Other scientific contributions

A Rozmiarek, K. S., Vaughn, B. H., Jones, T. R., Morris, V., Skorski, W. B., Hughes, A. G., Elston, J., **Wahl, S.**, Faber, A.-K., and Steen-Larsen, H. C. (2021)
An Unmanned Aerial Vehicle Sampling Platform for Atmospheric Water Vapor Isotopes in Polar Environments
Atmospheric Measurement Techniques, **accepted** (preprint)

B Harris-Stuart, R., Faber, A.-K., **Wahl, S.**, Hörhold, M., Kipfstuhl, S., Vasskog, K., Behrens, M., Zuhr, A. and Steen-Larsen H. C.
Exploring the role of surface snow metamorphism on the isotopic composition of the surface snow at EastGRIP (to be submitted to *The Cryosphere*)

C Zannoni, D., Steen-Larsen, H.C., Peters, A.J., **Wahl, S.**, Sodemann, H., Sveinbjörnsdóttir, A.E.,
Kinetic fractionation factors for ocean evaporation (to be submitted to *Science Advances*)

Contents

1 Introduction

1.1 Motivation

1.1.1 Stable water isotope records from ice cores

In the context of the current man-made climate change, information about past climate variability and the physical mechanisms behind it has become invaluable. Since instrumental climate records are limited to the past few hundred years, mankind relies on climate proxy data to learn about past climate and thus, be able to predict future climate. Stable water isotope records from ice cores are valuable climate proxies and have been used as paleothermometer based on observations of a direct dependency between annual isotopic composition in precipitation and mean annual temperatures (*Dansgaard*, 1964). This precipitation isotope temperature dependency, amongst other factors, has led to the search for past precipitation records. As ice sheets have been accumulating precipitation over several thousands of years, they are an excellent archive of polar snowfall events of the past. By drilling in locations on ice sheets and ice caps, that promise the oldest precipitation records, ice core paleo proxy data from the polar areas have been recovered dating back 130 thousand years (ka) on the Greenland Ice Sheet (GrIS) and up to 800 ka on the Antarctic Ice Sheet (AIS) (e.g. *Vinther et al.*, 2008; *Jouzel et al.*, 2007; *NEEM community-members*, 2013; *EPICA community-members*, 2004).
In addition, stable water isotopes from ice cores contributed to retrieving paleoclimate information beyond temperature alone:
Ice core records have provided insight into natural climate variability on (long) glacial-interglacial timescales (*Jouzel et al.*, 2007; *NEEM community-members*, 2013) and on (short) decadal and down to seasonal timescales (e.g. *Vinther et al.*, 2010). Isotope records have documented paleoclimate transitions (e.g. *Capron et al.*, 2021; *Buizert et al.*, 2014; *White et al.*, 2010; *Alley*, 2000) and the recent anthropogenic climate change (e.g. *Schneider et al.*, 2006). Further, the comparison of isotope records obtained from the GrIS and AIS have allowed studies of teleconnections between the two hemispheres and helped identifying the corresponding drivers (e.g. *Pedro et al.*, 2016; *Markle et al.*, 2017; *Jones et al.*, 2018). The second order parameters d-excess and ^{17}O-excess have been used to identify changes in atmospheric circulation patterns via precipitation source region identification (e.g. *Johnsen et al.*, 1989; *Jouzel et al.*, 2013; *Masson-Delmotte et al.*, 2005) and as proxy for environmental conditions in precipitation source regions (e.g. *Uemura et al.*, 2012; *Winkler et al.*, 2012).
Crucial for these kinds of ice core proxy interpretation studies is a detailed understanding of the signal formation processes that imprint the climate signal in the snow isotopic composition. Only when the governing equations and influencing parameters are identified, is it possible to retrieve the original climate signal. Conventionally, it has been assumed that the climate signal is captured in the isotopic composition of snowfall, which becomes conserved when the snow is transformed to ice. However, *Steen-Larsen et al.* (2014) showed that the surface snow isotopic composition undergoes changes in between precipitation events, indicating climate signal formation processes other than

precipitation alone. Subsequently, several mechanisms that could alter the snowpack isotopic composition before snow is transitioned into ice were outlined by *Casado et al.* (2018). These processes complicate the interpretation of isotope records in snow and ice and explain why the *transfer function* between ambient climate and ice core isotope signal has yet to be defined. Ongoing work strives to improve the understanding of relevant processes at play with the ultimate goal of answering the question of the validity of a direct dependency between the ratio of stable water isotopes in snow and mean temperatures at polar sites.

1.1.2 Transfer function between climate and ice core isotope record

There is growing evidence that the actual transfer function, describing the relationship between climate signal and ice core isotope signal, is more complex than a precipitation signal alone. *Jouzel et al.* (1997) summarized evidence for changing calibration functions of the paleothermometer in space and time, owing to elevation (*Vinther et al.*, 2009) and atmospheric circulation pattern changes (*Schlosser et al.*, 2004), as well as shifts in precipitation source regions (*Landais et al.*, 2008; *Masson-Delmotte et al.*, 2011) in changing climates. However, this inconsistency in the calibration function might not be attributed to changing precipitation signals alone, since the transfer function is more complex and consists of several phases that form the ice core isotope signal. Figure 1.1 shows a schematic of these phases that define snow structure and snow layering and hence, have the potential to influence the isotopic composition of a snow layer that is later transferred to ice and analyzed as climate proxy.

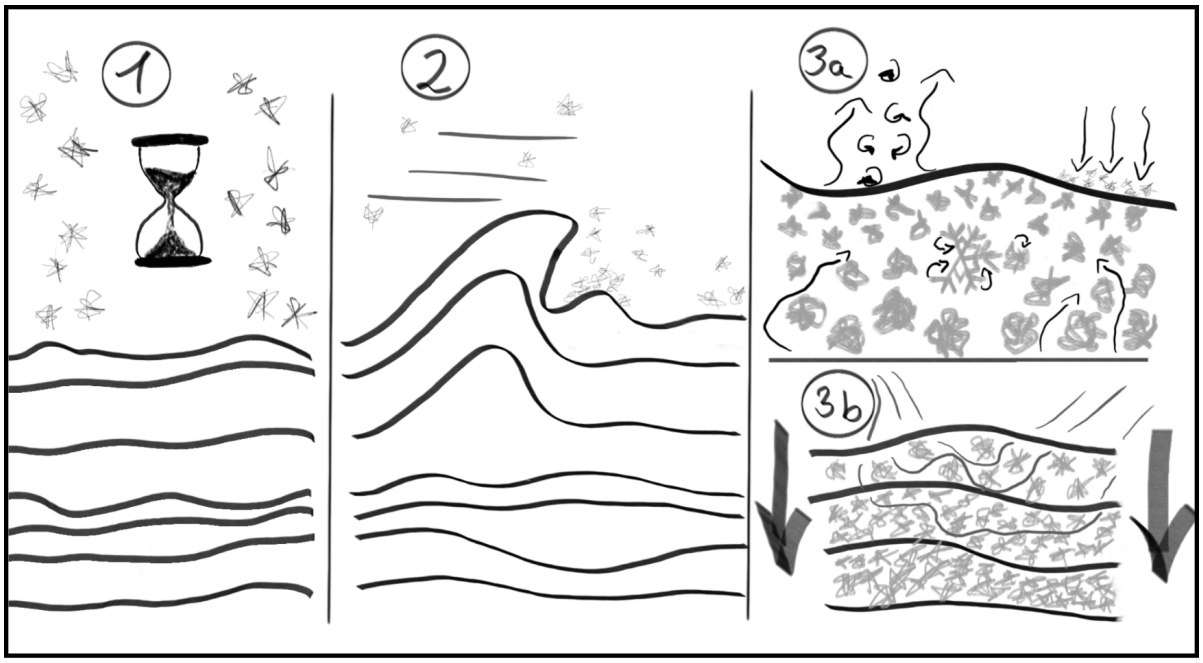

Figure 1.1: Transferring the climate signal to the ice core
The ice core isotope signal formation process is divided into three phases before snow turns into ice. (1) is the precipitation, (2) the deposition and (3) the post-deposition phase. Each individual phase has the potential to influence the isotope signal that is later recovered as part of the ice core isotope record. Not shown is the isotope diffusion in ice that smooths the isotope record.

First (1), there is the precipitation input signal consisting of snowfall and clear-sky precipitation (*Fujita and Abe*, 2006). The frequency, or the regular absence of precipitation events, also referred to as precipitation intermittency, is a factor influencing the information that can be retrieved from isotope records (*Casado et al.*, 2020). Additionally, seasonality of precipitation is discussed as bias introducing parameter (*Krinner and Werner*, 2003; *Sime et al.*, 2009). Both processes require the interpretation of ice core isotope records as precipitation-weighted mean instead of annual mean temperature (*Kohn and Welker*, 2005; *Persson et al.*, 2011; *Sturm et al.*, 2010).
Next (2) is the deposition phase, in which snow redistribution and drifting snow define local-scale spatial variability (*Zuhr et al.*, 2021). High spatial variability observed in firn cores questions the unambiguity of a single ice core drilled at one location (*Fisher et al.*, 1985; *Münch et al.*, 2021). Any process affecting the snow isotopic composition after deposition is discussed in literature under the term *post-depositional* process. However, it seems reasonable to divide this phase further.
Following deposition (3a), there is a period in which the top layer (several centimeters) of snow is in direct contact with the atmosphere. At this stage, diffusion of isotopes in air-filled pore spaces is a potentially important process, connecting the snow layers. Additionally, the surface humidity flux (*Ritter et al.*, 2016) and snow metamorphism (*Ebner et al.*, 2017; *Touzeau et al.*, 2018) are discussed as potentially influential for the snow isotopic composition.
Eventually, (3b) the surface snow gets buried. Snow turns first into firn and later into ice. Relevant processes at this stage are well-studied firn diffusion (*Johnsen*, 1977; *Johnsen et al.*, 2000), advection, and compaction processes as well as the potentially influential process of forced firn ventilation and associated diffusion (*Town et al.*, 2008).

This thesis focuses on the signal formation phase when the snow is in direct contact with the atmosphere before it gets buried. Specifically, it discusses the influence of *post-depositional* vapor-snow exchange at the snow surface for the isotope signal formation in snow.

1.1.3 Air-snow exchange and its role for snow isotopic composition

Steen-Larsen et al. (2013) pioneered in monitoring diurnal cycles in the stable water isotope signal in atmospheric water vapor at an ice core drilling site on the GrIS. *Casado et al.* (2016) observed the same pattern in the vapor above the AIS. These sub-diurnal changes of vapor isotopic composition are a locally sourced climate signal induced by the daily cycle of solar insulation and indicate an exchange of stable water isotopes between snow surface and atmosphere. *Madsen et al.* (2019) showed in a modeling study, that the observed diurnal cycles in vapor isotopes at different levels above ground required an amplified diurnal cycle signal at the snow-vapor interface level. This amplification could only be generated by enabling isotopic fractionation during sublimation from the snow surface. Fractionation during sublimation was formerly ruled out by the understanding of a layer-by-layer removal of snow crystals during sublimation, where mixing is prevented by the very low diffusion rates in the solid snow matrix (*Dansgaard et al.*, 1973; *Friedman et al.*, 1991; *Neumann et al.*, 2005). This is also the reason why isotope-enabled climate models to date, do not consider fractiona-

tion during sublimation in the parameterizations for isotope behavior within the water cycle (*Werner et al.*, 2011). Supporting the theory of fractionation during sublimation, *Ritter et al.* (2016) investigated sub-diurnal changes in the surface snow layer isotopic composition and found a diurnal cycle in phase with the vapor isotope cycle and an amplitude of 3 ‰ in δD . The foundation for the study by *Ritter et al.* (2016) was given when *Steen-Larsen et al.* (2014) provided evidence for a vapor-snow exchange that influences the snow isotopic composition on synoptic timescales. The authors showed that the isotopic composition of surface snow varied in parallel with changes in the vapor isotopic composition, even in between precipitation events hinting at a process that affects the snow isotopic composition continuously.
The surface humidity flux continuously exchanges water isotopes between the snow surface and atmospheric water vapor. It is therefore a post-depositional process with the potential to influence the isotopic signal in the surface snow layer. Depending on the climatic parameters that affect the humidity flux and potential isotopic fractionation processes involved, vapor-snow exchange could be a driver for a continuous climate signal formation in snow, bridging the precipitation intermittency. Hence, it is important to quantify the fractionation effects involved in vapor-snow exchange processes and investigate surface humidity and isotope fluxes on ice sheets, concerning their magnitude and net values. This will allow the determination of whether, when, and how surface fluxes are important for the signal formation of isotope records retrieved from ice cores. From this, the following research questions (RQ) have evolved that are the subject of this thesis:

1.1.4 Objectives

RQ 1 How can surface fluxes of different stable water isotopes be measured in the dry-snow region of the Greenland Ice Sheet?

RQ 2 What governs the isotopic composition of the humidity flux above a snow surface in the dry-snow region of the Greenland Ice Sheet during sublimation and deposition?

RQ 3 Does sublimation of snow in a low humidity environment affect the isotopic composition of the snow?

RQ 4 What are the governing parameters constraining the magnitude of sublimation effects on the snow isotopic composition?

RQ 5 How can we parameterize the sublimation flux isotopic composition in models?

RQ 6 Can atmospheric vapor-snow humidity exchange explain the observed temporal variability in the surface snow isotopic composition?

1.2 Scientific Background

1.2.1 Stable water isotopes in the hydrological cycle

The water molecule is composed of one oxygen (^{16}O) and two hydrogen (^{1}H) atoms which either or both can be replaced by a respective stable isotope (^{17}O, ^{18}O, ^{2}H also D), forming so-called isotopologues. The natural abundances of the most common water species in nature are given in Table 1.1.

Table 1.1: *Molecular mass and natural abundance of the most common water molecules as fraction of all water molecules. From Horita et al. (2008).*

	$\mathbf{H_2^{16}O}$	$\mathbf{H_2^{17}O}$	$\mathbf{DH^{16}O}$ $\mathbf{^2H^1H^{16}O}$	$\mathbf{H_2^{18}O}$
molecular weight [g·mol^{-1}]	18.011	19.015	19.017	20.015
abundance	0.99730	$3.788\cdot10^{-4}$	$3.106\cdot10^{-4}$	$1.999\cdot10^{-3}$

For practical reasons and to improve measurement precision, R^* was defined as the isotopic ratio between abundance of rare (*, i.e. $H_2^{18}O$, $H_2^{17}O$, HDO) and abundant ($H_2^{16}O$) isotopologue and is given instead of an absolute isotopologue content of a water sample. Phase transitions and mixing processes can alter this ratio because of small but noticeable differences in chemo-physical characteristics between isotopologues. These originate from differences in molecular weight between isotopologues, which influence the molecules' mobility and bonding strengths. Heavy isotopologues, therefore, have a lower diffusion velocity and tend to stay in the energetically lower phase (solid<liquid<gaseous). The resulting discrimination during chemical reactions or phase changes is called *isotopic fractionation*. To discuss the relative deviation in isotopologue content caused by various processes, *Craig* (1961) introduced the standard δ-notation following:

$$\delta^* = R^*/R^*_{reference} - 1, \tag{1.1}$$

reported in ‰ and with the *reference* being Vienna Standard Mean Ocean Water (VSMOW) with a δ-value defined as 0 ‰ (*de Laeter et al.*, 2003).

The origin of climate studies using stable water isotopes[1] is found in the work of the Danish professor Willi Dansgaard in the early 1950s, who documented a link between climatic conditions and stable water isotope content in freshwater and water vapor (*Dansgaard*, 1953, 1954). Ten years later, precipitation water samples from all around the globe revealed a strong correlation between stable water isotope content and mean annual air temperature (*Dansgaard*, 1964). Plotted in the δ^{18}O vs. δD space, the samples fall on a line with slope 8, referred to as the Global Meteoric Water Line (GMWL). The slope originates from the difference in saturation vapor pressure between isotopes resulting in different equilibrium fractionation coefficients. The equilibrium fractionation coefficient α_{eq} quantifies the amount of fractionation between two

[1] For readability reasons, *stable water isotope* will be used as synonym for *stable water isotopologue* throughout the rest of this thesis as well as *isotopic ratio* when referring to a water molecule ratio.

phases (l=liquid, v=vapour, s=solid) in equilibrium.

$$\alpha_{eq}^{l(s)/v}(T) = \frac{R_{l(s)}}{R_v} \tag{1.2}$$

Equilibrium fractionation is temperature (T) dependent and δD shows a higher temperature sensitivity compared to $\delta^{18}O$. At a temperature range between 30 °C and 40 °C, the ratio $\frac{^{D}\alpha_{eq}-1}{^{18}O\alpha_{eq}-1} \approx 8$, the origin of the slope of the GMWL (*Majoube*, 1971a). The dependency of the equilibrium fractionation factors and the resulting ratio on temperature is shown in Figure 1.2.

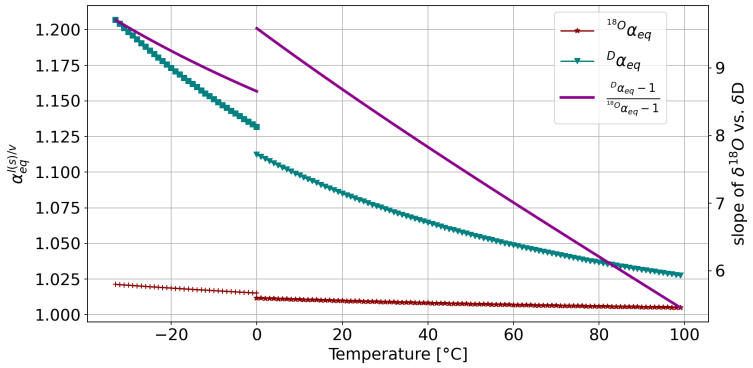

Figure 1.2: Surface temperature dependency on equilibrium fractionation *The temperature dependency of the equilibrium fractionation factors and the effect on the slope in a $\delta^{18}O$ vs. δD diagram. Fractionatino factors used are from Majoube (1971b,a); Merlivat and Nief (1967).*

An example for an equilibrium, i.e. reversible, process in nature is condensation at saturation during precipitation formation. The colder the air, the stronger the fractionation. Hence, precipitation forming at cold or warm temperatures is relatively more or less enriched in heavy water isotopes than the remaining vapor, respectively. Ice-vapor equilibrium fractionation factors used in this study were empirically determined for a temperature range from -33 °C - 0 °C for $H_2^{18}O$ by *Majoube* (1971b) and for HDO by *Merlivat and Nief* (1967). *Ellehoj et al.* (2013) suggested updated equilibrium ice-vapor fractionation factors for an extended temperature range down to -40 °C.

From the GMWL one can deduce the second order parameter d-excess; defined as d-excess=δD -8·$\delta^{18}O$. By this definition and to first order, a water parcel's d-excess value will not change as long as the water parcel experiences equilibrium fractionation processes alone since the isotopic composition will vary along the GMWL. This, however, is a simplification; As already mentioned, the equilibrium fractionation factors are temperature dependent and δD shows a relatively stronger dependency. As a consequence, the slope in a δ^{18}O vs. δD diagram increases with decreasing temperature resulting in a change of d-excess even under equilibrium conditions. This is referred to as the temperature effect. Therefore, alternative d-excess definitions have to be considered depending on the application area. The definition by *Pfahl and Wernli* (2008) accounts for the temperature effect during evaporation conditions, and *Dütsch et al.* (2017) proposed a d-excess definition accounting for an additional effect under very depleted conditions. This additional effect is referred to as the δ-scale effect and needs to be taken into account in high latitude or high altitude regions. However, the d-excess of a water sample is primarily influenced by processes other than equilibrium processes.

Apart from equilibrium fractionation during reversible processes, the isotopic composition of a water sample is influenced by kinetic fractionation during non-reversible processes. As soon as ambient conditions are sub-saturated and a humidity gradient is established kinetic fractionation influences the total resulting fractionation. While purely kinetic processes are hardly found in nature, processes like evaporation and condensation at supersaturation are examples for non-equilibrium processes and entail kinetic and equilibrium fractionation processes. Such non-equilibrium processes fractionate stronger compared to equilibrium processes. The driving force behind kinetic fractionation is the difference in molecular diffusivity between different isotopes in air, which affects the diffusion speed along the humidity gradient. Since δ^{18}O is slightly heavier, it is more strongly affected by kinetic fractionation compared to δD, as the molecular diffusivity is inversely proportional to the molecular mass ($mo^{-0.5}$). This difference gives rise to the influence of kinetic fractionation on the second order parameter d-excess[2]. Interestingly, the GMWL has the function δD =8$\cdot\delta^{18}$O +10‰ and therefore a d-excess value of +10‰, which shows that global precipitation is also slightly affected by non-equilibrium processes. The stronger the humidity gradient of a process, the stronger the relative difference of fractionation influences on the two isotope species and the higher the resulting d-excess value in the vapor (*Pfahl and Wernli*, 2008). Hence the non-equilibrium processes condensation at supersaturation during snow formation and evaporation, both fractionation types affect the resulting isotopic composition of the end members which can be summarized in an effective fractionation factor (α_{eff}) as:

$$\alpha_{eff} = \alpha_{eq}(T) \cdot \alpha_{kin}(h) \tag{1.3}$$

where $\alpha_{kin}(h)$ is a function of sub-saturation (h) and $\alpha_{eq}(T)$ is the temperature dependent equilibrium fractionation factor.

1.2.2 Stable water isotopes in models - process understanding & parameterizations

Rayleigh distillation model

To make use of the information stored in the relative abundance of stable water isotopes in any water parcel at any stage of the hydrological cycle, it is critical to understand and be able to model the processes at place. The fundamental principle of fractionation during phase change processes can easily be applied to a simplified model of the global water cycle. The atmospheric transport of water masses from the evaporation source regions towards the poles resembles a distillation process and is described by a Rayleigh distillation model (Figure 1.3). The ocean's isotopic composition is used as normalization factor for any reported stable water isotopic composition (SMOW). Consequently, a water parcel in the ocean at the beginning of the global water cycle has a δ-value of zero. As it is evaporated and transported polewards, it will progressively become more depleted in stable water isotopes (Figure 1.4). Reasons are first the transition to the gaseous phase including fractionation and afterwards the cooling of the air mass during transport and the subsequent reduction of its water holding capacity, that leads

[2]This is also the origin of the "excess" in d-excess. Since δ^{18}O is stronger affected, i.e. reduced, there is a surplus (excess) of δD .

to successive rain-out events and the associated fractionation of stable water isotopes. Therefore, the isotopic composition of a water parcel can be interpreted as an integrated signal of the path the water parcel has taken in the water cycle.

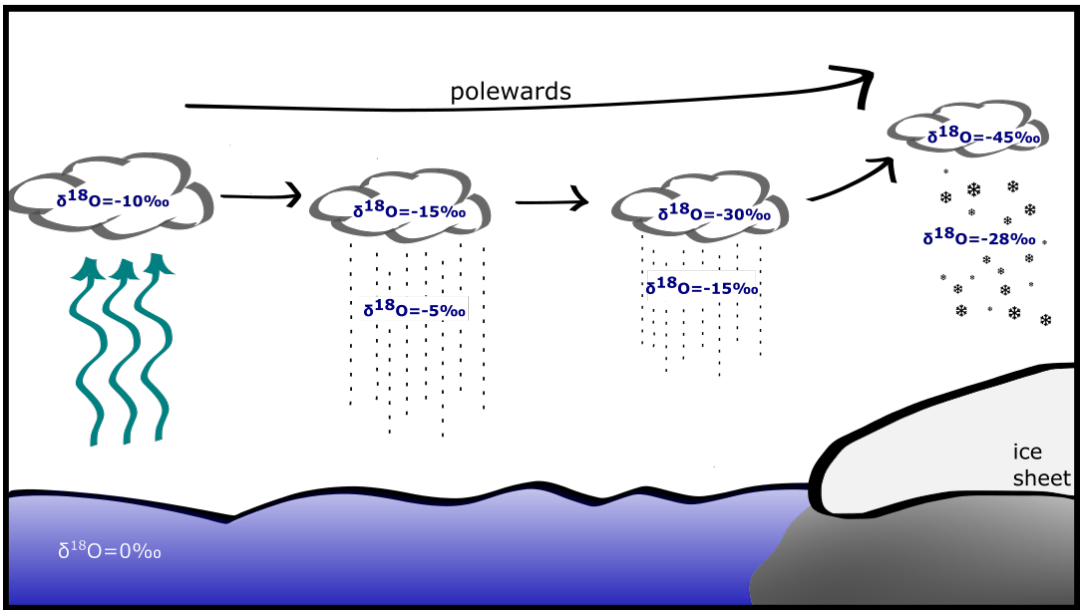

Figure 1.3: Scheme of Rayleigh distillation model
The evolution of the isotopic composition of a water parcel as it is transported polewards and subject to equilibrium fractionation.

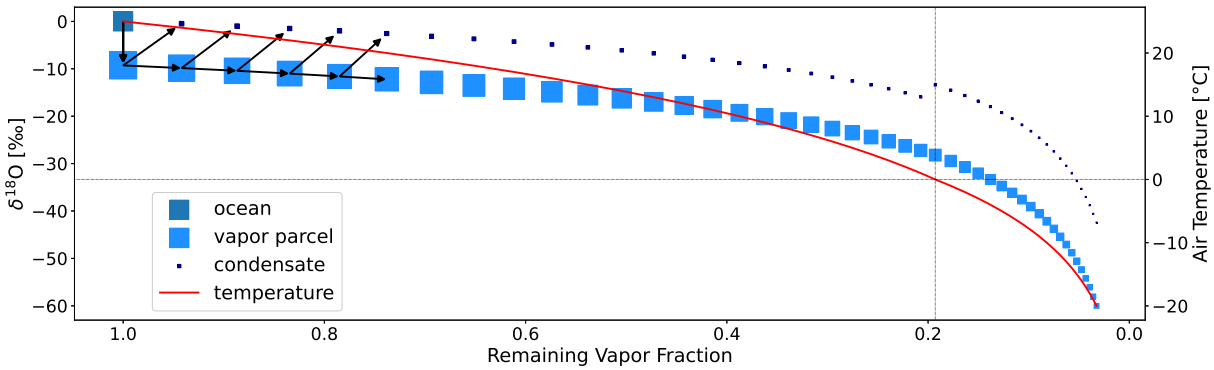

Figure 1.4: Rayleigh fractionation of a water parcel during poleward transport
A Rayleigh fractionation process calculated using Equation 1.4 for the conceptual understanding of consecutive rain-out events during poleward transport. The freezing point at 0 °C is indicated as the shift from vapor-liquid to vapor-ice equilibrium fractionation. Equilibrium fractionation factors from Majoube (1970, 1971a); Merlivat and Nief (1967).

In this simple model, that only considers equilibrium fractionation, the isotopic composition after precipitation formation is dependent on the ratio of remaining to initial mass and the condensation temperature. The corresponding equation is:

$$R_v = R_0 f^{\alpha(T)-1} \tag{1.4}$$

With R_v being the vapor isotopic composition at a given time, R_0 the initial vapor isotopic composition, f the fraction of remaining vapor, and $\alpha(T)$ the temperature dependent equilibrium fractionation factor for vapor-liquid or vapor-solid.

As explained earlier, natural phase transition processes are usually non-equilibrium processes with the evaporation process being the most important one, as it initiates the atmospheric part of the hydrological cycle. Since the beginning of isotopic studies of the hydrological cycle in the early 1960s, there has been one model describing the evaporation process from a water body that withstood the test of time: *Craig and Gordon* (1965).

Craig-Gordon evaporation model

Ever since its introduction, the *Craig and Gordon* (1965) (CG) evaporation model has been the basis for various experimental studies, climate model parameterizations, and biologically-motivated evapotranspiration studies. The idea behind the CG evaporation model is a formulation for the isotopic composition of the evaporation humidity flux that connects the vapor and liquid reservoirs. The fluxes of both humidity (E) and isotopes (E') are parameterized in analogy to a Langmuir linear resistance model. Conceptually, the evaporation surface system is divided into five sections: The liquid, interface, the diffusive and turbulently mixed vapor layers, and the free atmosphere (Figure 1.5).

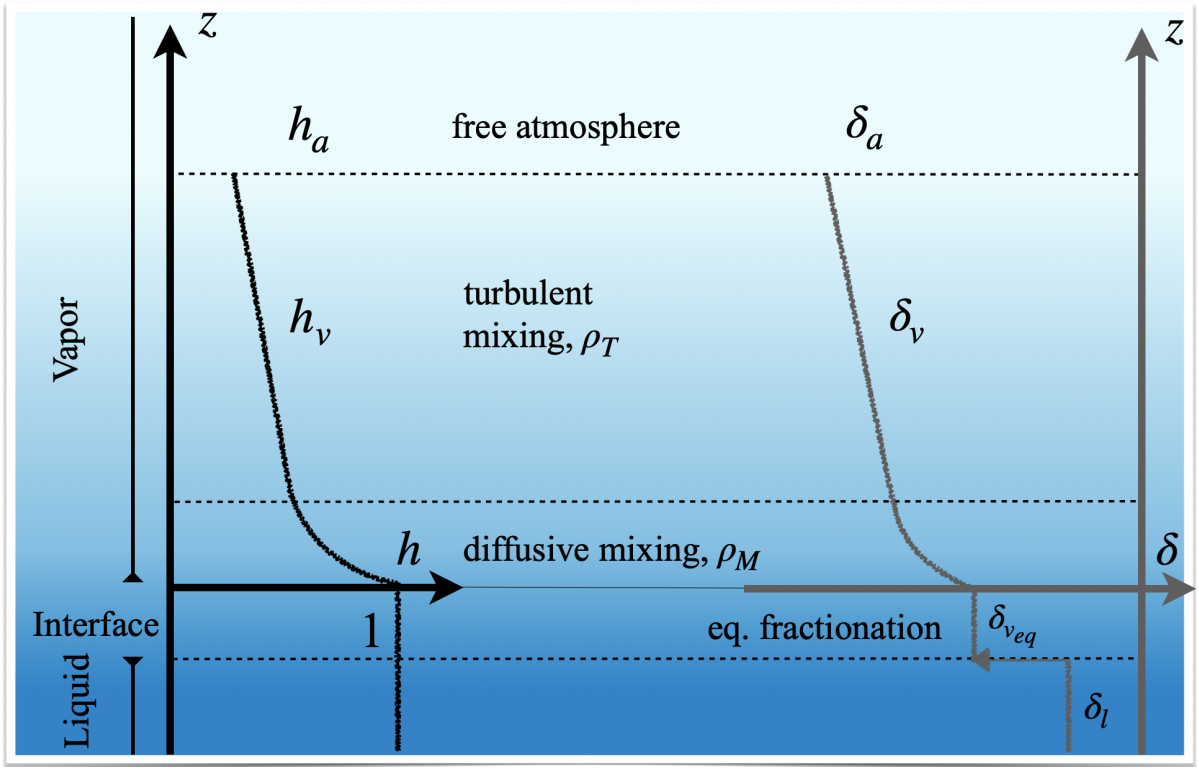

Figure 1.5: The evaporation process as parameterized by Craig and Gordon (1965).
The ocean-atmosphere boundary layer is divided into five sections: liquid, interface, the diffusive and turbulently mixed vapor layer, and the free atmosphere. Fluxes of both humidity and isotopes are parameterized with the flux-gradient method and their ratio taken as evaporation flux isotopic composition.

Gradients in humidity and isotopes between the water surface and the free atmosphere induce the fluxes and the resistances of the layers - summed in series - prescribe the flow speed. Equilibrium fractionation defines the isotopic composition at the lower

boundary and kinetic fractionation is realized through molecular (ρ_M) and turbulent resistance (ρ_T) in the laminar and turbulent section, respectively.

$$\begin{aligned} E &= \frac{(1-h)}{(\rho_M+\rho_T)} = \frac{(1-h)}{\rho} \\ E' &= \frac{\frac{1}{\alpha}R_l - hR_a}{(\rho'_M+\rho'_T)} = \frac{\frac{1}{\alpha}R_l - hR_a}{\rho'} \end{aligned} \tag{1.5}$$

The humidity profile is normalized with the surface humidity (q_{sat}), which is assumed to be saturated with respect to surface temperature (T_s). This yields the normalized humidity h at height z:

$$h(z) = \frac{q(z)}{q_{sat}(T_s)} \tag{1.6}$$

From this, the normalized humidity gradient (1-h) is defined. The ratio of both evaporation fluxes defines the evaporation flux isotopic composition following:

$$R_F = \frac{E'}{E} = \frac{\frac{1}{\alpha}R_l - hR_a}{(1-h)\frac{\rho'}{\rho}} \tag{1.7}$$

From the basic Equation 1.7, two formulations have evolved that both describe the same process but are formulated either in summation notation or as product. The product formulation,

$$R_F = \frac{(1-k)}{(1-h)}\left(\frac{1}{\alpha_{eq}}R_l - hR_a\right) \tag{1.8}$$

after *Merlivat and Jouzel* (1979) groups the kinetic fractionation influences in factor k.

$$k = 1 - \frac{\rho}{\rho'} = 1 - \frac{(\rho_M+\rho_T)}{(\rho'_M+\rho'_T)} \tag{1.9}$$

$$\rho_M \propto D^{-n};\ \rho'_M \propto D'^{-n} \tag{1.10}$$

Where the turbulent resistance parameter is dependent on aerodynamic properties and is assumed to be universal for all water molecule species, as turbulence is not a fractionating process. The molecular resistance, however, is specific for each species and is proportional to the $-n$ power of the respective isotope diffusivities D in air. The nature of the transport is described by the factor n, with n =1 for fully diffusive and n =0 for fully turbulent transport, respectively. According to *Brutsaert* (1975a,b) n can be estimated as n =2/3 for smooth and n =1/2 for rough water surface conditions, depending on the wind speed. The key parameter for the kinetic effects during evaporation is the ratio of the diffusivities of heavy and light isotopes.

$$\epsilon' = \frac{D}{D'} - 1 \tag{1.11}$$

There is some debate about the correct diffusivity ratios for HDO and $H_2^{18}O$, and consequentially about the ratio between them.

$$\frac{\epsilon_D}{\epsilon_{^{18}O}} = \frac{k_D}{k_{^{18}O}} \tag{1.12}$$

However, this ratio is an important parameter that gives rise to changes in d-excess under non-equilibrium conditions. Values for ϵ based on the kinetic theory of gases, taking into account the molecular masses of the isotopes and the surrounding pressure (*Craig and Gordon*, 1965), do not align with empirically determined values by *Merlivat* (1978) and others (Table 2 in *Horita et al.*, 2008). Possible explanations for this are differences in collision diameters between isotopes or experimental error sources like surface cooling and/or surface enrichment during the evaporation process (*Cappa*, 2003; *Kim and Lee*, 2011). To date, the most commonly used ϵ values are supported by two experimental designs from *Merlivat* (1978) with ϵ_D= 25.1 ‰ and $\epsilon_{^{18}O}$= 28.5 ‰ and a ratio between the two of:

$$\frac{\epsilon_D}{\epsilon_{^{18}O}} = 0.88 \tag{1.13}$$

Accordingly, the overall kinetic effects on the flux isotopic composition is an interplay between molecular and turbulent diffusion. *Merlivat and Jouzel* (1979) use the model of *Brutsaert* (1975a,b) to parameterize the k factor as a function of the aerodynamic conditions of the evaporation process, which define the ratio of turbulent over molecular diffusion, and hence the fractionation strength. Wind speed and corresponding friction velocity as well as roughness length of the water evaporation surface are the influencing parameters describing the aerodynamic conditions. The resulting k parameter is defined in analogy to the *Brutsaert* (1975a,b) model for a *rough* and a *smooth* regime (Figure 1.6). However, the separation into two regimes has not been supported by in-situ observations to day. In practice, a value of $k_{^{18}O}$=6 ‰ is often assumed for smooth conditions (*Johnsen et al.*, 1989).

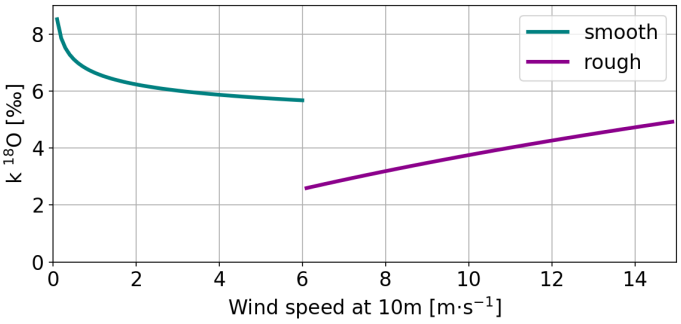

Figure 1.6: Wind influences on kinetic fractionation
The dependency of the kinetic fractionation parameter k for $H_2^{18}O$ on wind speed during rough and smooth conditions as proposed by Merlivat and Jouzel (1979).

The summation notation of the CG model is formulated with the δ instead of R values and explicitly contains the δ-enrichment due to equilibrium (ε^*) and kinetic fractionation ($\Delta\varepsilon$). As this formulation is not used in the rest of this work, the reader is referred to *Gat* (1996) for details.

Isotope-enabled climate models

The Rayleigh distillation model is a first order conceptual model to describe the observed temperature effect in global meteoric waters (*Dansgaard*, 1964). In reality, however, there are several other processes that affect the isotopic composition of a water parcel along a trajectory of the water cycle with the most important ones being evaporation and mixing processes. Hence, in order to discuss spatial and temporal variability of isotope ratios in water, higher order models are needed to model the transport of stable water isotopes within the water cycle. Consequentially, advances have been made

in equipping General Circulation Models (GCM) with stable water isotopes, making use of the holistic effort to describe the complex climate system in one set of equations. The first general circulation model was equipped with isotopes by *Joussaume et al.* (1984). For this task, all model code that describes the common water species is replicated for each individual isotope species and fractionation is implemented at phase change processes that are realized in the model. It is worth noting that various isotope-enabled climate models are using the same parameterizations and equations to describe isotope behavior within the water cycle. The fractionation processes that are implemented in most isotope-enabled climate models are shown in Figure 1.7. Notably, the models do not include fractionation during evaporation from any land area, including snow surfaces (*Cauquoin et al.*, 2019). Differences in the model performance, therefore, originate primarily from differences in the model's encoding of the water cycle itself. Hence, stable water isotopes offer the potential to be independent tracers in climate models that can be used to identify model biases caused by poor process parameterizations that would otherwise remain unnoticed (*Schmidt et al.*, 2005). Examples for such studies are *Risi et al.* (2012) for subtropical areas and *Werner et al.* (2001) for polar areas. Moreover, as stable water isotope records are used as paleoclimate proxies, a model, simulating isotopes, can be used to validate the model performance directly without the need for climate-proxy transfer functions (*Sturm et al.*, 2010). Likewise, they can improve our understanding of proxy signal formation and therefore proxy record interpretation (*Werner et al.*, 2000). For a full account of state-of-the art isotope-enabled climate models, the reviews by *Hoffmann et al.* (2000); *Sturm et al.* (2010); *Xi* (2014) are recommended.

1.2.3 Stable water isotopes in polar areas

Ice core paleothermometry

The discovery of the link between precipitation isotopic composition and mean annual temperature (*Dansgaard*, 1964) motivated the search for precipitation archives to infer information about paleoclimate. As perennial snow and ice is the prime archive for precipitation records, the first snow and ice core studies motivated by isotope paleothermometry followed closely in the late 1960s. The first deep ice core reaching bedrock below the GrIS was recovered at Camp Century in North-West Greenland in 1966. It contained a precipitation record of the past 100 ka. The resulting discrete stable water isotope record was interpreted as climate-proxy for paleotemperatures and informed about climate variability during the last glacial (*Dansgaard et al.*, 1969). Today, six and ten deep (>1000m) ice cores reaching bedrock and several shorter ones have been drilled on the GrIS and AIS, respectively (*Bentley and Koci*, 2007; *NEEM community-members*, 2013). Additionally, numerous ice cores were drilled on mountain and high latitude glaciers. Advances in isotope measurement technology allowed continuous flow analysis (CFA) while melting the ice core in addition to discretely cut ice samples. CFA has increased the record resolution to sub mm scales and allowed detailed analysis of relatively short-lived phenomena several thousand years ago (*Jones et al.*, 2017).

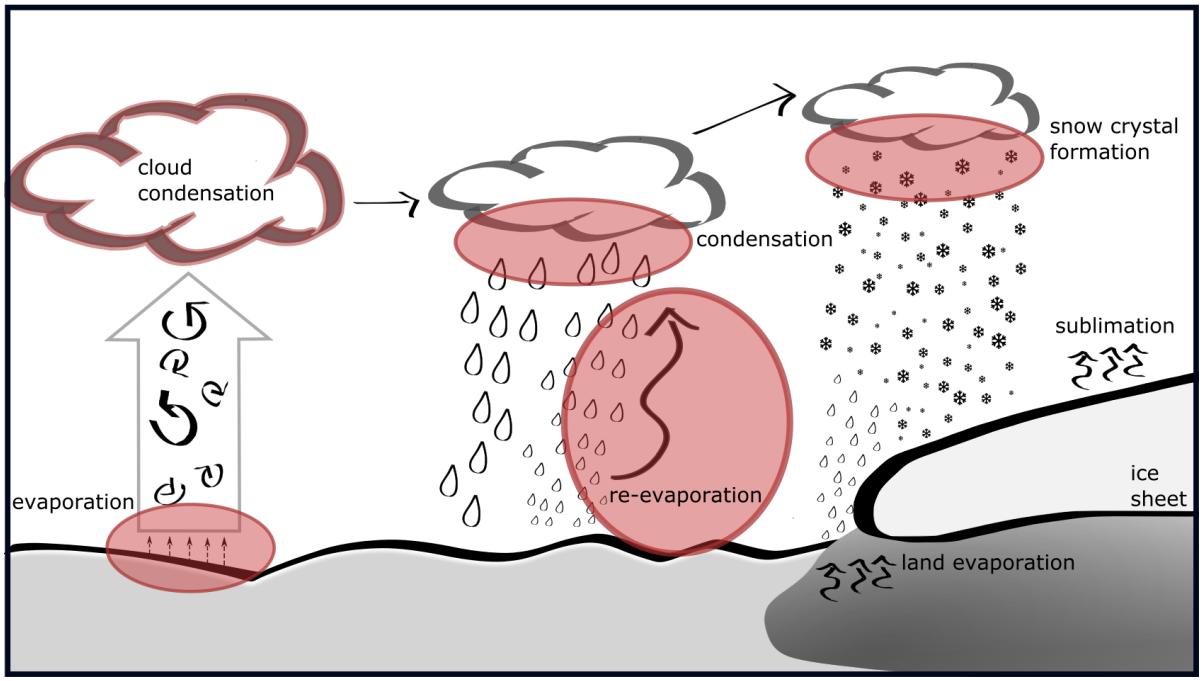

Figure 1.7: A schematic representation of the polar water cycle as realized in most isotope-enabled General Circulation Models

The fractionation-including processes that are represented in climate models are marked in red (Werner et al., 2011). Starting at the evaporation process in clockwise order the processes are: evaporation (kinetic (k) & equilibrium (eq) fractionation), condensation during cloud formation (eq), condensation of raindrops (eq), snow formation (k & eq), re-evaporation of droplets (eq). Some models contain sea-ice fractionation processes (Cauquoin et al., 2019).

However, the simple concept that the ice core isotope paleothermometer is based on is the assumption that the isotopic composition of the condensate, formed at the time of snowfall, captures the ambient climatic conditions and is conserved and transferred to the ice column. Like every simple concept, this is an oversimplification of the actual circumstances. Section 1.1.2outlines the various challenges arising from this simplification and their overall effects on the virtue of ice core isotope annual mean values as proxy for local mean annual near-surface temperatures. Important for the postulation of post-depositional influences on the snow isotopic composition was the development of laser-absorption cavity ring-down spectroscopy (CRDS) that opened the field for in-situ and continuous high-resolution monitoring of stable water isotopes in atmospheric water vapor. Previously, water vapor had to be sufficiently accumulated in cryogenic traps and analyzed by mass spectrometers before information about the isotopic composition of the atmospheric water reservoir was accessible. In low humidity areas like the high latitudes, this limited the time resolution of vapor samples to several hours (*Grootes and Stuiver*, 1997). With CRDS instruments, the (in some cases triple) isotopic composition of water vapor can directly be measured with a resolution of ~ 1 s and an uncertainty low enough to resolve small scale changes in space and time. Making use of this instrumental progress, *Steen-Larsen et al.* (2013) monitored the vapor isotopic composition on the GrIS with a frequency of ~1 Hz. The documented diurnal cycle signal and the subsequently observed co-evolution of surface snow and vapor isotopic composition (*Steen-Larsen et al.*, 2014) raised the question if post-depositional

vapor-snow exchange processes imprint on the snow isotopic composition and what consequences this has for ice core isotope record paleoclimate interpretations. To quantify the effect of post-depositional processes on the snow isotopic composition, one has to be familiar with the meteorological conditions at ice core drilling sites located in polar areas.

Meteorological conditions in the accumulation area of ice sheets

The GrIS, like the AIS and any large ice body, can be divided into an accumulation and an ablation zone according to the governing conditions regarding mass balance. In the ablation zone along the coast and up to a few hundred kilometers inland, melting and consequential runoff are the dominating processes and lead to an overall negative mass balance. In the interior of the GrIS, the accumulation zone, the net surface mass balance is positive with precipitation outweighing negative processes. Melting occurs rarely and turbulent surface fluxes become more important than in the ablation zone (*Lenaerts et al.*, 2019). The great rarity of melting and connected percolation of meltwater ensures an almost undisturbed annual layer stratigraphy in the snow and firn column; a prerequisite for accurate dating of proxy records for paleoclimate studies. Deep ice cores motivated by climate reconstruction have therefore been drilled predominantly in the accumulation zone of ice sheets. In addition, the locations were placed on domes or the ice divide to ensure negligible horizontal flow of ice (*Dansgaard and Johnsen*, 1969). Hence, the prevailing meteorological conditions at most ice core drilling sites, both on the GrIS and the AIS are similar regarding the surface energy balance:

First, snow has a high albedo between 80 % and 90 % and reflects most of the incoming shortwave radiation (*Lenaerts et al.*, 2019). This leads to year-round low air temperatures mainly below the melting point with summer monthly mean temperatures below -10 °C in central Greenland and Antarctica (*Turner et al.*, 2020; *Hanna et al.*, 2021). Consequently, the specific humidity in the interior of ice sheets is low, with summer maximum values of ~5 $g\,kg^{-1}$ on the GrIS and <1 $g\,kg^{-1}$ on the AIS despite the endless frozen water reservoir at hand (*Steen-Larsen et al.*, 2013; *Casado et al.*, 2016). In the winter, during polar night conditions, the air is principally saturated and the atmosphere stably stratified resulting in very weak deposition surface fluxes (*Box and Steffen*, 2001). In the summer, however, a small fraction of the continuously incoming solar radiation is absorbed by the snow which leads to a prominent diurnal cycle signal in the snow surface temperature. The diurnal warming and cooling of the surface trigger vertical gradients in air temperature and humidity which lead to turbulent surface fluxes contributing to the surface energy balance. Cold air advection and long-wave heating can further contribute to the formation of temperature gradients in the air (*Anderson and Neff*, 2008). So formed convective boundary layers with unstable atmospheric stratification that favor turbulent surface fluxes have been observed on ice sheets (*King et al.*, 1996; *Cullen and Steffen*, 2001). The predominant creation mechanism for turbulence in the accumulation zone of ice sheets is the buoyancy term as the surface is rather smooth which limits the wind shear contributions. The relevant determining parameter for turbulence induced by shear is the surface roughness length, which is difficult to measure. Generally, the bedrock topography below the ice sheet does not influence the ice sheet surface topography. Therefore, the surface is generally

flat with wind-generated snow formations defining the surface roughness length (*Albert and Hawley*, 2002; *Filhol and Sturm*, 2015). Typical roughness lengths for snow surfaces reported in literature range from $2{\cdot}10^{-5}$ m to $5{\cdot}10^{-4}$ m depending on the season and local wind patterns (*van As et al.*, 2005; *Van den Broeke et al.*, 2005; *Gromke et al.*, 2011; *Amory et al.*, 2017). Since bulk or gradient estimations of surface fluxes depend heavily on an accurate estimation of the surface roughness length, this is often an error source.

Whereas the turbulent surface fluxes play a minor role in the surface energy balance at ice core drilling sites (*King et al.*, 1996; *Box and Steffen*, 2001; *van As et al.*, 2005), the humidity flux can constitute a significant part of the surface mass balance in the accumulation zone of the ice sheets (*Cullen et al.*, 2014) which is dependent on the local accumulation rate; a parameter that varies substantially depending on the location on the ice sheets.

In Greenland, observed accumulation rates in the interior of the ice sheet range from ~10 cm water equivalent (w.eq.) a^{-1} to ~50 cm w. eq. a^{-1} (*Mernild et al.*, 2015; *Mosley-Thompson et al.*, 2001; *Koenig et al.*, 2016). In the interior of the AIS, the annual accumulation rates are significantly less. Observed accumulation rates range from less than 2 cm w. eq. a^{-1} to ~10 cm w. eq. a^{-1} (*Thomas et al.*, 2017; *Palerme et al.*, 2014). This is due to even lower atmospheric humidity and limited influence of coastal synoptic conditions that could bring warm and humid air masses needed for precipitation inland (*Masson-Delmotte et al.*, 2011). Instead, precipitation events in the form of *diamond dust* is a frequently, often daily observed phenomenon (*Fujita and Abe*, 2006; *Schlosser et al.*, 2016) on the AIS. It also occurs on the GrIS, but less frequently. Diamond dust forms through radiative cooling of saturated or near-saturated air at very low temperatures and is also referred to as clear-sky precipitation. It can contribute the majority of annual accumulation at some places on the AIS (*Ekaykin et al.*, 2004; *Ricaud et al.*, 2017). However, the contribution from diamond dust to total precipitation is subject to interannual variability (*Stenni et al.*, 2016). It further seems to be highly dependent on interannual variability and location, whether the snowfall events show a seasonal pattern (*Burkhart et al.*, 2004) or not (*Porter and Mosley-Thompson*, 2014; *Dibb and Fahnestock*, 2004; *Fujita and Abe*, 2006). However, even if there is no clear accumulation seasonality, snowfall events are spread unevenly throughout the year and the majority of the annual accumulation can be attributed to few, major snowfall events (*Fujita and Abe*, 2006; *Servettaz et al.*, 2020).

2 Methods & Data

2.1 Methods

In order to answer the research questions outlined in Chapter 1.1.4, I used observational in-situ data from EastGRIP (see Chapter 2.2.1) in the accumulation zone of the GrIS. Besides meteorological parameters, vapor and snow samples were analyzed for their isotopic composition using a CRDS. The measurement technique and necessary data processing steps are outlined in the next section of this chapter. A full description of the site and an account of the available data sets is given in Chapter 2.2.
For Paper I, we developed a new measurement method to monitor the exchange of stable water isotopes between snow surface and lower atmosphere in-situ through direct isotope flux measurements. The method is based on the combination of fast eddy-covariance humidity flux measurements and slower vapor isotope measurements.
Additionally, a laboratory experiment was designed and is presented in Paper II. The chamber set-up allowed control of the environmental parameters and hence the monitoring of the effect of the sublimation process on the snow isotopic composition under ideal conditions. The study was supplemented by similar experiments carried out at EastGRIP under characteristic environmental conditions and an additional control snow surface sampling scheme.
Paper III makes use of the acquired meteorological and isotope data from EastGRIP as input parameters for a simple numerical mass-balance model simulating vapor-snow exchange processes and their influence on the isotopic composition of the snow. For this, the observations of the snow isotope content serve as benchmark for the model results.

2.1.1 Stable water isotope measurements

To analyze a sample's water isotopic composition as defined by equation 1.1, the ratio of molecular concentrations of rare and abundant water species needs to be measured. The two ways to measure such concentrations are either using the indirect mass spectrometry (MS), or the direct optical spectroscopy method.
The technique behind Isotope Ratio Mass Spectrometers (IRMS) is the separation of charged ions or molecules based on their weight using an electromagnetic field (*Ghosh and Brand*, 2003). Due to the highly adsorbing behavior of water molecules, however, they can not be analyzed directly using a mass spectrometer. Instead, water molecules need to be transferred into gases with less sticky characteristics like CO_2, H_2 or O_2 through chemical reactions. For measurements of δD the reduction to pure hydrogen gas (*Bigeleisen et al.*, 1952) or pyrolisys into CO and H_2 (*Gehre et al.*, 2004) is commonly performed, whereas for δ^{18}O the equilibration method with CO_2 gas (*Epstein and Mayeda*, 1953) is used. Hence δ^{18}O and δD need to be analyzed separately. Despite highly precise and accurate, the MS method is therefore a slow and costly measurement technique, which is usually used for characterizing calibration standards. Moreover, samples need to be available in liquid or solid phase and MS is therefore not suitable as in-situ method to measure water vapor directly.

The alternative optical spectroscopy measurement technique relies on the specific light absorption characteristics of the different water species. Hence water molecules of different species can be identified by analyzing the absorption peaks at different wavelengths in an optical spectrum. The area under the respective absorption peak is directly linked to the number of molecules of the respective species in the sample volume. There are several instruments commercially available that all rely on the same principle but use slightly different analysis methods. The instrument I used to analyze liquid samples and water vapor was a cavity ring-down spectrometer (CRDS) type L2140-i from the manufacturer Picarro Inc. This instrument introduces a gaseous sample into a chamber kept at 50 Torr (~67 mbar) and exposes it to two lasers of known wavelength. The chamber (cavity) includes semi-transparent mirrors that increase the optical path length to 6.7 km. The measurement starts when the lasers are stopped and the fading of the light intensity, i.e. the "ring-down" is measured. In an empty cavity, this takes 22 μs (*Casado*, 2016). The presence of target molecules within the cavity will lead to a decrease of this ring-down time, as the absorbance increases according to the Lambert-Beer law. Once the absorption spectrum in the respective bandwidth is generated, the area under the absorbance peak for the respective molecules is calculated and the ratio inferred (see Figure. 2.1). Instead of integrating the spectra directly, a fit is calculated taking into account the physical principle of absorption and relevant environmental factors, such as pressure and temperature that define the peak shape.

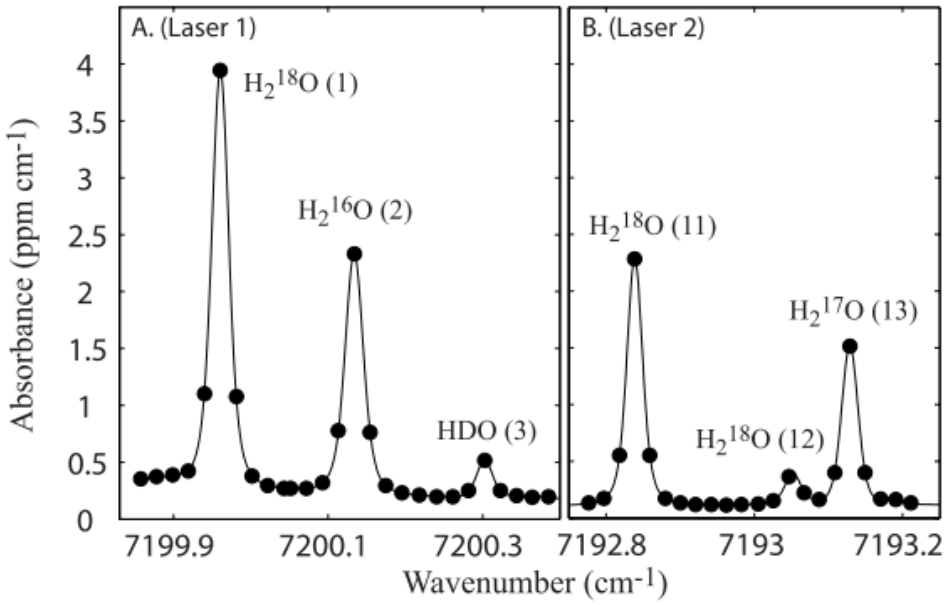

Figure 2.1: Absorption spectrum of CRDS analyzer type L2140-i
Measurements were performed at 20.000 ppmv in dry air carrier gas. The peaks are labelled with the associated isotopologue. Lines are least-square fits to the data using Galatry profiles. From Steig et al. (2014).

The measurement precision and accuracy of the CRDS technique depends on the goodness-of-fit to these absorbance peaks, the instrument's ability to keep the measurement conditions constant and on the humidity level in the cavity. The same water standard measured at different humidity levels results in different CRDS readings of the

isotopic ratio. This is referred to as the humidity-isotope response of the instrument and has shown to be different for different water standard values (*Weng et al.*, 2020). Additionally, the noise on the measurement increases with lower humidity as the shapes of the absorption peaks change and the fit becomes worse. The manufacturer, therefore, recommends measuring at humidity levels of ~20.000 ppmv when measuring liquid samples in the laboratory. However, when measuring vapor in-situ on the GrIS, ambient humidity varies in the range of 500-8000 ppmv. Consequently, the measurements have to be calibrated.

CRDS calibration

Generally, measurements obtained by a CRDS have to be corrected for the instrument's 1) humidity-isotope response and 2) drift and 3) calibrated against the VSMOW-SLAP scale, to obtain highly accurate and comparable data. The reasons are, as outlined above, the instrument's limited ability to obtain a good fit to the absorption peaks and the absence of a calibration of peak height to VSMOW-SLAP scale. Moreover, the aforementioned stickiness of water molecules leads to memory effects in the measurements when the isotopic composition of the sample changes abruptly, for example, when the vapor sampling level is switched or when liquid samples are analyzed in sequence in the laboratory. Memory effects become larger the more contact surfaces are present in the sampling system, including the cavity. As a result, CRDS measurements require the routine performance of a calibration protocol. In the following, I will briefly outline the calibration protocol followed for the liquid sample analysis performed at the stable water isotope laboratory of the AWI in Bremerhaven, Germany, and the protocol for the in-situ measurements at EastGRIP.

Liquid samples calibration protocol

Snow samples were kept frozen until the day of the analysis. The samples were melted at room temperature in closed plastic *Whirl-Paks* to prevent fractionation. Afterwards, 1.8 ml of sample were transferred to 2 ml glass vials, which were closed with a septa-cap and placed in the tray of a PAL autosampler. The samples were vaporized with a Picarro high-throughput vaporizer heated to 110 °C. Following the *van Geldern and Barth* (2012) measurement protocol, each sample is injected four times and analyzed at a humidity level of 20,000 ppmv, making humidity-isotope calibrations unnecessary. To account for memory effects, three distinctly different standards are injected ten times each (one twice) at the beginning of each measurement run. The resulting memory effect curves are used to calculate run-specific memory coefficients with which the sample injections are post-run corrected in order to avoid discarding sampling injections and to reduce measurement time. Drift monitoring samples along with a quality control sample are measured throughout the run. The deviation of this quality control run from the true value can be used to describe the measurement accuracy.

Vapor sample calibration protocol

As in the laboratory, it is important for in-situ measurements to keep environmental conditions for the CRDS as stable as possible to limit the instrument's tendency for drift. Similar to the laboratory routine, the measurements have to be calibrated to the VSMOW-SLAP scale. For this purpose, one of two standards bracketing and one (quality) standard in the expected range of observed isotopic composition is measured in alternating sequence once a day. The custom-made calibration unit (similar to *Steen-Larsen et al.* (2013)) used for the EastGRIP calibration runs allows the regulation of the humidity level. In the daily calibration routine, standards are measured at a high humidity level (~7000 ppmv) and at a low humidity level (~3000 ppmv) and the drift over the season is monitored. The 3000 ppmv level was chosen as it was perceived as low enough to be a reference level for the low humidity observations at the same time as being high enough to assure sufficient precision of the standard measurement. Additionally, humidity calibrations are performed once at the beginning, during and at the end of the season. For these, all three standards are measured at several humidity levels, spanning the expected range of humidity (*Steen-Larsen et al.*, 2013).

If the drift does not outweigh the noise on the calibration pulses, all humidity-isotope response curves are averaged to estimate the season specific humidity-isotope correction function that is used to calibrate all measurements after the season. In case of visible drift in the measured quality and calibration standard values, it has to be accounted for during calibration. During the field seasons 2018 and 2019, the secondary standards listed in Table 2.1 were used.

Table 2.1: *Standards used for EastGRIP Vapor Analysis*

Standard	Purpose	δ^{18}O [‰]	δD [‰]
Boulder Water	Upper Boundary	-14.15	-111.65
South Pole	Lower Boundary	-55.39	-435.31
Arctic Water	Quality Check	-30.30	-239.13

2.1.2 Surface humidity flux measurements

An important part of this thesis, besides the field of stable water isotopes, is the analysis of turbulent surface fluxes that exchange heat and humidity between the earth's (snow) surface and the atmosphere. Only by knowing how much and under which conditions snow is sublimated and deposited, is a quantification of effects of vapor-snow exchange on snow properties possible. However, although studied for over a century (*Foken et al.*, 2006), turbulence or turbulent transport, as opposed to laminar transport (*Schmitt*, 2017), remains a quantity difficult to measure. Turbulence is the irregular movement of air, different from the mean wind, that can be thought of as variously sized swirls of motion, so-called eddies, superimposed on the mean wind and on each other. The largest eddies are generated by forcing mechanisms at the surface and contain the highest levels of energy. This energy is passed on to smaller eddies (and so forth) until it dissolves in molecular viscosity (also referred to as Energy Cascade). Turbulent eddies of all sizes move atmospheric quantities such as momentum, heat and scalars, e.g. water molecules, by their motion. Since this is a chaotic movement without direction, it acts as a mixing process, spreading the quantity in space.
Turbulence is created through shear or buoyancy production. Wind shear is always enhancing turbulence whereas it depends on the temperature gradient if buoyancy intensifies or counteracts turbulence. These two forcing mechanisms are used to define the atmospheric stability (ξ), a measure for the atmosphere's tendency to en- or discourage vertical motion. For this, the Obukhov-length L is calculated which can be interpreted as the height at which buoyancy dominates over shear (*Stull*, 1988). It follows with measurement height z:

$$\xi = \frac{z}{L} = \frac{-zkg\,(\overline{w'\Theta_v'})}{\overline{\Theta_v}\,u_*^3} \approx \frac{zkg\,\Delta\overline{\Theta_v}}{u_*\,\overline{\Theta_v}\Delta\overline{U}} \tag{2.1}$$

$$u_* = \left(\overline{u'w'}^2 + \overline{v'w'}^2\right)^{0.25} \tag{2.2}$$

with u_* being the shear parameter (friction velocity) and $(\overline{w'\Theta_v'})$ the buoyancy term, which can be approximated by the vertical gradient of the virtual potential temperature $\Delta\Theta_v$. Otherwise, k=0.4 is van Karman constant, g is gravity acceleration, U wind speed and u, v, w the three dimensional wind components. Typical averaging times are between 10 min and 1 hour. A negative ξ indicates unstable atmospheric stability that allows for large fluxes and convective movements, whereas a positive ξ value indicates stable atmospheric conditions. For an unstable atmosphere (ξ<0), the ground needs to be heated above the temperature of the overlying air. This seems implausible for snow-covered areas but has been observed at EastGRIP and other locations on an ice sheet (Chapter 1.2.3 & 2.2.1).
This chapter focuses on the measurement of scalar fluxes, as the humidity or latent heat flux (LE). There are two main approaches to measuring turbulent transport: the *flux-gradient method* and the *eddy-covariance* method. Both methods are used throughout this thesis and will be briefly explained in the following.

Flux-gradient method

The flux-gradient method understands turbulence as transport along a gradient in analogy to a diffusive transport. The constraining parameters are a vertical gradient in the quantity that is transported and a diffusivity parameter (K), characteristic for the transport conditions (*Foken and Wichura*, 1996). As K is unknown, the transport is often parameterized by following the Monin-Obukhov similarity theory (*Monin and Obukhov*, 1954). Using the bulk method with a gradient defined by one measurement height and the surface, the latent heat flux can thus be approximated by (*Van AS*, 2011):

$$LE = \rho L_{v/s} \kappa^2 \frac{u}{\left(ln\frac{z_u}{z_{0u}} - \psi_u\right)} \frac{(q - q_{sat})}{\left(ln\frac{z_q}{z_{0q}} - \psi_q\right)} \tag{2.3}$$

with ρ being the density of air, $L_{v/s}$ the latent heat of vaporization or sublimation, z_u, z_q the measurement heights of humidity (q) and wind (u), z_{0u}, z_{0q} the corresponding roughness lengths (see Chapter 2.2.1) and ψ_u, ψ_q the atmospheric stability correction functions. Commonly used empirically-derived correction functions are from *Paulson* (1970); *Businger et al.* (1971); *Högström* (1988); *Holtslag and De Bruin* (1988). The physical explanation of the roughness length for momentum z_0 is the height above the (bare) ground at which the wind becomes zero. It can be calculated during neutral atmospheric stability by assuming a logarithmic wind profile. Roughness lengths in nature span several orders of magnitude from ice surfaces with $z_0 = 1 \cdot 10^{-5}$ m to forests with $z_0 = 1$ m (*Stull*, 1988). The roughness lengths of temperature and humidity are inferred from z_0 (e.g. for snow *Andreas*, 1987). If measurements from two levels are available, the gradient can also be calculated between the levels, given that the measurement uncertainty is small enough to resolve, at times, small vertical gradients.
The flux-gradient method is an indirect way for estimating the turbulent fluxes because it relies on empirical functions and is therefore associated with high uncertainties. It is highly dependent on and sensible to the used roughness lengths, which are difficult to measure and therefore a great uncertainty risk (*Optis et al.*, 2016). It further does not account for potential counter-gradient transport and poses high requirements for the instrument precision and accuracy. Further, the applicability of the flux-gradient method under stable conditions can be limited as underlying assumptions may be violated under stable conditions (*Sorbjan and Grachev*, 2010)

Eddy-covariance method

The eddy-covariance (EC) method is a direct method for measuring turbulent surface fluxes. A sonic anemometer records three-dimensional wind speed while the scalar of interest is measured simultaneously in the same sampling volume (*Swinbank*, 1951). The idea is to measure eddies of all relevant sizes, i.e. frequencies, by measuring at a high frequency (>10 Hz) for a long enough but necessarily short averaging period to avoid sampling signals outside the turbulence spectrum. The optimal length of the averaging period varies, depending on the atmospheric stability and surrounding topography. The covariance of vertical wind and humidity time series is computed for the

averaging period.

$$covar(w,q) = \frac{1}{N}\sum_{i=1}^{N}(w_i - \bar{w})(q_i - \bar{q}) = \frac{1}{N}\sum_{i=1}^{N} w_i' q_i' = \overline{w'q'} \tag{2.4}$$

This way, vertical air movements are associated with the respective humidity measurements and a net vertical humidity flux $\overline{w'q'}$ can be monitored. From this, the latent heat flux can be obtained with:

$$LE = \overline{w'q'} \cdot \rho \cdot L_{v/s} \tag{2.5}$$

The EC method does not rely on empirical functions or the similarity theory assumption. However, the accuracy of the method relies on the compliance with underlying assumptions regarding measurement location, instrument installation and nature of transport (*Foken and Wichura*, 1996). The most important requirements are that:

- *Taylor* (1915) hypothesis of stationarity is fulfilled
- *Reynolds* (1894) averaging can be applied, i.e. mean vertical flow is zero
- the terrain is flat and homogeneous
- fetch area of the flux system is the area of interest
- instrument is installed horizontally, directed in the mean wind and flow is undisturbed
- the transport is of fully turbulent nature

The data has to be quality controlled with respect to the mentioned requirements. Compliance with some can be ensured through post-processing of the data, e.g. small deviations from the mean wind direction can be corrected for by rotating the wind vectors, i.e. setting $v = 0$. Additionally, several frequency-correction functions are applied to the calculated cospectrum during post-processing, necessary due to instrument limitations and data processing effects like averaging. Similar to the flux-gradient method, the EC method's applicability to stable atmospheric conditions might be limited. The assumption, that transport is only realized through turbulence might be violated under stable conditions as submeso-motion like structures can play a crucial role in this atmospheric state (*Mahrt*, 2009).

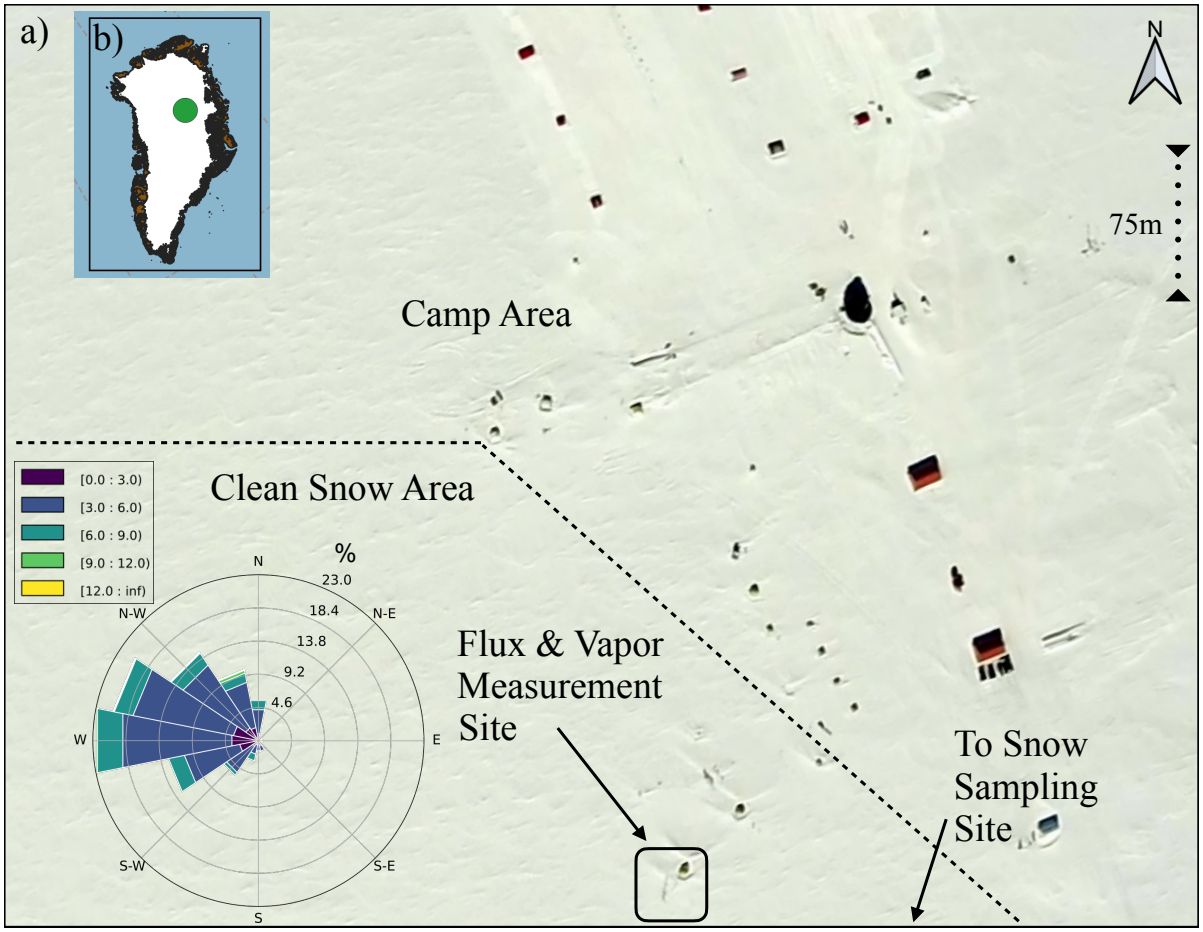

Figure 2.2: EastGRIP camp site
The location of the EastGRIP camp on the GrIS is shown in b) and the outline of camp and clean snow area as viewed from above in a). The windrose shows the wind direction distribution of the summer season 2019. Due to the rather constant wind direction, the flux, vapor and snow sampling site are largely unaffected by camp activities. Aerial picture credit: J. Box and A. Hubbard

2.2 Data & Field Site

2.2.1 East Greenland Ice Core Project (EastGRIP) site

Field observations used throughout this thesis were obtained from the *East Greenland Ice Core Project (EastGRIP* or *EGRIP)* site (75°37'47" N, 35°59'22" W in July 2019) on the GrIS at about 2700 m above sea level. The EastGRIP camp is located in North-East Greenland (Figure 2.2 b) at the onset of the north-east Greenland ice stream (NEGIS) (*Fahnestock et al.*, 1993) in the accumulation zone of the GrIS.

The camp was set up in 2016 to accommodate an ice core drilling project with the aim to drill through a fast-flowing ice stream motivated by an improved understanding of characteristics and flow behavior of ice streams. In 2021 the project is ongoing and supposed to reach bedrock in 2022. All drilling activities are performed during the summer months (May-August) in trenches below the surface. At peak times, the camp hosts about 40 scientists and staff who carry out research projects above and below the surface. The SNOWISO project is part of EastGRIP's surface science division and has set up a dedicated clean snow area upstream of

the camp in the direction of the prevailing wind (Figure 2.2 a). This way, impact from the camp on the monitored atmospheric and snow properties are minimized. The SNOWISO project has monitored the isotopic and meteorological conditions, including surface fluxes, each summer season between and including 2016 to 2019. Thereby, unstable atmospheric conditions were observed, which is an important factor for sublimation (see Figure 2.3). Additionally, the Geological Survey of Denmark and Greenland has been operating an automatic weather station (AWS) at the EastGRIP field site since 2016 through the Programme for Monitoring of the Greenland Ice Sheet (*Fausto et al.*, 2021) such that basic meteorological information is available continuously between May 2016 up to today. The meteorological conditions at the EastGRIP site within the period May 2016 to April 2020 are characterized by an annual mean 2 m air temperature of -28.7 °C (min daily avg: -61.6 °C, max daily avg: -1.9 °C) and a mean annual specific humidity of 0.81 g kg^{-1} (min daily avg: 0.01 g kg^{-3}, max daily avg: 4.1 g kg^{-1}). Such conditions are representative for other accumulation zone locations on ice sheets (see Chapter 1.2.3). The annual cycles of monthly means of air temperature, specific humidity and net radiation are shown in Figure 2.4. The mean annual accumulation rate at Eastgrip is ~10-15 cm w. eq (*Karlsson et al.*, 2020).We have observed a seasonality in accumulation with the majority of snowfall occurring in late summer and autumn.

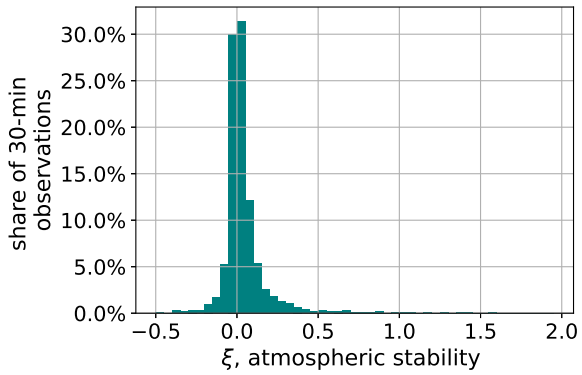

Figure 2.3: Atmospheric stability recorded at EastGRIP during summer 2019
The stability was calculated with the EC data according to equation 2.1. Bins are spaced in 0.05 increments. Negative values report unstable atmospheric conditions.

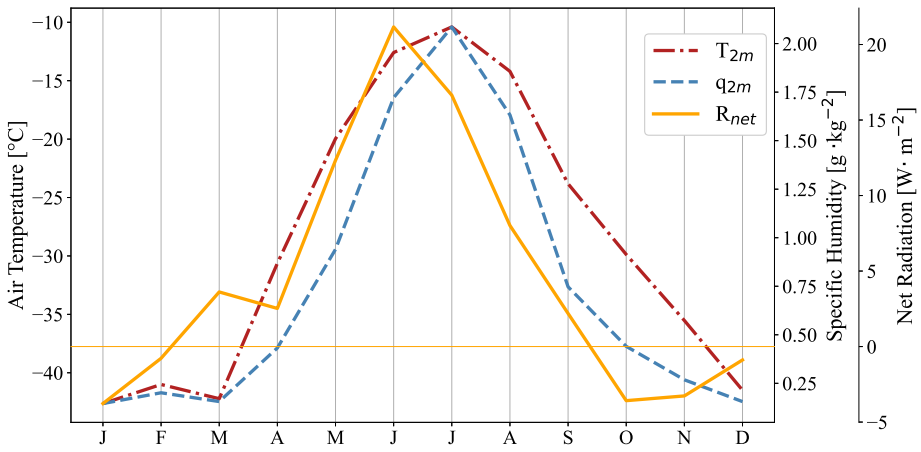

Figure 2.4: Meteorological conditions at the EastGRIP site *The annual cycle of monthly mean temperature, specific humidity and net radiation are shown as recorded by the local AWS station in the four years from May 2016 to April 2020. The net radiation is defined as positive for downward fluxes. Humidity and radiation data are missing in the period 11.2019 - 04.2020.*

2.2.2 Data sets from EastGRIP

The SNOWISO project repeatedly set up a combination of instrumentation to observe near surface atmospheric parameters up to a height of ~7m using tower installations in the dedicated clean snow area of the EastGRIP camp. Besides the standard meteorological parameters, surface fluxes and vapor isotopic composition were measured throughout the summer months between 2016 to 2019 (Figure 2.5 a). Further, a comprehensive snow sampling protocol was followed to monitor the temporal and spatial variability of snow properties, such as specific surface area, density, temperature, and isotopic composition. Figure 2.5 b shows an exemplary snow sampling event for various depths.

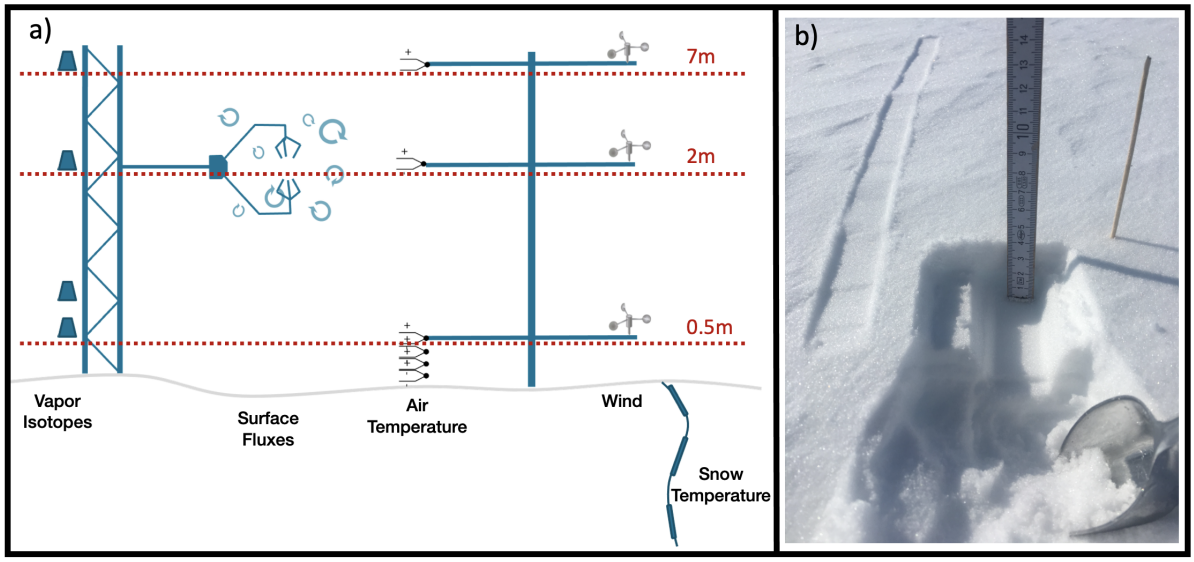

Figure 2.5: EastGRIP sampling of snow and atmospheric parameters
The regularly observed parameters are presented schematically in a) and a typical snow sampling scheme with snow samples of different depths shown in b). Picture credit: A. Thayer.

The respective data sets are being made available on publicly accessible data repositories, and an overview is given in Table 2.2.

Table 2.2: *Data sets from EastGRIP*

	Parameter	Temporal / Spatial Resolution	Height / Depth	Observation Period	doi
Meteorology	Wind Speed &	10min	0.5,1,2m	14.06-04.08.2016	
	Wind Direction	10min	0.4,0.8,1.7m	08.05-07.08.2017	
		1s	0.3,1.8m	19.05-07.08.2018	
		1s	0.5,1,5m	26.05-31.07.2019	[128]
	Temperature	10min	50,100,200cm	14.06-04.08.2016	
		10min	40,80,170 cm	08.05-07.08.2017	
		1s	2,5,10,30,80,180cm	19.05-07.08.2018	
		1s	5,10,30,50,200cm	26.05-31.07.2019	[128]
	LE&H	10min	180cm	14.06-28.07.2016	
	surface	10min	160cm	08.05-07.08.2017	
	fluxes	30min	180cm	19.05-17.08.2018	
		30min	215cm	23.05-31.07.2019	[129]
	Humidity	hourly	0.5,1,2,7m	11.06-07.08.2016	
	mixing	hourly	0.3,0.7,1.7,7m	14.06-10.08.2017	
	ratio	hourly	0.3,0.8,1.8,7m	07.05-06.08.2018	
		hourly	0.5,1,2,7m	25.05-27.07.2019	[130]
Snow	Accumulation	~3days / 200x1m		11.06-02.08.2016	
		~3days / 200x1m		12.05-13.08.2017	
		~3days / 200x1m		25.05-05.08.2018	[124]
		~3days / 200x1m		17.05-30.07.2019	
	Temperature	1s	0,5,10,20,30,50,75,100 cm	25.05-31.07.2019	
		1s	surface	25.05-31.07.2019	
	SSA	daily / 10x10m	0-2.5cm	09.06-02.08.2016	
	& Density	daily / 10x10m	0-2.5cm	30.06-03.08.2017	
		daily / 10x10m	0-2.5cm	05.05-06.08.2018	
		daily / 10x10m	0-2.5cm	27.05-31.07.2019	
Stable Water Isotopes	Surface Snow	daily / indi. 10x10 & 20x50m	0-1,6-7cm	11.06-03.08.2016	
		daily / indi. 10x50m	0-1,6-7cm	03.05-11.08.2017	
		daily / con. 10x10m	0-0.5,0-1,0-2cm	11.05-05.08.2018	
		daily / con. 10x10m	0-0.5,0-1,0-2,0-5cm	17.05-31.07.2019	
	Surface Snow	daily / indi. 10x10m	0-2.5cm	09.06-02.08.2016	
		daily / indi. 10x10m	0-2.5cm	30.06-03.08.2017	
		daily / indi. 10x10m	0-2.5cm	05.05-06.08.2018	
		daily / indi. 10x10m	0-2.5cm	27.05-31.07.2019	
	Snowpack	~2 days / 2cm	0-30cm (x2)	26.06-04.08.2016	
		bi-weekly / 2cm	0-1m (x5)	03.05-12.08.2017	
		bi-weekly / 2cm	0-1m (x5)	12.05-06.08.2018	
		bi-weekly / 2cm	0-1m (x5)	29.05-24.07.2019	
	Vapor	hourly	0.5,1,2,7m	11.06-07.08.2016	
		hourly	0.3,0.7,1.7,7m	14.06-10.08.2017	
		hourly	0.3,0.8,1.8,7m	07.05-06.08.2018	
		hourly	0.5,1,2,7m	25.05-27.07.2019	[130]

3 Summary of Papers

Paper I: **Quantifying the Stable Water Isotopologue Exchange Between Snow Surface and Lower Atmosphere by Direct Flux Measurements.**

***Sonja Wahl**, Hans Christian Steen-Larsen, Joachim Reuder, and Maria Hörhold (2021)*
Journal of Geophysical Research: Atmospheres, *126 (13)*

Paper I presents in-situ observations of stable water isotope fluxes from the interior of the GrIS measured with the eddy-covariance technique. With these unprecedented direct observations from the GrIS, we investigate the vapor-snow exchange process by calculating the isotopic composition of the humidity flux.

The outlined method of combining high-frequency turbulence and simultaneous vapor isotope measurements allows a quantification of the isotope fluxes without relying on empirical models (**RQ 1**). These are the first observations of this kind performed in polar conditions on an ice sheet. The study entails a thorough quality control procedure to ensure reliable results which shows that the presented method is most accurate in unstable to slightly stable atmospheric conditions. We further estimate the measurement uncertainty of the eddy-covariance method which shows to be within the uncertainty range of other methods given in the literature. A comparison with isotope flux estimates using bulk methods shows a satisfying agreement, albeit the necessary exclusion of some measurement points due to violation of compliance with bulk method criteria. Our observations show that, as expected, the isotope fluxes closely follow the pattern of the humidity flux and continuously exchange water isotopes between snow and atmosphere by deposition and sublimation. During deposition conditions, we find a dependency of the humidity flux isotope signal on the vapor isotopic composition and the observations suggest an isotopically enriched deposition flux compared to the near-surface vapor (**RQ 2**, Figure 3.1a). During sublimation conditions, the isotopic composition of the humidity flux is dependent on the snow isotopic composition and relatively depleted in heavy isotopes compared to the snow (**RQ 2**, Figure 3.1b). This provides indisputable in-situ evidence of fractionation during sublimation (**RQ 3**). A comparison with established fractionation functions suggests a sublimation flux that is, averaged over the season, close to vapor in equilibrium with the snow surface.

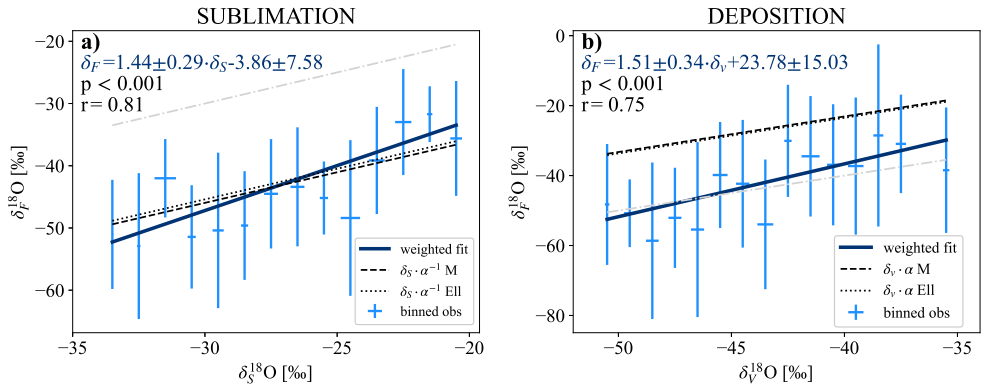

Figure 3.1: *The dependency of observed humidity flux isotope signal (δ_F) on snow (δ_S) and vapor (δ_V) isotopic composition during sublimation (a) and deposition (b), respectively (Wahl et al., 2021).*

Paper II: **The Role of Sublimation as a Driver of Climate Signals in the Water Isotope Content of Surface Snow: Laboratory and Field Experimental Results**

Abigail G. Hughes, ***Sonja Wahl****, Tyler R. Jones, Alexandra Zuhr, Maria Hörhold, James W. C. White, and Hans Christian Steen-Larsen (2021)*
The Cryosphere*, (15)*

Paper II investigates the role of vapor-snow isotope exchange for the formation of the snow isotopic composition on hourly timescales; with a focus on the sublimation process. Through a set of laboratory and field experimental observations, we evaluate the effect of sublimation from the snow perspective.

In the controlled laboratory experiments, we find that the sublimation process affects the snow isotopic composition through fractionation during sublimation and show the consequential enrichment of heavy isotopes in the snowpack and an accompanying decrease in the snow's d-excess value (**RQ 3**, Figure 3.2). Although strongest at the surface, the sublimation signal affects underlying layers down to a depth of 2-3 cm, which can be explained by diffusion. Despite different experimental runs under varying temperature and dry-air flow conditions, we can not identify a dependency between rate of change in δ^{18}O and sublimation rate (**RQ 4**). However, the change in d-excess shows a strong dependency on sublimation rate. With this study, we contribute to the existing series of experimental studies about fractionation including sublimation by co-measuring, for the first time, the isotopic composition of the vapor in contact with the snow surface both in the laboratory and during the field experiments. In the intermediate experiment, with isolated snow samples under field conditions, we find the same enrichment behavior, albeit less extreme owing to less sublimation compared to the laboratory settings. Additional probing of the undisturbed snow surface showed both enrichment and depletion on hourly timescales, with a significant correlation between vapor and snow isotopic composition in three of four experiments (**RQ 4**). The results of our study demonstrate that the snow surface isotopic composition is variable on hourly timescales. A simple zero-order mass balance calculation concludes that the vapor-snow exchange process imprints on the seasonal snow isotopic signal, while there is a seasonal net sublimation flux.

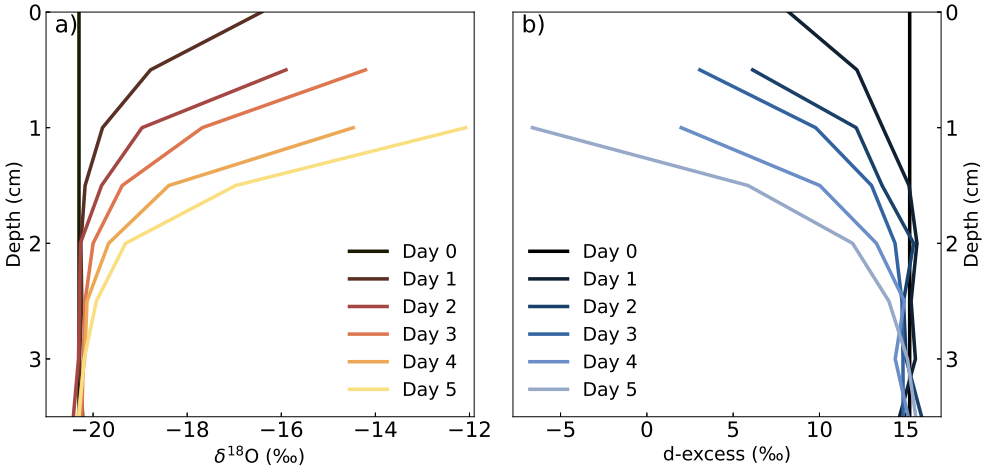

Figure 3.2: *Gradual, sublimation-induced isotopic enrichment (a) and decrease of d-excess (b) in snow samples from laboratory experiments (modified from Hughes et al., 2021).*

Paper III: **Challenging Old Axioms: Interpretations of Water Isotopes in Ice Cores**

***Sonja Wahl**, Hans Christian Steen-Larsen, Abigail Hughes, Laura J. Dietrich, Alexandra Zuhr, Melanie Behrens, Anne-Katrine Faber and Maria Hörhold (submitted to Nature Geoscience)*

Paper III studies the influence of vapor-snow isotope exchange on the temporal evolution of the surface snow isotopic composition that was observed during the summers of 2018 and 2019 at the EastGRIP location. Based on a mass balance approach, we set up a simple surface snow model to explore whether surface humidity fluxes can explain the observed temporal variability in the snow isotopic composition.
To exclude influences from snow drift or precipitation, we make use of the daily collected snow surface samples that were unaffected by snowfall and wind and model the evolution of the snow isotope signal in-between sampling events. We use the in-situ measured meteorological parameters to drive the model and benchmark the model's performance against observed day-to-day changes. By parameterizing sublimation in analogy to the CG-evaporation model, the snow model can explain 35% (52%) of the observed variability in the δ^{18}O (δD) signal (**RQ 5**). By contrast, when assuming equilibrium fractionation, the model's ability to capture the temporal variability is worse. When fractionation during sublimation is switched off, the R^2 value approaches zero. This result clearly shows that vapor-snow exchange is an important driver for the snow isotopic composition on short timescales (**RQ 6**). With a sensitivity analysis, we identify the most influential parameters determining the magnitude of the change in snow isotopic composition to be the net latent heat flux (defined by flux strength and duration), the vapor isotopic composition and the deviation from the latter to vapor in equilibrium with the snow (**RQ 4**). We further show that the impact of vapor-snow exchange on the snow isotopic composition is not constant throughout the observation period. Since the magnitude of sublimation effects is constrained by the vapor-snow isotope gradient and the humidity flux strength, a climate signal gets imprinted in the snow isotopic composition through the surface humidity flux. We hypothesize that surface fluxes could therefore be a process linking the climate and snow isotope signal by damping the influence of individual precipitation events on the seasonal isotope signal through a tendency to bring snow and vapor closer to equilibrium. This paper stresses the need for the implementation of a fractionation-including sublimation process in isotope-enabled climate and complex snow models.

Other scientific contributions

Paper A: An Unmanned Aerial Vehicle Sampling Platform for Atmospheric Water Vapor Isotopes in Polar Environments

Kevin S. Rozmiarek, Bruce H. Vaughn, Tyler R. Jones, Valerie Morris, William B. Skorski, Abigail G. Hughes, Jack Elston, ***Sonja Wahl****, Anne-Katrine Faber and Hans Christian Steen-Larsen, (2021), Atmospheric Measurement Techniques, (accepted)*

This paper presents a sampling technique for stable water isotopes from high altitudes, specifically designed for sampling across the atmospheric planetary boundary layer (PBL). Air is sampled into flasks mounted on an autonomous fixed-wing aircraft and afterwards analyzed for its water vapor isotopic composition using the established laser spectroscopy method. Six flights were performed at the EastGRIP location in summer 2019. The measurement precision was 0.45 ‰ (2.8 ‰) for δ^{18}O (δD) inferred from two flasks sampled at the same height. This method promises to generate important results in future field campaigns that will allow the analysis of the evolution of the PBL in the course of a day and the exchange processes across it, both of which are largely unconstrained processes in polar areas and above an ice sheet.

For this study, I contributed to the generation of reference vapor tower measurements and I assisted with test sampling in the field. I provided feedback on the analysis and the manuscript.

Paper B: Exploring the role of surface snow metamorphism on the isotopic composition of the surface snow at EastGRIP

Romilly Harris Stuart, Anne-Katrine Faber, ***Sonja Wahl****, Maria Hörhold, Sepp Kipfstuhl, Kristian Vasskog, Melanie Behrens, Alexandra Zuhr, and Hans Christian Steen-Larsen, (to be submitted to The Cryosphere)*

In this paper, snow metamorphism at the EastGRIP location is quantified and analyzed as possible driver for post-depositional changes in snow isotopic composition. With the help of daily snow samples, collected over the course of three summers (2017-2019), an empirical decay model is defined that describes the evolution of the snow's specific surface area (SSA), a measure for snow microstructure, after snowfall events. Prominent SSA decay events identify periods of strong snow metamorphism. In over 70% of prominent SSA decay events, snow metamorphism corresponds to decreases in the snow's d-excess value over a period of two days. During these periods, a net sublimation flux was measured. Further, it was identified by principal component analysis, that d-excess and SSA variability shows coherent structures during periods of low spatial variability in snow parameters. This suggests that the precipitation d-excess value is altered by processes driving surface snow metamorphism, i.e. firn diffusion, sublimation and deposition.

For this study, I took part in the snow surface sampling in the field and provided the processed latent heat flux data. In addition, I assisted in analyzing and interpreting the data and contributed to the manuscript.

Paper C: **Kinetic fractionation factors for ocean evaporation**

Daniele Zannoni, Hans Christian Steen-Larsen, Andrew J. Peters, ***Sonja Wahl****, Harald Sodemann, Árný E. Sveinbjörnsdóttir, (to be submitted to Science Advances)*

For this paper, ocean evaporation flux isotopic composition is calculated from six months of in-situ vapor isotope measurements from Bermuda in the northwest Atlantic. The data allows the deduction of the kinetic fractionation factor (k) involved in evaporation and an evaluation of its two-regime dependency on wind speed as proposed by *Brutsaert* (1975a,b) (Figure 1.6). The two-level gradient measurements are precise enough to calculate the evaporation flux' isotopic composition using a flux-gradient method. From these, mean values of $k_{^{18}O} = 5.2 \pm 0.6$ ‰ and $k_D = 4.3 \pm 3.4$ ‰ and an average ratio of $k_D/k_{^{18}O} = 0.83$ are inferred which agrees well with theory (*Merlivat and Jouzel*, 1979). The results showed to be highly sensitive to sea surface temperatures, with k_D being more sensitive due to the higher temperature dependency of the equilibrium fractionation factor. We find evidence for a dependency of fractionation factors on 10 m wind speed, albeit with low sensitivity of ~ -0.2 ‰ $\mathrm{m\,s^{-1}}$, yet the data suggest a monotonous decrease of k with wind speed, without a separation into two regimes.

For this study, I contributed to discussions regarding the calculations of the evaporation flux isotopic composition. Additionally, I provided edits to the manuscript.

4 Concluding Discussion

4.1 Synergy of the papers

This thesis explores the influence of vapor-snow isotope exchange on the climate signal imprinted in the snow isotopic composition in a holistic way: I used laboratory experiments and in-situ observations to test the influence of sublimation on the snow isotopic composition by studying both the humidity flux (**Paper I**) and the snow isotopic composition (**Paper II**). I further investigated the process understanding of post-depositional influences on the snow isotopic composition by setting up a simple, in-situ observation-driven snow surface model, using a mass balance approach (**Paper III**). Field observations of the evolution of the isotope signal in the surface snow were used to benchmark the model's performance. The three studies combined have demonstrated that sublimation from a snow surface involves fractionation and, together with deposition, causes changes in the snow isotopic composition throughout the summer. These post-depositional alterations of the snow isotopic composition therefore have the potential to imprint permanently on the climate signal in the snow. In the following, I will explore what consequences my findings have for the interpretation of ice core isotope records as paleoclimate proxies.

4.2 Perspectives

Climate signal recording in snow

The isotope signal in global precipitation is not governed by the local condensation temperature alone and is therefore not a proxy for local climate. Instead, it is the global mean temperature and the difference in evaporation to condensation temperature that define the initial vapor isotopic composition and the successive amount of rainout (*Johnsen et al.*, 1989; *Sodemann et al.*, 2008), and hence constrain the isotope signal of vapor, rain and snowfall. Changes in the isotope signal of snow or firn cores can therefore not merely be interpreted as local temperature signal but rather as regional climate signal. However, precipitation is an intermittent phenomenon and can therefore not record the climate continuously (*Persson et al.*, 2011). In contrast, the vapor isotopic composition is continuously modulated by both the local diurnal cycle signal and by regional synoptic-scale weather phenomena and seasonal temperature variations (*Bagheri Dastgerdi et al.*, 2021). Hence, the vapor isotopic composition is directly linked to regional climate and if there were an archive for water vapor isotopic composition, it would be a better climate archive than the precipitation archive found in ice cores.

Paper I and III suggest that vapor-snow exchange of stable water isotopes could be the link between snow and atmospheric vapor signal and could, given that fluxes are large enough, tie the snow isotopic composition tighter to ambient conditions. Specifically, the vapor signal gets imprinted by forming small amounts of frost and rime at the surface during deposition, which includes fractionation (*Casado et al.*, 2016). During sublimation, the *Craig and Gordon* (1965) (CG) formulation of the sublimation flux allows for an influence of the vapor on the sublimation flux isotopic composition. In this way, the climate signal in the vapor defines the sublimation flux isotopic composition and thus the magnitude of the change in the snow signal associated with sublimation. These processes seem to restore the snow-vapor equilibrium because, on average, the vapor is in thermodynamic equilibrium with the snow (Casado 2021,

Paper III). Supporting this, the results of **Paper I** show a sublimation flux isotopic signature that is, averaged over the season, close to vapor in equilibrium with the averaged snow surface. This could indicate the existence of a process that restores isotopic equilibrium after precipitation events when new air masses are advected. This process would need to be able to deplete or enrich the snow isotopic composition, depending on the disequilibrium between snow and vapor. The CG model assumes that fluxes of different isotope species can be described through their independent gradients and their ratio taken as the evaporation flux isotopic composition. If the CG model is suitable for sublimation conditions, we can, indeed, formulate a scenario in which the snow gets depleted during sublimation.

The influence of vapor isotopic composition on the change in snow isotopic composition during sublimation

The isotopic composition of the humidity flux is prescribed by the ratio of heavy to light water isotope flux, which is, in turn, constrained by the isotope specific gradient and the specific turbulent diffusion coefficient (Chapter 1, equation 1.7). Assuming the two isotope species are independent from each other, one can formulate some interesting theoretical perspectives. With regards to **RQ 4 & 5**, I use the *Merlivat and Jouzel* (1979) formulation of the CG model for thought experiments regarding the isotopic composition of the humidity flux. The CG humidity flux isotopic composition is influenced by the surface temperature (T_S), which influences equilibrium fractionation, and the prevalent sub-saturation which causes kinetic fractionation. However, a factor that is of fundamental importance, even for the sign of the flux isotope signal, is the deviation of the vapor isotopic composition from vapor in isotopic equilibrium with the snow. I will refer to this deviation as *disequilibrium*. Figure 4.1 shows the

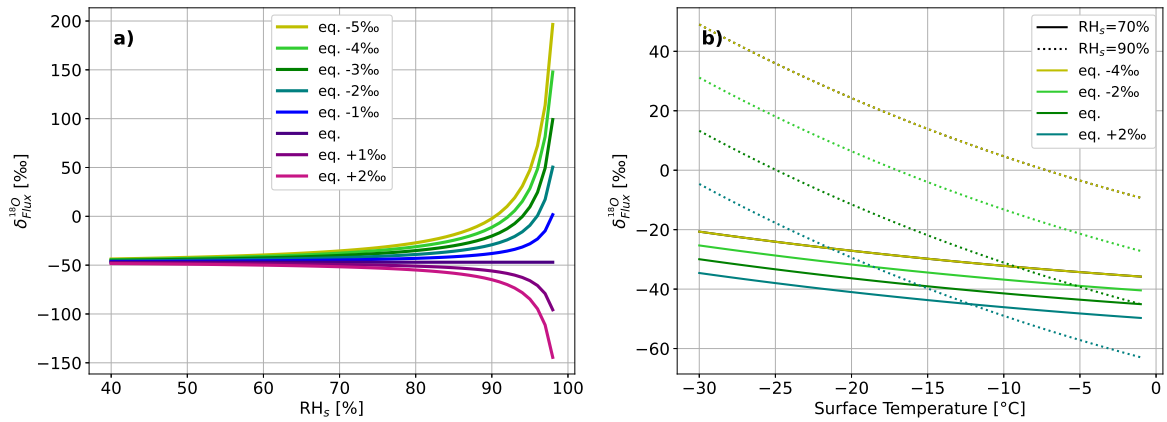

Figure 4.1: Influences on the isotopic composition of the evaporation flux
The flux isotopic composition dependency on disequilibrium and sub-saturation conditions in a) and on surface temperature in b). For a) the surface temperature is -12 °C. For both plots, the snow has a $\delta^{18}O$ value of -25‰ . Different colors represent varying deviation from vapor that is in equilibrium with the snow.

calculated δ^{18}O value of the humidity flux as a function of a) sub-saturation (RH_s) and b) surface temperature. As can be seen, the flux isotopic composition is highly sensitive to the disequilibrium. Similarly, *Benson et al.* (1994) discuss the highly variable humidity flux isotopic composition in the context of advected vapor mixing-in with local evaporated vapor from a lake surface. Analogies can be drawn from the lake setting to the ice sheet, where synoptic weather events can bring in significantly depleted or enriched vapor and therefore

create the disequilibrium (*Steen-Larsen et al.*, 2017; *Schlosser et al.*, 2010). An important difference between sublimation and evaporation conditions, however, is that mechanical and diffusive mixing in a liquid water body will counteract the evaporation effect at the surface relatively quickly, whereas mixing with lower layers is very slow in the solid snow matrix. This is why the influences of sublimation in the snow surface isotopic composition are visible. The disequilibrium in the vapor-snow system resulting from advected vapor with strongly anomalous isotope signature can lead to extreme values in the humidity flux isotopic composition. Under very depleted vapor conditions, this results in humidity fluxes that are more enriched in heavy water isotopes compared to the source (snow/water) isotopic composition. Under these conditions, relatively more heavy water isotopes are transported compared to a layer-by-layer removal and therefore the snow becomes depleted during sublimation. Following *Merlivat and Jouzel* (1979) (Chapter 1, Equation 1.8) and assuming a constant k of $k_{18_O} = 6.2\,‰$ and $k_D = 0.88 \cdot k_{18_O}$, the disequilibrium threshold can be calculated at which sublimation leads to isotopic depletion of the snow surface. This threshold is dependent on temperature, subsaturation and kinetic fractionation factors. As can be seen from Figure 4.2, weaker humidity gradients and warmer surface temperatures favor sublimation-depleting conditions.

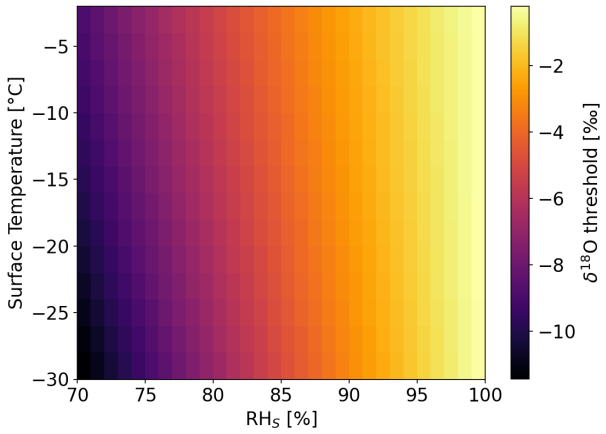

Figure 4.2: *The disequilibrium threshold at which sublimation causes isotopic depletion of the snow assuming $k_{18_O} = 6.2\,‰$ and $k_D = 0.88 \cdot k_{18_O}$. Ice-vapor equilibrium fractionation factors used from Ellehoj et al. (2013).*

To evaluate the rate of change in the snow isotopic composition expected from different disequilibrium conditions, one can calculate the effect of sublimation on a 5 cm snow layer using a simple mass balance approach, similar to the one used in **Paper III**. The rate of change observed in snow is dependent on the amount of mass that sublimates (**Paper II**). To combine the dependency of change in snow isotope signal on mass transfer and environmental conditions, the mass of snow removed is calculated from the humidity gradient (1-RH_s) and mean observation values of snow temperature, roughness length (z_0) and wind (u) using a flux-bulk formula. This way, implausible combinations of mass transfer and environmental conditions are ruled out. For average obser-

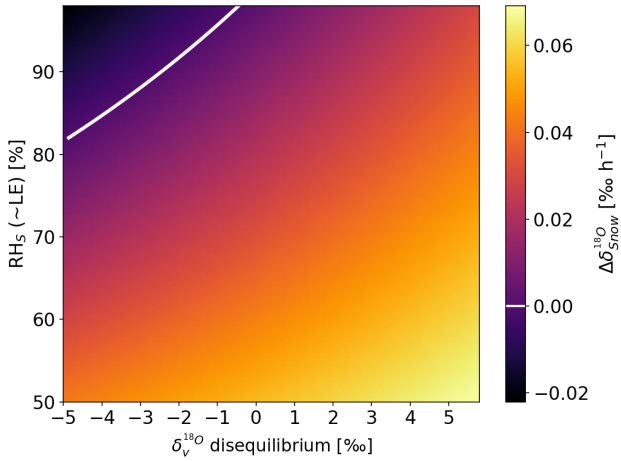

Figure 4.3: *Vapor-snow disequilibrium influences on the rate of change in $\delta^{18}O$ snow isotope signal ($\Delta\,\delta^{18}O$) assuming δ_S=-25‰ , T_S=-12 °C, u=4.5ms^{-1}, z_0=1.3e^{-4}m. The mass transfer rate (LE) is calculated from RH_s.*

vation values of T_S=-12 °C, u=4.5 m s^{-1} and median z_0=1.3·e^{-4} m, this leads to a latent heat flux (LE) of ~2.8 W m^{-2} and 0.6 W m^{-2} for RH_s values of 50 % and 90 %, respectively. Figure 4.3 shows the results of the calculations for a range of disequilibrium conditions. Depending on the disequilibrium between vapor isotopic composition and vapor in equilibrium with the snow, the flux and therefore the effect on the snow isotopic composition can vary greatly. The more enriched the vapor, the higher the enrichment in the snow. Even at equilibrium, the snow will become enriched owing to kinetic fractionation. It also becomes apparent, that under average environmental conditions, depletion during sublimation conditions are rare.

The comprehensive set of meteorological and isotopic observations at the EastGRIP location allows to investigate whether conditions favoring depletion during sublimation have been observed during the field campaigns. For mean daily sublimation conditions, the threshold for depletion during sublimation is not reached. However, the vapor was significantly depleted compared to equilibrium conditions in the period between 11th July 2019 and 26th July 2019, a pre-requisite for depleting conditions. To investigate sub-daily conditions, we make use of half-hourly meteorological data sets and, in the absence of high resolution samples, the daily snow surface samples, that were taken before noon. These sub-daily calculations show, that the sublimation-depletion threshold has been reached several times during late July 2019 (Figure 4.4). Supporting this theory, the snow surface samples show a gradual depletion during this period which could hint to combined depletion effects during sublimation and deposition conditions.

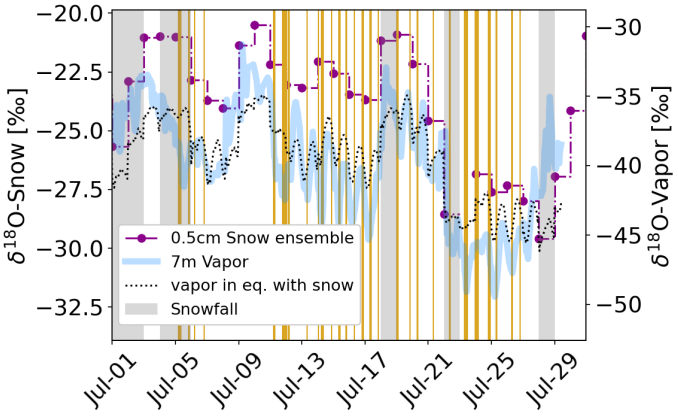

Figure 4.4: Observations of strongly depleted vapor compared to equilibrium vapor

Daily snow and hourly vapor isotopic composition during July 2019. Equilibrium vapor was calculated using ice-vapor equilibrium fractionation factors of Ellehoj et al. (2013) and observed snow surface temperatures. The orange lines indicate times at which the threshold for snow depletion during sublimation is passed.

Relevance of vapor-snow exchange for the ice core signal

The overarching question that arises from the findings of my thesis is: Is vapor-snow exchange important for the ice core isotope signal that is analyzed as climate proxy?
If so, how much of the precipitation input signal is overprinted by vapor-snow exchange and how does it influence climate reconstructions from ice core isotope records?
In the literature, arguments for both, noise or signal, can be found. *Stichler et al.* (2001) argues for ice cores from high alpine glaciers, that the influence of surface fluxes is negligible for the interpretation of ice core records, provided that the characteristics of surface fluxes do not change in time. *Münch et al.* (2017) states that post-depositional vapor-exchange processes are irrelevant for the firn isotope record. However, they focus on the signal formation phase after the snow is buried, i.e. phase (3b) after the influences of surface fluxes have ceased. In contrast, *Pang et al.* (2019) states that moisture recycling, including sublimation, may be potentially

influential for the AIS summer snow surface isotopic composition but that observations, of the kind presented in this thesis, are missing to draw further conclusions. A study by *Casado et al.* (2020) discusses vapor-snow exchange as both a possibly noise introducing mechanism due to spatial and temporal variability of surface fluxes or as a possibly noise reducing mechanism, if vapor-snow exchange significantly imprints a climate signal during times of precipitation absence, therefore bridging the intermittency gaps. Recently, *Casado et al.* (2021) identified summer snow metamorphism, induced by surface sublimation and condensation from sub-surface vapor, as an important contributor for the formation of Antarctic seasonal isotopic composition in two case studies by studying the second-order parameters d-excess and ^{17}O-excess. In their study, the authors implemented fractionation during sublimation and support it with **Paper I & II** of this thesis. The authors conclude that major post-depositional snow metamorphism events imprint on the snow to an extent, that the signal is conserved during ice formation. Interestingly, they conclude that post-depositional effects were not equally relevant for all observation periods studied. This indicates that lasting effects of post-depositional influences are highly dependent on the length of precipitation free periods in which the snow is in direct contact with the atmosphere. *Neumann et al.* (2008) further concludes that the humidity flux magnitude and its relative importance on the surface mass balance compared to accumulation is determining the effect of surfaces fluxes on the ice core record. This suggests that regions of high impact of vapor-snow surface exchange on the climate signal in snow can be identified by studying the humidity flux relevance to the surface mass balance and its net sign, i.e. net deposition or sublimation flux.

As straightforward as this might sound, estimating the contribution of the humidity flux to the surface mass balance is difficult to assess for the interior part of ice sheets. Local EC flux observations are sparse and flux-gradient measurements highly uncertain since they are sensitive to choices of scaling parameters like roughness lengths. As climate models likewise rely on the bulk flux-gradient method, modeled estimates of the surface flux contribution are equally uncertain. There are few existing literature estimates for the net humidity flux, as fluxes are generally assumed to be negligible for the surface mass balance in the interior of ice sheets (*Lenaerts et al.*, 2019). For the interior GrIS, a net annual deposition flux was estimated from observations by *Box and Steffen* (2001) and from a mass balance model by *Cullen et al.* (2014). Both studies calculate a net sublimation flux during the summer months, in agreement with observations from EastGRIP (**Paper I & III**). The latest unpublished work within the SNOWISO research group estimates, for EastGRIP, that up to ~30% of precipitated snowfall sublimates during the summer months. Such high values indicate that vapor-snow surface exchange is important for the summer snow signal. For the AIS, *Genthon et al.* (2017) estimates that the net surface humidity flux sublimates up to 10 % of the annual accumulation input at Dome C based on observations. A net sublimation flux is also reported in *Stearns and Weidner* (1993) for the South Pole area. Despite small net fluxes, the integrated mass turnover, i.e. sublimation and deposition in sum, might be the relevant parameter for estimating the imprint of vapor-snow exchange on the snow isotope signal, since the effects of deposition do not necessarily counteract the effects of sublimation. Based on spatially variable humidity flux balances on both ice sheets, as well as changing accumulation rates on longer timescales, it is reasonable to assume that the contribution of the humidity flux to the surface mass balance has not been constant in time. Consequentially, it can not be assumed that the impact of post-depositional vapor-snow exchange for the ice core isotope signal has been stable on ice core record time scales. To conclude, an in-depth evaluation of the extent to which the precipitation signal is overprinted by vapor-snow exchange requires a snow or climate model that is able to simulate both the precipitation isotope signal and the vapor-snow exchange signal.

4.3 Outlook

Future work

From the findings of my thesis, several follow-up work tasks emerge. First and foremost, my work stresses the necessity of implementing fractionation during sublimation from snow surfaces in isotope-enabled climate models. Given that 12.5 % of global land area is permanently covered with snow (*Bamber et al.*, 2018), this is critical for tracer studies. For this purpose, further experimental studies have to be conducted in order to identify the fractionation factors associated with sublimation and deposition. Hence, more in-situ observations of the humidity flux isotopic composition are necessary. As motivated in **Paper I**, the use of so called *flux-CRDS* with higher sampling frequency (*Chazette et al.*, 2021) could extend the applicability of the EC method for isotope fluxes to more stable conditions and likewise increase the database of humidity flux isotopic composition over snow surfaces. From such an extensive set of in-situ observed flux data, it should be possible to deduce the kinetic fractionation factor for sublimation as done in Paper C, and similarly for deposition. Alternatively, laboratory experiments similar to the experiments in **Paper II**, could be used to infer the kinetic fractionation coefficient for sublimation. If moist air with a known isotopic composition were pumped through the experimental chamber, one could draw direct comparisons to the CG model. Similar experiments have been conducted for the estimation of the kinetic fractionation factor for evaporation (*Kim and Lee*, 2011; *Cappa*, 2003; *Gonfiantini et al.*, 2020). The same set-up could be used to test the thought experiments of Chapter 4.2, i.e. to investigate if snow can get depleted of heavy isotopes during sublimation. For this experiment, very depleted vapor would need to be advected over enriched snow.

Climate model performance benchmarking with ice core isotope records

The ultimate goal for the ice core paleoclimatology community is an in-depth understanding of the signal formation process with all important drivers identified and parameterized. Besides vapor-snow exchange at the surface, this entails other processes such as snow metamorphism, snow ventilation and stratigraphic noise. By being able to simulate all processes constituting the transfer function between climate and snow signal, we could use climate models to simulate isotope records and compare them directly against snow, firn and ice core isotope records. Without the need for paleothermometer calibration functions, this would unlock past climate history in drilling places, where no instrumental measurements have been available and extend model validation periods back in time. A thorough signal formation understanding would further allow to reduce the signal-to-noise ratio in isotope records. As a consequence, natural climate variability could be studied in more detail by using existing high-resolution isotope records of the Holocene as well as records from future ice core drilling projects that promise Antarctic ice dating back one million years.

5 Scientific results

Paper I

Quantifying the Stable Water Isotopologue Exchange between Snow Surface and Lower Atmosphere by Direct Flux Measurements

Sonja Wahl, Hans Christian Steen-Larsen, Joachim Reuder, Maria Hörhold
Journal of Geophysical Research: Atmospheres, **126/13** (2021)

JGR Atmospheres

RESEARCH ARTICLE
10.1029/2020JD034400

Quantifying the Stable Water Isotopologue Exchange Between the Snow Surface and Lower Atmosphere by Direct Flux Measurements

S. Wahl[1], **H. C. Steen-Larsen**[1], **J. Reuder**[1], **and M. Hörhold**[2]

[1]Geophysical Institute and Bjerknes Centre for Climate Research, University of Bergen, Bergen, Norway, [2]Alfred-Wegener-Institut Helmholtz-Zentrum für Polar- und Meeresforschung, Bremerhaven, Germany

Key Points:

- Direct measurements of the stable water isotopologue fluxes between the snow surface and atmosphere
- Combination of eddy covariance method with cavity ring-down spectroscopy isotopologue measurements
- Isotopic composition of sublimation flux shows isotopic fractionation during sublimation

Supporting Information:

Supporting Information may be found in the online version of this article.

Correspondence to:

S. Wahl,
sonja.wahl@uib.no

Citation:

Wahl, S., Steen-Larsen, H. C., Reuder, J., & Hörhold, M. (2021). Quantifying the stable water isotopologue exchange between snow surface and lower atmosphere by direct flux measurements. *Journal of Geophysical Research: Atmospheres*, *126*, e2020JD034400. https://doi.org/10.1029/2020JD034400

Received 9 DEC 2020
Accepted 30 MAY 2021

Author Contributions:

Conceptualization: S. Wahl, H. C. Steen-Larsen
Data curation: S. Wahl, H. C. Steen-Larsen, M. Hörhold
Formal analysis: S. Wahl
Funding acquisition: H. C. Steen-Larsen
Investigation: S. Wahl, H. C. Steen-Larsen
Methodology: S. Wahl, H. C. Steen-Larsen, J. Reuder
Project Administration: H. C. Steen-Larsen
Resources: H. C. Steen-Larsen, M. Hörhold

Abstract Surface processes in high latitudes play an important role in global climate and thus understanding the physics of these systems is critical for improving climate projections. The characterization of the stable water isotopologue flux between the surface and the atmosphere offers the potential to constrain parameterizations of these physical surface exchange processes in numerical models. In addition, observations of isotopologue surface fluxes allow the evaluation of surface fluxes as a process influencing the formation of the climate signal retrieved from ice core isotopologue records. Here, we present a record of stable water isotopologue surface fluxes measured in-situ in the accumulation zone of the Greenland Ice Sheet at the East Greenland Ice Core Project site. We measured isotopologue fluxes above the snow surface directly by combining high-frequency eddy covariance measurements with low-frequency isotopologue measurements from a cavity ring-down spectrometer (CRDS). We developed a method to correct for the high-frequency loss of the CRDS by combining humidity measurements from both the CRDS and eddy covariance instruments. Using this approach our measurements provide the first direct observations of water isotopologue fluxes in polar areas. We observed a clear diurnal cycle in the fluxes of the different water isotopologues. The isotopic composition of the sublimation and deposition flux showed to be dependent on the snow and vapor isotopic composition, respectively. To a first order, the isotopic composition of the sublimation flux could be derived assuming equilibrium fractionation during sublimation.

Plain Language Summary Heavy water molecules behave differently than light water molecules during phase change processes. By measuring both, the heavy and light water concentration throughout the atmospheric water cycle, we gain a better understanding of the processes involved. Processes that are not well understood and therefore difficult to represent in climate models, are surface exchange processes in the polar areas. Including heavy water molecules as an additional parameter in climate models can improve our understanding of the water exchange between snow and atmosphere. In order to test model results, we need observations of the exchange of heavy and light water molecules between snow and air. We have therefore developed a method that allows us to measure the flux of heavy water molecules directly. To do so, we combined high-frequency wind and humidity measurements from a flux system, with slower laser spectroscopy heavy water measurements to obtain the flux. We correct for the losses in the high-frequency range of the slower instrument, by combining the humidity measurements of both the fast and the slow instruments. With this method, we observed that the heavy water flux follows the diurnal cycle, and that, on average, the snow surface defines the heavy water content in the sublimation flux.

1. Introduction

The turbulent humidity flux at the Earth's surface continuously exchanges water between the land and marine reservoirs to the atmosphere. On the global scale, sublimation and evaporation move up to half a million cubic kilometers of water per year (Bengtsson, 2010; Trenberth et al., 2007). This water vapor flux has important implications for the frozen reservoir of water in the form of ice sheets. The humidity flux influences the surface mass balance (SMB) of the ice sheet, both directly in the form of sublimation and deposition, and indirectly, as part of the local energy balance (Fausto et al., 2016; Lenaerts et al., 2019). Currently, the net water vapor flux between the snow surface and the atmosphere in the interior dry snow region of the

Supervision: H. C. Steen-Larsen
Validation: H. C. Steen-Larsen, J. Reuder
Visualization: S. Wahl
Writing – original draft: S. Wahl
Writing – review & editing: S. Wahl, H. C. Steen-Larsen, J. Reuder

Greenland Ice Sheet (GrIS) helps to maintain the total mass of the ice sheet (Box & Steffen, 2001; Lenaerts et al., 2019). In a warming climate, however, this contribution could change sign to a net mass loss, accelerating the ongoing shrinking of ice sheets (Cullen et al., 2014). Such future changes, influencing SMB and energy balance, can only be predicted by climate models and rely on an accurate parameterization of humidity fluxes. Recent studies indicate, however, that climate models seem to systematically underestimate turbulent surface fluxes over ice surfaces (Box & Steffen, 2001; Fettweis, 2007; Noël et al., 2015).

Stable isotopologues of water act as natural tracers within the water cycle and provide an independent constraint on the parameterization of the exchange between the snow surface and the atmosphere. Each time a water parcel undergoes a phase change process, its characteristic isotopic fingerprint is modified. The isotopic composition of a water parcel can therefore be interpreted as an integrated signal of its path in the water cycle (Galewsky et al., 2016). As a consequence, the isotopic composition of, for example, the atmospheric water vapor can be used as an observable quantity to evaluate isotopologue-enabled model performance (e.g., Gryazin et al., 2014; Steen-Larsen et al., 2017). In isotope-enabled models, the individual water isotopologues are simulated independently. This way, difficult to observe processes like atmospheric entrainment and other mixing processes can be constrained through observations of water isotopologues (e.g., Benetti et al., 2018; Benson et al., 1994). Using multiple isotopologue-enabled General Circulation Models, Steen-Larsen et al. (2017) documented biases in the simulated water vapor isotopic composition above the GrIS despite only small differences between the observed and simulated specific humidity. They argued that this could indicate that the models did not accurately capture the moisture sources for the vapor above the ice sheet and hence illustrated how water isotopologue observations provide additional information on the modeling of the atmospheric hydrological cycle.

To identify the relevant processes responsible for potential model biases using water isotopic composition, the logical next step is to investigate the fluxes connecting the reservoirs with respect to their isotopic fingerprint. Such model verification requires accurate in-situ observations of the water isotopologue fluxes between the surface and the atmosphere. Those can be obtained either indirectly, by the Flux-Gradient (FG) method (Yakir & Wang, 1996) or the Keeling-Plot (KP) method (Keeling, 1958), or directly, by eddy covariance (EC) measurements (Swinbank, 1951). Based on the typical time resolution of the measurement systems for stable water isotopologues in the order of seconds, the FG method would be the natural choice. Measurements of CO_2 and H_2O isotopologue fluxes using the FG method have been used to quantify ecosystem activity in areas with moderate humidity levels (Griffis et al., 2005; Lee et al., 2007, 2009; Welp et al., 2008). Good et al. (2014) and Wei et al. (2015) used the isotopic signal of the humidity flux to differentiate between evapo- and transpiration using the KP method. Both approaches are based on the assumption that turbulent fluxes can be interpreted as gradient induced diffusion and are the foundation for flux parameterizations in models. The quality of these flux estimates are based on measurements of high precision and assumptions of source and sink homogeneity and the absence of counter-gradient transport (Griffis et al., 2008). However, those bulk methods experience inherent shortcomings, in particular when it comes to polar areas, characterized by low atmospheric humidity content and predominantly stable conditions (Anderson & Neff, 2008). The established gradient-flux relationships are based on the Monin-Obukhov similarity theory (MOST), but the underlying assumptions for the use of this approach may be frequently violated under stable conditions (Grachev et al., 2013; Mahrt, 2008; Sorbjan & Grachev, 2010). This issue can be expected to become more severe with increasing atmospheric stability in the surface layer. In addition, the gradient measurement strategy requires simultaneous measurements at different levels, and thus, optimally two analyzers that have to be carefully calibrated and maintained to provide the corresponding measurements with sufficient precision.

To overcome the inherent drawbacks of the gradient dependent approaches, the EC method is often applied. The EC technique is widely accepted as a direct and robust method for measuring latent and sensible heat fluxes (e.g., Foken et al., 2012; Lee et al., 2005) and has previously also been used for measurements of trace gas exchange (e.g., Baldocchi, 2014; Wohlfahrt et al., 2009) and isotopologue fluxes (e.g., Braden-Behrens et al., 2019; Griffis et al., 2008, 2010). The EC method is based on the understanding of the eddy energy cascade which states that transport happens over a wide range of frequencies (Kolmogorov, 1991). This implies the demanding requirement of high precision and high temporal resolution measurements (Foken et al., 2012). Measurement systems, which do not meet the sampling requirements due to instrument

limitations and set-up, have to rely on cospectral frequency loss corrections to obtain accurate flux measurements (Moore, 1986). Depending on the system set-up, both high and low-frequency corrections, might be required. Such corrections of measured covariances can be done by applying empirically derived models (Kaimal et al., 1972), utilizing analytical approaches (Massman, 2000; Spank & Bernhofer, 2008) or using on-site reference measurements for comparison, as outlined by Ferrara et al. (2012).

To establish isotopologue-enabled climate models as tools to improve our understanding of climate dynamics and climate projections, they need to have accurate process parameterizations implemented. Expanding on the limited numbers of stable water isotopologue flux measurements and adding observations, especially in the polar areas, is therefore a necessity to contribute to isotopologue-enabled climate model advancement. Unfortunately, this adds the complications emanating from low humidity and low temperature polar environments to the inherent challenges of scalar flux measurements. Hence, there is a need for a robust method to obtain stable water isotopologue fluxes.

This study presents a method for measuring stable water isotopologue fluxes in polar areas by combining high-frequency EC measurements with ∼1 Hz water vapor isotopologue cavity ring down spectroscopy (CRDS) measurements. CRDS instruments have previously demonstrated a good performance of continuous, high precision in-situ water vapor isotopologue measurements in high latitude locations (Berkelhammer et al., 2016; Bonne et al., 2014; Casado et al., 2016; Steen-Larsen et al., 2013). To assure robust isotopologue flux estimates in such environments, a stringent quality control based on integrated one-sided cospectra (ogive) analysis is outlined. Measurements obtained with this method will help to improve the process of understanding throughout the water cycle, whenever isotopologues are exchanged. We demonstrate the use of this method by presenting stable water isotopologue flux measurements between the snow surface and the atmosphere at the *East Greenland Ice-Core Project* (EastGRIP) site in the summer of 2019. Our results show that the isotopic composition of the humidity flux is dependent on vapor and snow isotopic composition, and that fractionation processes take place during sublimation.

2. Data & Set-Up

2.1. Measurement Site

The measurement site was located at 75° 37′ 47′′ N, 35° 59′ 22′′ W in North-East Greenland at 2,700 m altitude on the GrIS. Measurements were conducted as part of the surface science division of the ongoing international deep ice core drilling project EastGRIP. Turbulent fluxes of heat, moisture, and water isotopologues were sampled continuously throughout the summer of 2019 from 25 May to 29 July. The local time (LT) corresponds to the UTC-2 timezone. Instruments for this study were installed on a tower in a dedicated clean snow area, with other camp and housing facilities downwind, to ensure undisturbed measurements (Figure 1).

Radiation and relative humidity data were obtained from a continuously operating automatic weather station (AWS) from the *Program for the Monitoring of the Greenland Ice Sheet* (PROMICE) (Ahlstrøm et al., 2008; Fausto & van As, 2019), installed roughly 1 km SE from the flux measurement site. The synoptic conditions throughout the measurement campaign were characterized by a prevailing and rather stable wind direction of 285°N ($\pm 1\,\sigma = 53°$), a mean 2 m air temperature of −9.9 °C (max = 1.3 °C, min = −25.4 °C), low average specific humidity of 1.9 g/kg (max = 4.7 g/kg, min = 0.4 g/kg) and a distinct diurnal cycle visible in all relevant meteorological parameters on clear sky days.

2.2. Instruments

The instrumentation on the measuring tower used for monitoring isotopologue fluxes directly, consisted of a combination of two instruments. An IRGASON 2-in-1 sonic anemometer and open-path mid-**I**nfra**R**ed absorption **G**as **A**nalyzer (IRGA) by Campbell Scientific measured high-frequency three-dimensional wind and humidity and an optical **C**avity **R**ing-**D**own laser absorption **S**pectrometer (CRDS), type L2140-i from Picarro measured stable water isotopologues in the vapor. The relative concentrations of naturally occurring stable water isotopologues $DH^{16}O$ (also D), $H_2^{18}O$ (also ^{18}O) and $H_2^{17}O$ were measured simultaneously

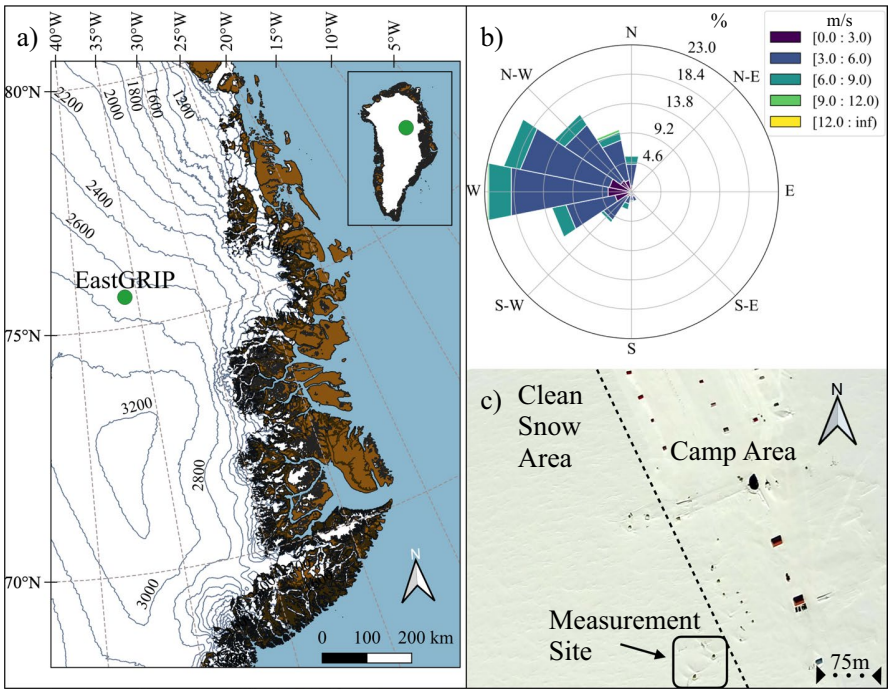

Figure 1. The location of the EastGRIP measurement site in the accumulation zone of the GrIS (a) and with respect to the surrounding camp (c). The tower was set up in a dedicated clean snow area away from camp in the direction of the prevailing wind (b). (Background picture in (c) taken 24.06.2017 at 300 m altitude, Credit: J. Box and A. Hubbard) (Data for map (a): I. M. Howat et al., 2014; I. Howat et al., 2015).

together with specific humidity by the CRDS. Specific humidity was reported in ppm_v. Since the rare and heavy water isotopologues occur in small amounts compared to the abundant species ($H_2^{16}O$), the rare species were reported in ‰ following the standard δ-notation after H. Craig (1961):

$$\delta^* = R^* / R^*_{VSMOW} - 1 \tag{1}$$

R^* is the ratio of concentrations between the rare(*) and abundant isotopologue and R^*_{VSMOW} is the ratio of the reference Vienna Standard Mean Ocean Water (VSMOW) (de Laeter et al., 2003).

The IRGA was installed at an initial measurement height of 2.15 m above the snow (2 m-level), facing the prevailing wind direction. There was no significant change in the snow height observed throughout the season and all calculations were made using the initial height throughout the campaign. The IRGA measured 3D-wind components $\vec{U} = (u, v, w)$ and absolute humidity ρ_w in the same measurement sample-volume. The CRDS inlet for vapor probing was mounted at 2.15 m, receiving the air sample just as it left the IRGA sampling volume with an offset of 10 cm in the prevailing wind direction (Figure 2). Three additional vapor inlets were installed on the tower at 0.47, 0.96, and 7.13 m height, referred to as the 0.5 m-, 1 m- and 7 m-level. The four inlets merged into one tube at the base of the tower using three three-way solenoid valves (EVT317-6DZ-02F-Q). From this junction, the air sample was pumped through a 15 m heated copper tube (OD: 1/4") using a KNF pump (N811 KN.18) with a flow rate of 10 L/min to the CRDS, which was kept in a tent at a constant temperature of 15° C. The overall measurement set-up is schematically presented in Figure 2.

2.3. Sampling Strategy

The IRGA measured wind, humidity, and sonic temperature continuously at a sampling frequency (f_s) of 20 Hz. The raw data were stored on a CR6 Campbell Scientific Datalogger and the data were monitored using the Campbell Scientific program *LoggerNet*.

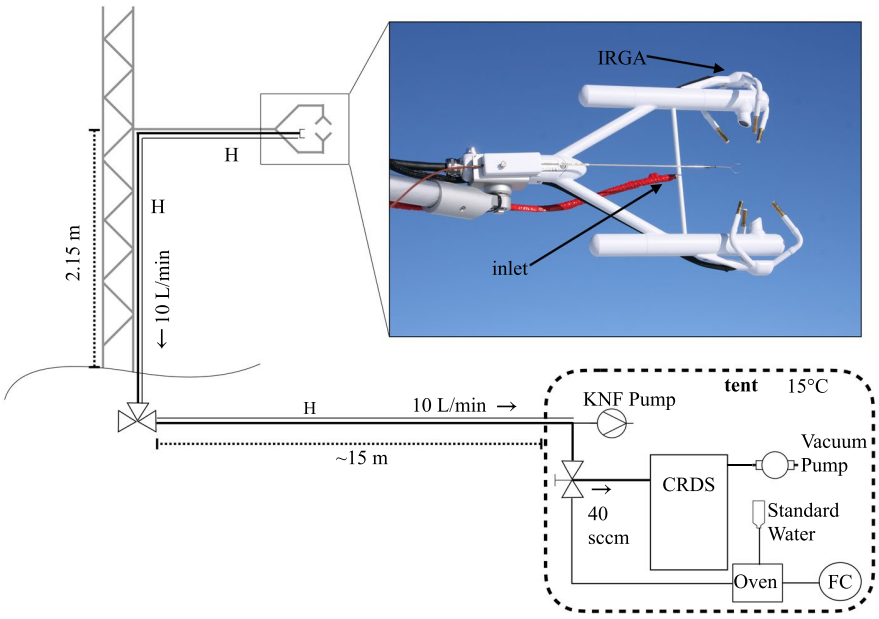

Figure 2. A schematic drawing of the system set-up comprising of the tower installations and the instrumentation inside the tent. Proportions are not to scale.

Vapor was pumped from four levels using the Picarro's valve sequencer software in a repeated one hour cycle of 10 min at levels 0.5, 1, and 7 m, and 30 min at the 2 m-level together with the IRGA high-frequency measurements. This resulted in a total of 1,350 30 min-periods for eddy covariance flux computation at the 2 m-level, hereafter called EC-periods. The CRDS ran in the ^{17}O-sampling-mode and vapor data of humidity and isotopologue concentration were generated at a f_s of ~1 Hz.

For comparison with the snow surface isotopic composition, half centimeter surface snow samples were sampled daily from 10 locations along a 100 m long transect. The samples were shipped frozen to the stable water isotope laboratory at Alfred-Wegener-Institut, Bremerhaven, Germany and analyzed on a CRDS as one consolidated sample following the Van Geldern and Barth (2012) measurement protocol.

2.4. Calibration and Uncertainty

The in-situ CRDS measurements of the isotopic composition of the vapor were calibrated against the VSMOW-SLAP scale using secondary laboratory standards fully spanning the range of observed water vapor isotopologue values provided by the Institute of Arctic and Alpine Research, University of Colorado (see Table S1). The CRDS instrument was calibrated once every day by providing a stream of vapor from individual standards using a custom made calibration system. As the CRDS instrument was observed to be very stable, the measurements were combined to one set of VSMOW-SLAP calibration curves for δ^{18}O and δD to reduce the influence of the measurement noise from the day-to-day standard measurements. To account for the expected humidity dependency on the isotopologue measurements, humidity-isotopologue response curve calibration runs were performed several times during the campaign to test for stability (Steen-Larsen et al., 2014). The humidity-isotopologue response curve was established by creating a stream of water vapor with a constant isotopic composition at different humidity levels (Steen-Larsen et al., 2013). No drift in the humidity-isotopologue response curve was observed during the campaign, but the humidity-isotopologue response curve was dependent on the isotopic composition of the individual standards as previously observed by Weng et al. (2020) (Figures S6–S9). Linear interpolation in the isotopologue space between the humidity-isotopologue response curves was applied to correct for this dependency. The uncertainties on the CRDS vapor isotopologue measurements were assumed to be 0.23 and 1.4‰ for δ^{18}O and δD, respectively and similar to that observed by Madsen et al. (2019) after Steen-Larsen et al. (2014).

To calibrate all available instruments for humidity, the AWS humidity data quality was tested and confirmed to be accurate by comparing the measurements with observations of an additional on-site CRDS analyzer. This analyzer had been calibrated against a custom made dew point generator spanning saturation vapor pressure levels from −40°C to 5°C. The average of the bias between the humidity measurements of these two was less than 0.001 g/kg for the specific humidity range of 0.4–1.6 g/kg. The bias in higher humidity conditions is assumed to be of the same order of magnitude. The AWS humidity measurements were then used as reference for CRDS and IRGA humidity post-season calibration.

Flux error computation required the specification of uncertainties of the individual parameters. The precision statements of the manufacturer for the IRGA were 0.006 mmol/mol on the humidity readings and 0.5 mm/s on the vertical velocity measurements. We defined the uncertainty of averaged vertical wind data to be the standard deviation of the mean over the averaging period.

The manufacturer does not give a precision value for the CRDS humidity readings, so the CRDS precision was estimated using controlled humidity calibration pulses. The obtained precision values for the isotopologues, as well as the humidity measurements, are conservative estimates of the actual instrument uncertainty, since the vapor stream, provided by the calibration system, was variable in itself. Furthermore, it is stated by the manufacturer, that the CRDS precision is humidity dependent. In agreement with this, we inferred a 0.2% uncertainty on the isotopologue as well as the humidity readings of the CRDS.

3. Flux Calculation Method

In the following section, we describe the protocol for calculating kinematic isotopologue fluxes (F_D^{kin} and $F_{18_O}^{kin}$) with units gm/(kgs) directly from the raw field data. An overview of the workflow is provided in Figure 3. The protocol for the humidity flux ($F_{q_{IRGA}}^{kin}$) follows established procedures as in Mauder et al. (2006).

3.1. Preconditioning of Data

All 1350 EC-periods, in which CRDS and IRGA measured at the same height, were evaluated for isotopologue flux calculations. Data of the first and last 2.5 min were excluded from the beginning and end of each EC-period to avoid influences from the valve switching and allow for synchronization between instruments. The CRDS data set was interpolated to homogeneous 1 Hz-frequency. Humidity and isotopologue concentrations were converted to mass mixing ratios (q_{CRDS}, q_{18_O}, q_D) with units g/kg. Absolute humidity measurements of the IRGA (ρ_w) were likewise converted into mass mixing ratio (q_{IRGA}). The 20 Hz IRGA data were despiked following the procedure of Schmid et al. (2000) and periods with more than 1% of missing data were excluded (319 EC-periods discarded). Individual 25 min wind data sets were rotated into the mean wind direction using the double-rotation method, setting the mean w and v wind vectors to zero ($\overline{w} = 0$, $\overline{v} = 0$). The despiked and rotated IRGA time series of w and q_{IRGA} were downsampled to averaged 1 s-resolution for isotopologue flux computation.

3.2. Humidity Flux Computation

The IRGA humidity flux ($F_{q_{IRGA}}^{kin}$) was calculated from the IRGA's mixing ratio and vertical wind data. Covariances ($\overline{w'q'_{IRGA}}$) were computed for a 25 min integration time (τ) after linear detrending. We evaluated shorter integration times, but found no significant improvement in the quality of the flux estimates. Integrated one-sided cospectra, called ogives (Og) (Desjardins et al., 1989), were computed from w and q_{IRGA} for all despiked EC-periods following:

$$Og_{q_{IRGA}}(f) = \int_{f=f_{Nyquist}}^{f=f_N} cospectrum_{w,q_{IRGA}}(f)\,df \tag{2}$$

with :

$$\begin{aligned} f_{Nyquist} &= 0.5\, f_s \\ f_N &= 1/(\tau.60) \end{aligned}$$

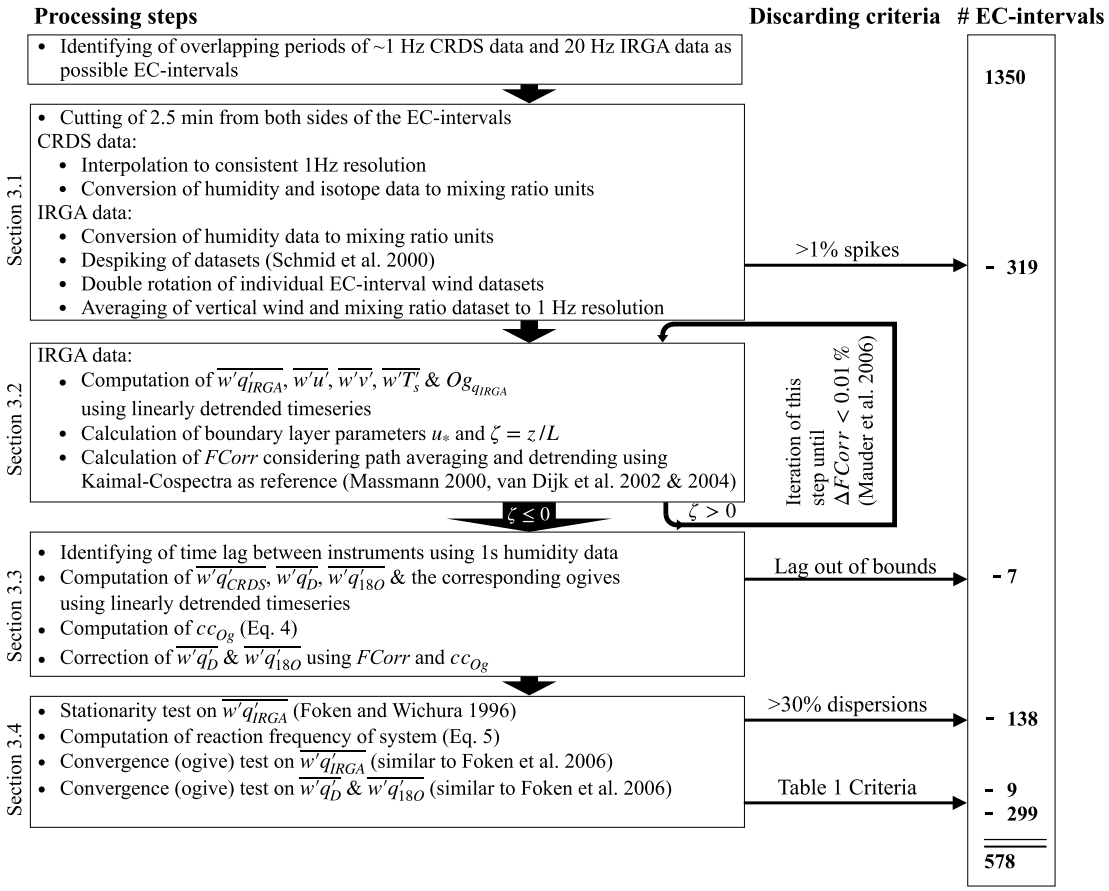

Figure 3. This workflow scheme presents a summary of the processing steps undertaken to generate quality controlled kinematic isotopologue fluxes from the raw field data. Details are given in the indicated subsections of the method section.

This presentation method of fluxes has two advantages. It illustrates how the total flux energy is distributed over the frequency range and it provides a method for evaluating the quality of the flux estimate with a given τ (Foken et al., 2006). The endpoint of the ogive (i.e., the value at lowest frequency f_N) is equal to the covariance $\overline{w'q'_{IRGA}}$ with units in g m/(kg s) (Mann & Lenschow, 1994).

$$\overline{w'q'_{IRGA}} = Og_{q_{IRGA}}(f_N) \tag{3}$$

Frequency corrections applied to $\overline{w'q'_{IRGA}}$ comprised of low-frequency-loss corrections originating from linear detrending and high-frequency loss corrections due to path-averaging (Massman, 2000; Van Dijk, 2002; van Dijk et al., 2004). Webb-Pearman-Leuning corrections due to buoyancy effects (Webb et al., 1980) were not necessary, since fluxes were computed from the mixing ratio data directly (Businger, 1986). We used the established cospectral models of Kaimal et al. (1972) (Co_{Kaimal}) for estimating the total frequency correction transfer function (TF) and calculated kinematic humidity fluxes ($F^{kin}_{q_{IRGA}}$) with the resulting frequency correction factor ($FCorr$):

$$F^{kin}_{q_{IRGA}} = \overline{w'q'_{IRGA}}^{*} FCorr = \overline{w'q'_{IRGA}}^{*} \left[\frac{\int_{10^{-6}}^{10^{4}} Co_{Kaimal}(f)df}{\int_{10^{-6}}^{10^{4}} TF(f) Co_{Kaimal}(f)df} \right]. \tag{4}$$

3.3. Isotopologue Flux Computation

Due to the lower sampling resolution of the CRDS and likely additional tube attenuation effects, frequency corrections of covariances, computed from CRDS, were necessary. In this context, the kinematic humidity flux of the IRGA and its ogive is considered to represent the total humidity flux of each EC-period. It is used to compute the correction coefficient (cc_{Og}) to correct calculated isotopologue fluxes. The IRGA humidity flux measurements themselves could be verified by good agreement with two other independent on-site EC-systems operated during the field campaign.

To account for expected lag times between the IRGA and CRDS data, 1s - q_{IRGA} and q_{CRDS} were lag time-cross-correlated. The identified lag showed to be nonuniform in time throughout the season (Figure S1), which was due to a drift in time of the CRDS software system. Hence, respective lag times yielding maximum correlation between 1 s-q_{IRGA} and q_{CRDS} time series were used to shift the CRDS data accordingly. EC-periods with lag times exceeding the values within the observed trend were excluded (7 EC-periods discarded).

$\overline{w'q'_{CRDS}}$, $\overline{w'q'_{D}}$, $\overline{w'q'_{18_O}}$ and corresponding ogives were calculated using the 1 s vertical wind data from the IRGA. The ratio between the end values of the humidity IRGA and CRDS ogives yields the cc_{Og} as:

$$cc_{Og} = \frac{Og_{q_{IRGA}}(f_N)}{Og_{q_{CRDS}}(f_N)} \tag{5}$$

All covariances computed from the CRDS data were corrected with the interval-specific cc_{Og}. Finally, the frequency correction factor ($FCorr$) established for the humidity flux, was likewise applied to the CRDS isotopologue fluxes.

Knowing both, the total humidity and the isotopologue flux, one can calculate the isotopic composition of the humidity flux (δ_F) as,

$$R_F^* = F_{q*}^{kin} \; / \; F_{q_{IRGA}}^{kin} \tag{6}$$

which can be converted to δ-notation as introduced in Equation 1.

3.4. Alternative Methods to Calculate Isotopic Composition of the Humidity Flux

In order to compare our estimates of the isotopic composition of the humidity flux with estimates from methods like the Keeling-Plot or Flux-Gradient approach, we recalculate δ_F with information from all four levels of the measurement tower. It is important to notice that neither of those two methods as presented below is suitable to estimate total isotopologue surface fluxes.

3.4.1. Flux-Gradient Method

For the FG approach, we made use of the 0.5 m-, 1 m- and 7 m-level 10 min measurements (Section 2.3) together with the 2 m measurements that were used in the EC calculations. Averages were computed for the three 10 min levels cutting the first 3 min after each valve switch, resulting in one measurement point at each level per hour. Likewise, 3 min were cut from the beginning of the 2 m measurement period. The remaining data were split into three subsets and averaged, yielding three sample points per hour at the 2 m- level. Subsequently, measurements at each level were linearly interpolated to the mid-point of each EC-period. Assuming equal turbulent diffusivities for all three isotopologues, the isotopic composition of the humidity flux can then be calculated from the ratio of heavy isotopologue gradient to light isotopologue gradient. Making use of information from all four levels, we calculated $R_F^*(FG)$ as slope of the linear regression of q_{CRDS} at each level against q_* at each level using the following relationship (Good et al., 2012):

$$q_* = c_{FG} + R_F^*(FG) \cdot q_{CRDS} \tag{7}$$

Table 1
Criteria for Flux Estimation Quality Based on $\overline{w'D'}$-Ogive Shape

Flag	Quality	$\lvert m_{norm}\rvert$	$\lvert RMSE_{norm}\rvert$	# EC-periods
*QC*1	accepted	< 0.1	< 0.1	371
*QC*2	accepted	$0.1 < m_{norm} < 0.2$	< 0.1	207
*QC*3	discarded	$0.2 <$	any	242
*QC*3	discarded	any	$0.1 <$	57

Again, $R_F^*(FG)$ was converted to $\delta_F^*(FG)$ using Equation 1. The standard error of the regression slope was taken as the uncertainty estimate for the $\delta_F\left(\mathrm{FG}\right)$ value.

3.4.2. Keeling-Plot Method

For the KP estimates of δ_F, we assumed a steady-state within each EC-period and the half hour that followed. We averaged the last 5 min of each level yielding four measurement points in 35 min. The KP approach is essentially a two end-member mixing model with one mixing source being the free atmosphere and the other mixing source being the humidity flux coming from the ground. Measurements at several levels in the atmospheric boundary layer then fall on the mixing line of those end-members. Consequently, and without knowing the actual value of the free atmosphere, we can estimate $\delta_F^*(KP)$ by linear regression. Therefore, we establish the linear relationship between the reciprocal of q_{CRDS} and $\delta*$ and extrapolate to $q_{CRDS}^{-1} = 0$ which is the unknown $\delta_F^*(KP)$ following:

$$\delta^* = \delta_F^*(KP) + m_{KP} \cdot q_{CRDS}^{-1} \tag{8}$$

The standard error of the regression intercept was taken as uncertainty estimate for the $\delta_F\left(\mathrm{KP}\right)$ value.

3.5. Quality Assurance–Correction Coefficient Analysis

Calculation of fluxes using the EC method requires the check for compliance with the eddy covariance flux theory. The most important assumptions underlying the EC theory are homogeneity of the terrain, the absence of divergence or convergence and stationarity within the integration period (Foken & Wichura, 1996). Our measurement site satisfied the first two requirements, being a vast, open and homogeneous flat surface in the direction of the wind. Stationarity within the τ was assured through the IRGA mixing ratio covariance ($\overline{w'q'_{IRGA}}$) dispersion of <30% following Foken and Wichura (1996), and periods with higher divergence were discarded (138 EC-periods discarded). Furthermore, we investigated possible measurement errors introduced by the measuring system by performing an extensive ogive analysis:

First, CRDS-ogives of all three isotopologues were tested for their minimum responding frequency (f_{res}) and the difference between the f_{qCRDS}^{res} and f_{qD}^{res} or $f_{q18_O}^{res}$ was computed. f_{res} was defined as:

$$f_*^{res} = 0.1 \cdot \overline{w'q'_*}_{norm} \tag{9}$$

where $*_{norm}$ denotes any normalized covariance from the CRDS. This was done to assure that cc_{Og} can be used to correct fluxes of all three isotopologues.

Second, convergence analysis was performed on the ogives of the q_{IRGA}-flux and the q_D-flux as representative for the CRDS fluxes, following a similar approach as Foken et al. (2006). In contrast to continuous EC measurements at one height, our intermittent data set could not satisfy the originally proposed evaluation criteria, since a maximum analysis period of six times τ would be required. Hence, a quality criterion based on the ogive shape was developed. For an adequate τ, the ogive of a flux measurement will converge. Consequently, if a log-linear fit through the low-frequency end of the ogive had a slope close to zero, that is, it converged, and this EC-period was accepted. The fit was calculated for ogive values with frequencies $<4.5 * 10^{-3}$ Hz using the least squares method. Ogives were characterized according to absolute values of the normalized slope (m_{norm}) and normalized root mean square error ($RMSE_{norm}$) of the fit as defined in Table 1. EC-periods with nonconvergent q_{IRGA}-ogives were excluded from further flux calculation (9 EC-periods discarded). The $\overline{w'D'}$-ogives were classified as defined in Table 1. In *QC*2 EC-periods, the absolute value of the computed fluxes was slightly underestimated, as the ogive either had not reached its asymptote yet or had passed the extreme value already.

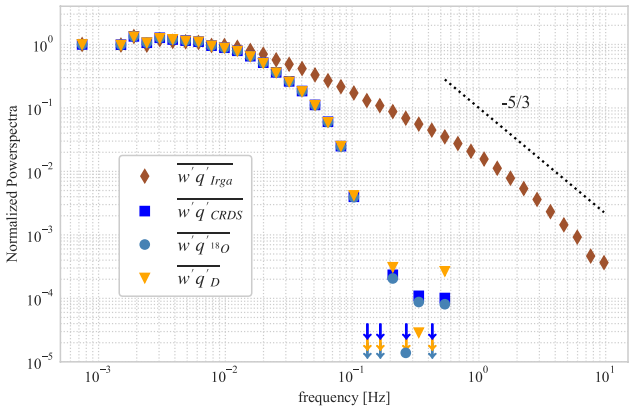

Figure 4. Spectral density analysis of the IRGA humidity covariance ($\overline{w'q'_{Irga}}$) together with the powerspectra of the CRDS covariances ($\overline{w'q'_{CRDS}}$, $\overline{w'q'_{18_O}}$, $\overline{w'q'_D}$). Normalized powerspectra were computed from all 578 accepted 25 min EC-periods and were bin averaged using 10 logarithmically spaced intervals per decade. $\overline{w'q'_{Irga}}$ was calculated from the 20 Hz time series, whereas the others were computed from the 1 Hz time series of the CRDS. The expected slope of the inertial subrange is shown as a black dotted line. The negative values of the averaged CRDS spectra (noise influences) are indicated as arrows.

3.6. Isotopologue Flux Error Estimation

Conventionally, errors on EC flux measurements are either inferred from multiple instruments measuring the same flux or measuring during similar conditions, that is, comparing several days (Good et al., 2012). A more statistical approach was developed by Mann and Lenschow (1994) (ML) in which the integral length scale (τ_f) and the correlation coefficient (r) between the time series of the vertical wind (w) and the scalar of interest (s) are considered. τ_f can be estimated by the ratio of measurement height to averaged wind speed within the τ. The standard deviation of the flux estimation after ML then reads:

$$\sigma_{ML}(\overline{w's'}) = \left|\overline{w's'}\right| \sqrt{\frac{2\tau_f}{N}} \sqrt{\frac{1+r^2}{r^2}} \tag{10}$$

with N being the number of samples in τ and $r = \overline{w's'} / (\sigma_w \sigma_s)$. Finkelstein and Sims (2001) (FS) estimated the error on the flux obtained from EC measurements by calculating the variance of the covariance. Following this approach and adopting the notation from Fuller (1976), the standard deviation of the covariance between w and s is defined as:

$$\sigma_{FS}(\overline{w's'}) = \sqrt{\frac{1}{N} \sum_{p=-m}^{m} \left(\overline{w'w'_p} \cdot \overline{s's'_p} + \overline{w's'_p} \cdot \overline{s'w'_p} \right)} \tag{11}$$

where the time lag (p) is defined by $m = N/2$ and is added to either w or s in the auto-($\overline{w'w'}$ / $\overline{s's'}$) and cross-($\overline{w's'}$ / $\overline{s'w'}$) covariances. For comparison, we calculated the relative error on the isotopologue flux values using both Equations 10 and 11. Since the calculated isotopologue fluxes are corrected using observed differences in humidity ogives between the two instruments (cc_{Og}), the final flux isotopic value is essentially a product of three individually computed covariances. We therefore propagated the relative errors on the individual covariances, assuming they are not independent, to yield a final error estimation of the corrected isotopologue flux. However, this method produced rather high uncertainties that originate mainly from the uncertainty of the correction coefficient.

In order to differentiate errors stemming from instrument noise and sampling errors of the covariances (Businger, 1986), we set up an empirical error estimation using the Monte Carlo (MC) method. We carried out 1000 MC simulations for each EC-period that passed the quality control by adding random normally distributed noise based on the precision estimations of the respective instrument on the individual time series. The error on the final isotopologue flux value due to instrument noise was obtained from the standard deviation of the MC generated distributions. All three approaches were used to compute a relative error of the final isotopologue flux measurements and to separate instrument noise from stochastic (sampling) noise.

4. Results

4.1. Measuring System Characteristics

We evaluated whether our sampling set-up resulted in unequal sampling of different water isotopologues due to potential tubing effects. For this, the minimum responding frequency (f_{res}, Equation 9), defining the noise and signal range, was calculated. The differences in minimum responding frequency between the total humidity and the heavy isotopologues were evenly centered around zero (Figure S2). No systematic bias between the different water isotopologues was observed and the distribution around zero indicated randomness. Based on this analysis, we concluded that the isotopologues were not affected differently by the system. Hence, all measured isotopologue fluxes for a given interval could be corrected accurately with the calculated cc_{Og} of this interval.

The equal treatment of different isotopologues was further supported by spectral density analysis of the individual isotopologue flux time series. Figure 4 shows no apparent difference in the averaged powerspectra

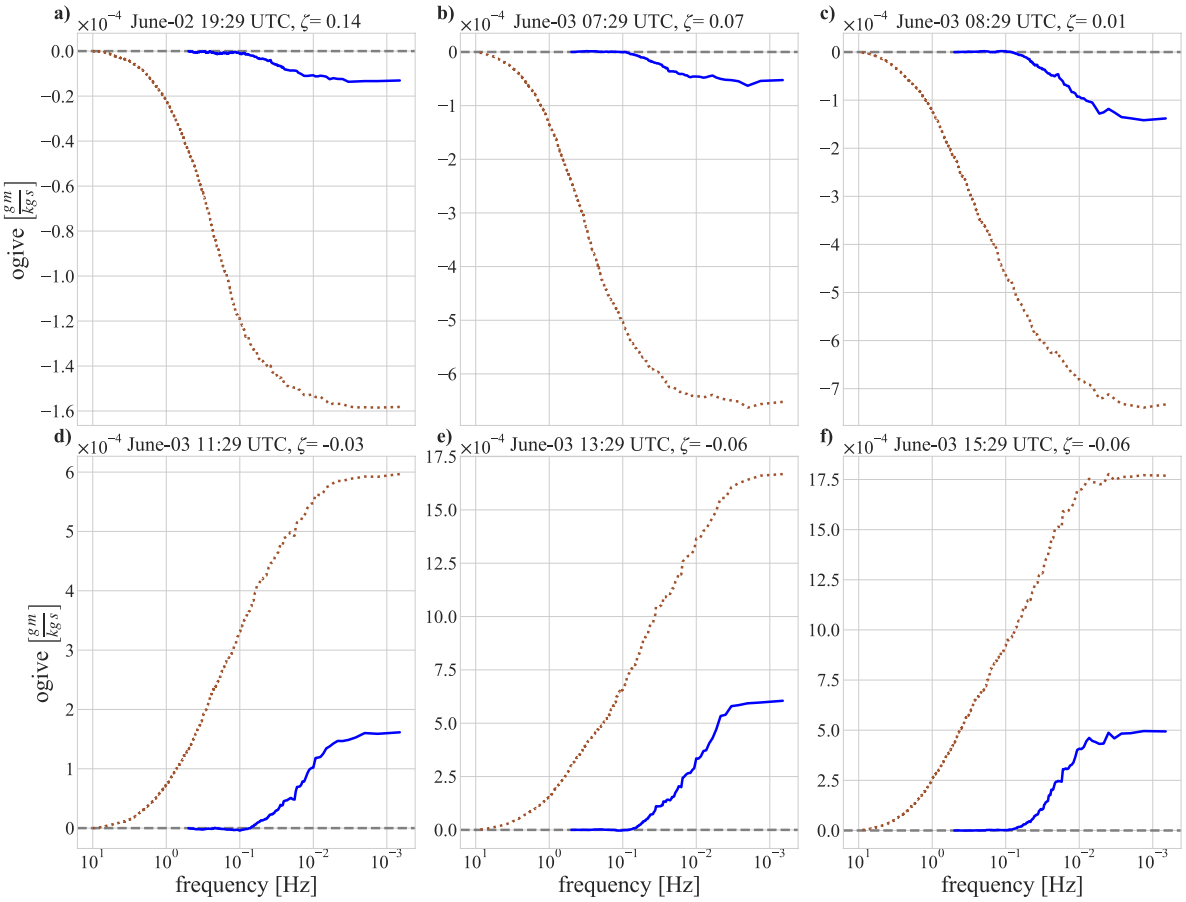

Figure 5. Exemplary 25 min ogives of mixing ratio humidity covariances $\overline{w'q'_*}$ for negative nighttime fluxes (upper row: a,b,c) and positive daytime fluxes (lower row: d,e,f). The atmospheric stability parameter ζ is given for each period. The IRGA ogives ($Og_{w,q_{IRGA}}$, brown dotted curves) were calculated from the 20 Hz time series and the CRDS ogives ($Og_{w,q_{CRDS}}$, blue solid curves) from the downsampled 1 Hz vertical wind and CRDS mixing ratio time series. The ratio of the end values yield the ogive correction coefficient for the specific EC-period.

of the individual water isotopologues measured with the CRDS. The averaged IRGA powerspectrum follows the expected slope for the inertial subrange. In contrast, the averaged CRDS isotopologue powerspectra show a dampening at high frequencies and a minimum responding frequency of ~0.1 Hz, with higher frequencies being influenced by noise.

4.2. Ogive Correction Coefficient

For obtaining the cc_{Og}, the humidity mixing ratio ogives of CRDS and IRGA of each individual EC-period were compared and evaluated according to Equation 5. The value of cc_{Og} is directly linked to the shape of the ogives in the respective EC-period, and therefore the atmospheric stability. To demonstrate this dependency, ogives of example EC-periods are shown in Figure 5. The ogives of the CRDS humidity flux only start increasing at a frequency of ~0.1 Hz, which corresponds to the signal-noise threshold as observed in Figure 4. In contrast, the ogives of the IRGA, being an open-path instrument and measuring at a higher frequency, start increasing at a frequency of ~5 Hz.

4.2.1. Dependency on the Atmospheric Stability and Friction Velocity

Turbulence is created by the interplay of two influencing mechanisms: buoyancy and wind shear. The two corresponding key variables are the buoyancy flux ($\overline{w'T'}$) and the friction velocity (u_*). The friction velocity is always reinforcing a turbulent transport and increases with increasing wind speed. Depending on the

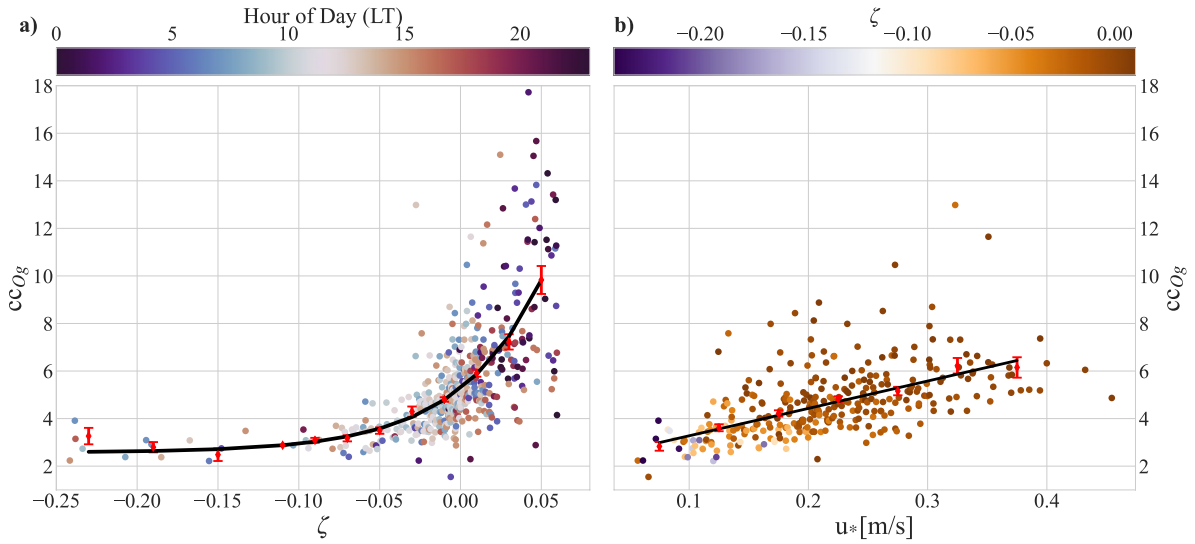

Figure 6. The cc_{Og} dependency on the stability in (a) and on the friction velocity in (b). In (a), the individual cc_{Og}-values are color coded by the local hour of the day, whereas they are color coded by the stability in (b). Red markers are bin-averaged values with the corresponding mean standard error. Regression curves are fitted to the binned values, using the minimum least squares method. Periods of very stable conditions ($\zeta > 0.06$) were excluded in (a) and periods with $\zeta > 0.01$ were excluded in (b). Figures S3 and S4 in the supplementary material show the same analysis including all available EC-periods and the dependency on wind speed, respectively.

sign of $\overline{w'T'}$, buoyancy can enforce or counteract turbulence. The ratio of shear and buoyant turbulent forcing is defined as the Monin-Obukhov length L as developed by Obukhov (1946). Taking into account the measurement height $z = 2.15$ m, the atmospheric stability can then be described by the stability parameter $\zeta = z/L$. Unstable and stable atmospheric conditions are characterized by a negative or a positive stability parameter, respectively.

We used the accepted EC-periods (Table 1) to investigate the dependency of our method's correction coefficient (cc_{Og}) on ζ and u_*. We limited our analysis to a stability range of $-0.3 < \zeta < 0.06$, which includes weakly stable regimes but excludes very stable conditions of $\zeta > 0.06$ (Mahrt, 1998). We concentrate on this stability range, as transport in very stable conditions is likely not predominantly governed by the two turbulence parameters ζ and u_* as further discussed in section 5.1.1. To analyze the dependency of cc_{Og} on u_*, we analyze the stability range of $-0.3 < \zeta < 0.01$, as the stability influence would otherwise mask the friction velocity dependency. The reader is referred to the supporting information to see the same analysis including very stable conditions and the dependency on wind speed (Figures S3 and S4).

The cc_{Og} was found to increase exponentially with increasing stability as shown in Figure 6a). When focusing on the near-neutral and unstable regimes ($-0.3 < \zeta < 0.01$), a dependency of cc_{Og} on the friction velocity becomes apparent. Values of cc_{Og} increased linearly with the friction velocity (Figure 6b).

4.3. Quality of Data

During the analysis of the low-frequency shape of the $\overline{w'D'}$-ogives (Section 3.5) 578 of the evaluated EC-periods were accepted; 371 as $QC1$ and 207 as $QC2$ (Table 1). A dependency on stability was observed. In stable conditions, the measured $\overline{w'D'}$-ogives did not develop a pronounced S-shape which would indicate that both, the high and low frequency fluctuations were appropriately covered by the chosen averaging period and the instrument sampling frequency. Therefore, those ogives had small end values close to zero resulting in corresponding high cc_{Og} values. Using the quality criteria, the majority of all discarded ($QC3$) $\overline{w'D'}$-ogives (#298) fall in stable atmospheric conditions (#257) and about half in the very stable conditions $\zeta > 0.06$ (#159) (Figure S5). In addition, the flux error analysis showed highest error values during the stable regime (Section 4.4) which is discussed in section 5.2.

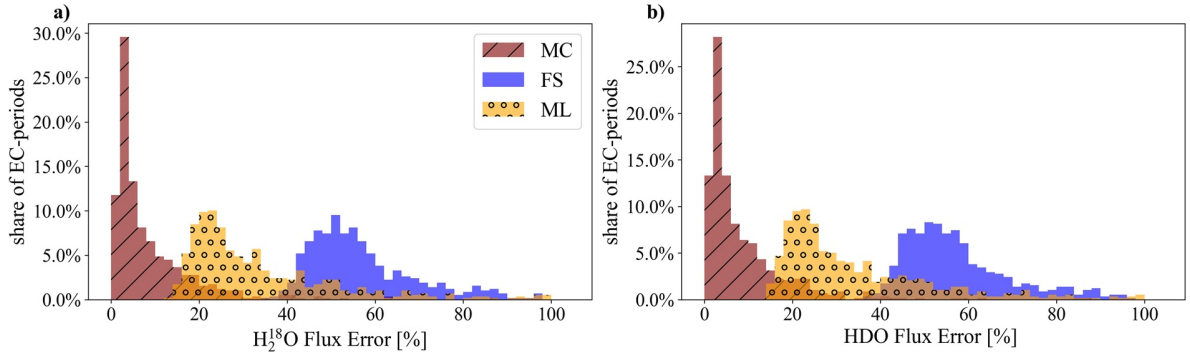

Figure 7. The relative error distributions of final isotopologue flux values calculated with three different approaches: FS (Equation 11), ML (Equation 10), and MC (Monte Carlo). Corrected $H_2{}^{18}O$ flux error estimations are given in (a) and errors of corrected HDO fluxes in (b). For all three methods, values > 100% were excluded (MC: 2.2%, ML: 3.9%, FS: 5.7%).

4.4. Flux Error Analysis

The three different error calculation methods resulted in three clearly separated distributions for the relative error of the final isotopologue flux values (Figure 7). All three error distributions are skewed to the right but their median is located at different values for the error sum of 5%, 29%, and 56% for the MC, ML, and FS approach, respectively. Generally, high relative error values of the ML and MC methods could predominantly be associated with a stably stratified atmosphere and low absolute flux values, whereas values from the FS method could not readily be assigned to one regime only. The errors obtained from the MC method were an order of magnitude smaller than the errors calculated by the FS method. This was to be expected, as the MC approach only takes into account instrument noise and omits stochastic error contributions, that is, the number of independent observations. Both the ML and FS method are estimates of the total uncertainty of the flux measurements.

4.5. Computed Isotopologue Flux Values

Three clear sky periods (one each in May, June, and July) were chosen to demonstrate and compare the behavior of isotopologue surface fluxes during ideal summer conditions in the interior of the GrIS (Figure 8). In all three periods, the averaged net latent heat flux (*LE*, Figure 8c) was slightly positive, that is, sublimation outweighed deposition and the humidity flux contributed negatively to the surface mass balance. Likewise, the net surface flux of isotopologues was directed away from the surface and the snowpack lost heavy isotopologues to the atmosphere through sublimation. In general, the isotopologue fluxes co-varied with *LE*. Between May and June, the amplitude of the ^{18}O-isotopologue surface flux increased from an averaged daily maximum value of 0.5 10^{-5} g/kg to 1.5 10^{-5} g/kg (Figure 8a). The measured D-isotopologue flux was of an order of magnitude smaller than the measured ^{18}O-isotopologue flux but showed the same pattern (Figure 8b). This increase in mass exchange was also observed in the sublimation rate (calculated from *LE* assuming a latent heat of sublimation of 2.834 10^6 J/kg) with averaged net daily values during the June period (0.14 mm water equivalent [w.eq.]) being five times larger compared to the averaged 0.03 mm w.eq. that sublimated during the May period. During July, the net sublimation rate decreased again to 0.08 mm w.eq. The mass exchange increase between May and June is accompanied by higher temperatures (Figure 8e) and increasing humidity. Absolute humidity observations (not shown) recorded an increase in water vapor content throughout the season from values of around 1 g/m^3 in May to 3 g/m^3 in July. The air temperature and relative humidity were near inversely proportional and on diurnal time scales driven by the net radiation (Figure 8h). Consequently, and characteristic for polar areas, the air had a general high relative humidity level (mean: 86%) despite the low absolute humidity. Saturation (with respect to ice) was repeatedly reached during night time hours in the May period. However, it was not reached in the June period and only registered around local midnight for the July period, resulting in longer periods of sublimation conditions (Figure 8f). A weak diurnal cycle signal in the wind speed was observed but no considerable change in wind conditions between the three periods was recorded (Figure 8g). In all three periods, the average net sensible heat flux (*H*, Figure 8d) was negative, indicating a gradual warming of the snowpack over the season which

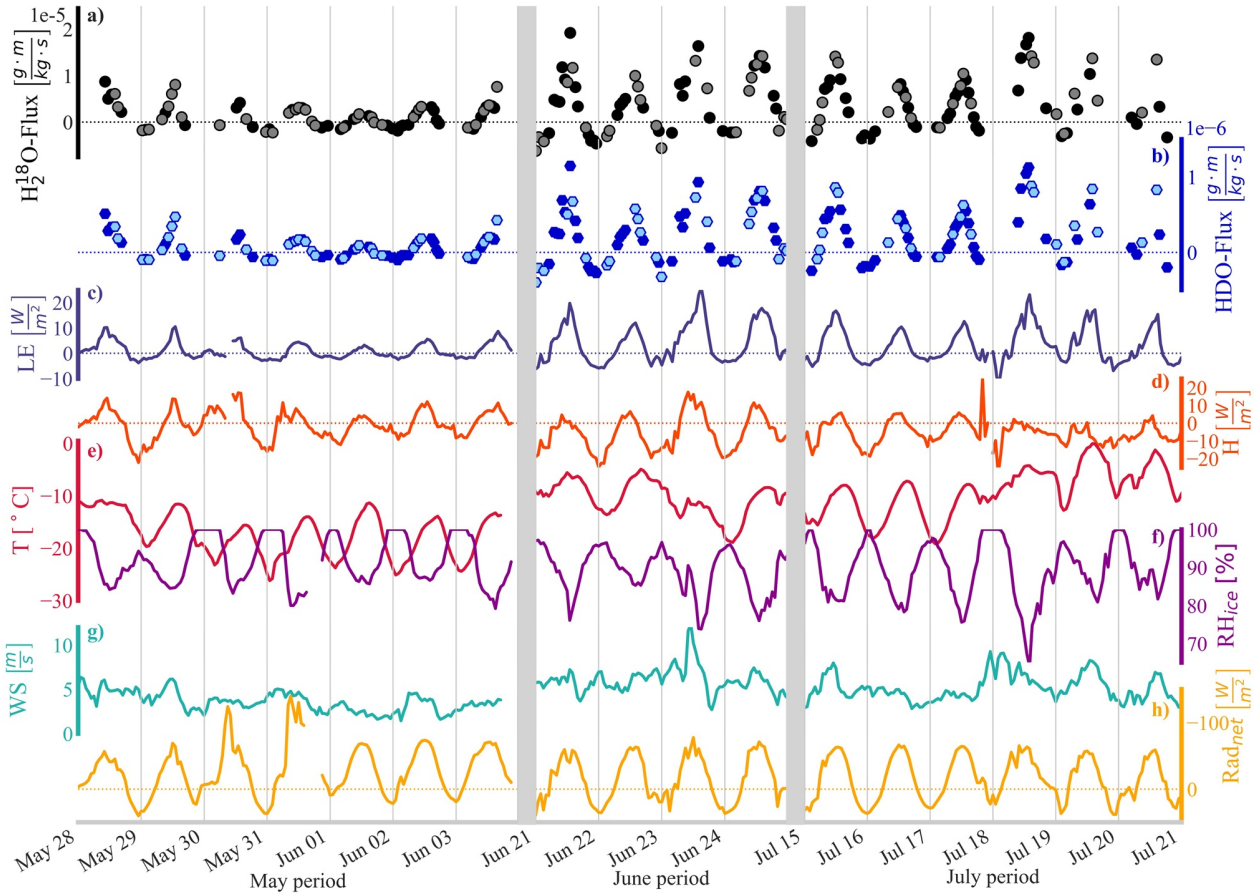

Figure 8. The measured surface isotopologue fluxes together with key meteorological parameters are shown for three clear sky periods throughout the EastGRIP 2019 season. *QC*2 isotopologue flux measurements are indicated with lighter colors in panels (a) and (b). Hourly surface flux measurements of latent (c) and sensible heat (d), ambient 2 m air temperature (e) and 2 m wind speed (g) are reported from the flux tower, whereas 2.5 m relative humidity (f) and net surface radiation (h) were measured at the PROMICE station. The sign convention is positive for upward fluxes. Note the discontinuous time axis.

was supported by snow temperature measurements (not shown). Strong negative daytime, but weak positive nighttime, temperature gradients between snowpack and air temperature resulted in high H daytime values and only slightly negative daily mean H values of -0.7 W/m^2 in May, when the air temperatures were still low. Further into the summer, a decreased net H flux showed stronger nighttime snow–air temperature differences during the clear-sky periods and a corresponding amplification of the energy uptake of the snow with a daily mean H of -5.8 W/m^2 and -5.4 W/m^2 in June and July, respectively.

4.6. Computed Isotopic Composition of the Humidity Flux

Although, in general, the isotopologue fluxes co-varied with the humidity flux, the relative abundance of isotopologues in the humidity flux changed depending on the underlying process. The identification of influencing parameters required the knowledge of the isotopic composition of the humidity flux. Therefore, δ_F was calculated with the eddy-covariance method using the 1 Hz CRDS measurements following Equation 6. For comparison, δ_F was also calculated assuming the Flux-Gradient theory (δ_F(FG), Equation 7) and following the Keeling-Plot approach (δ_F(KP), Equation 8). A detailed quality control procedure for the EC method was outlined in section 3.5 and summarized in Table 1. For the KP and FG approach, the estimated uncertainty of the δ_F value was dependent on the R^2 value of the linear regression and on the humidity difference between the observation levels (Δq) within the calculation period, as previously observed by Santos et al. (2012). High uncertainties were observed in the KP calculations when $R^2 < 0.9$. We therefore used

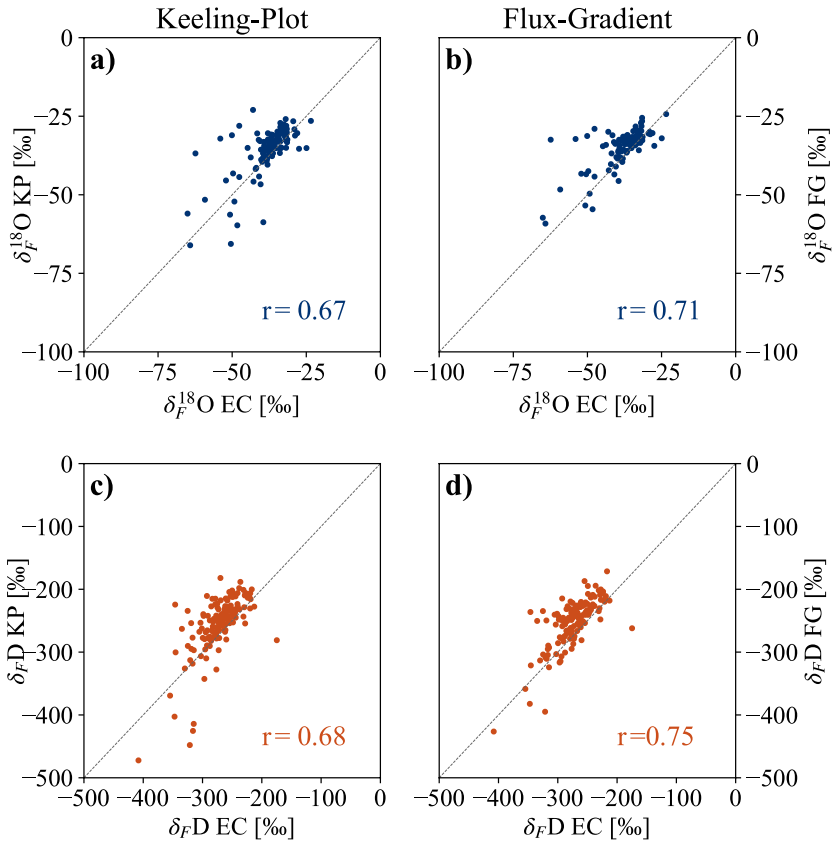

Figure 9. Comparison of isotopic composition of sublimation flux as estimated by KP (a and c) and FG (b and d) method. δ_F^{18}O comparison shown in blue in (a and b) and $\delta_F D$ shown in red in (c and d). Shown are the share of KP and FG estimates that passed the quality control (28% for δ_F^{18} and 36% for $\delta_F D$) and the corresponding correlation coefficients (r). The estimates were matched on hourly resolution and the 1:1 line is shown in gray.

$R^2 > 0.9$ as the quality criterion for the KP estimates. Concerning the second criterion, Δq of the FG data was always smaller than Δq of the KP data. This is because we interpolated the humidity levels to the same point in time for the FG method and the corresponding Δq therefore does not include a time component unlike Δq of the KP method. We inferred a quality criterion of $\Delta q > 50$ mg/kg^{-1} for the FG method from the uncertainty analysis. Of the 578 available *QC*1 & *QC*2 EC-periods, 36% fulfilled the two criteria for δ_FD and 28% for δ_F^{18}O (Figure S6).

The result of the comparison between δ_F(EC), δ_F(FG), and δ_F(KP) for sublimation conditions ($LE > 0$) is shown in Figure 9. Only the reduced data set, that passed the quality criteria, is shown. In general, the FG estimates (Figures 9b and 9d) had a higher correlation ($r > 0.70$) with EC results than KP estimates ($r > 0.65$) (Figures 9a and 9c). Furthermore, $\delta_F D$ (Figures 9c and 9d) showed a slightly better agreement between methods than δ_F^{18}O (Figures 9a and 9b).

During deposition conditions ($LE < 0$), δ_F between the three methods compared less well with values not falling on the one-to-one line (Figures S7–S8). The correlation coefficients were smaller than 0.55 in both comparisons and for both isotopologues.

In the course of the season, isotopic enrichment of the sublimation flux was recorded. During sublimation conditions within the three example periods, the averaged isotopic composition from the EC method was δ^{18}O = −47‰ in May, δ^{18}O = −41‰ in June and δ^{18}O = −31‰ in July. This temporal isotopic enrichment of the sublimation flux was consistent with the observed isotopic enrichment of the top snow layer. Figures 10a and 10c show the dependency between observed snow surface isotopic composition (δ_S) and measured EC δ_F values. For this analysis, we removed outliers of δ_F that exceeded a range from −100 to

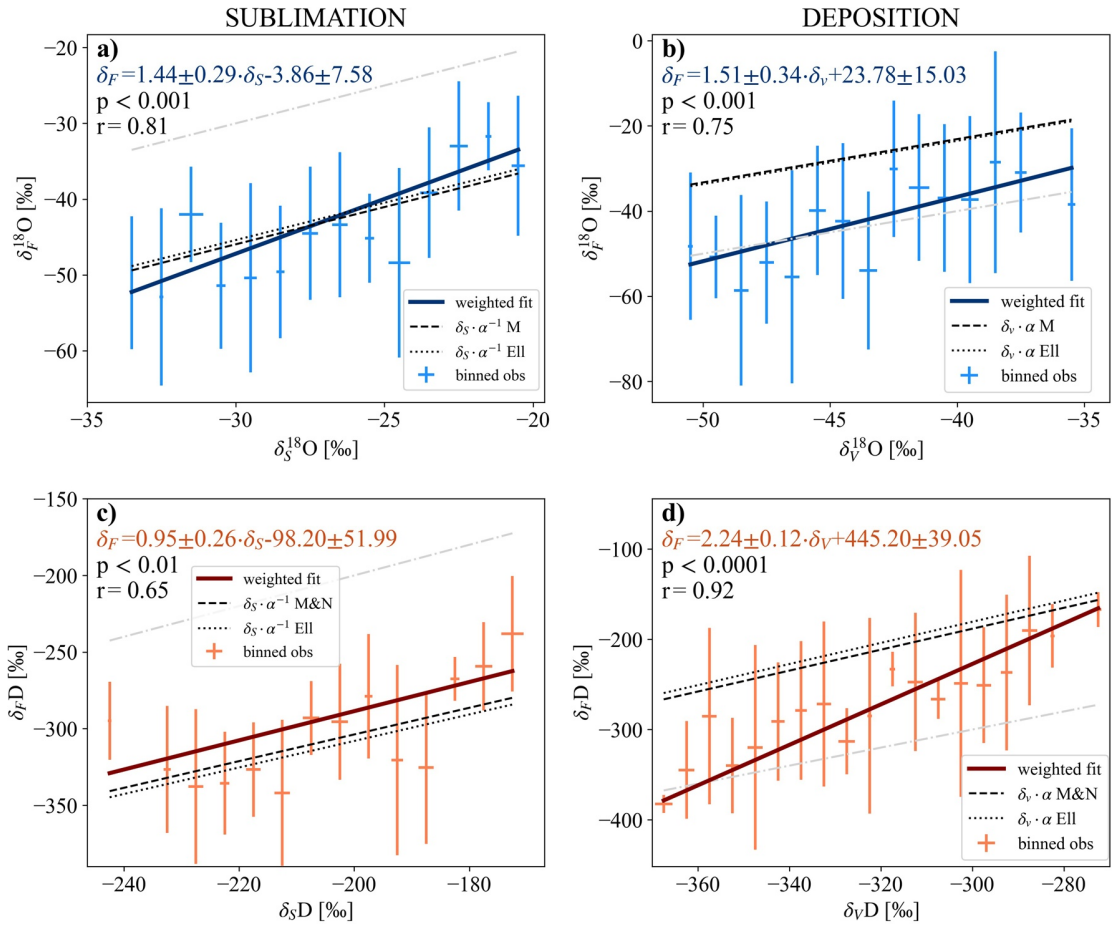

Figure 10. The isotopic composition of the sublimation (a and c) and deposition (b and d) flux as a function of the snow and vapor isotopic composition, respectively. δ_F^{18}O dependency shown in blue (a and b) and δ_FD shown in red (c and d). The snow and vapor observations were binned in 1‰ (5‰)-intervals for δ18O (δD) and the standard deviations within each bin are given as error bars. Linear weighted fits with corresponding significance levels (p-values) are given for each panel. Equilibrium vapor [ice] isotopic composition calculated assuming a surface temperature of −9°C [−14°C] (mean of snow surface during observation period) and taking fractionation factors (α) from Majoube (1971) (M), Merlivat and Nief (1967) (M&N) and Ellehoj et al. (2013) (Ell) for sublimation [deposition] conditions are shown in black. The 1:1 line is shown as gray dash-dot line.

0‰ for δ^{18}O and from −500 to 0‰ for δD. To account for the expected noise in the signal, the data was bin averaged (δ18O bin size: 1‰, δD bin size: 5‰) and the error bars indicate the standard deviation in each bin. The correlation between snow and flux isotopic composition was higher for δ^{18}O ($r = 0.81$) than for δD ($r = 0.65$). Weighted linear regressions were performed for both isotopologue species and were significant. The corresponding equations and p-values are given in Figure 10. The sublimation flux was isotopically depleted compared to the snow surface isotopologue content. For comparison, we calculated the expected isotopic composition of vapor under the assumption of ice-vapor equilibrium fractionation. We used the observed mean surface temperature during sublimation conditions (−9 °C) and fractionation factors of Majoube (1971), Merlivat and Nief (1967) and Ellehoj et al. (2013) for this calculation.

For deposition conditions, a significant dependency of δ_F on the isotopic composition of the 2 m vapor (δ_V) was observed (Figures 10b and 10d). Contrary to sublimation conditions, the correlation coefficient was higher for δD ($r = 0.94$) than for δ^{18}O ($r = 0.75$). Again, both weighted linear regression fits are given with corresponding significant p-values. The linear regressions suggest an isotopic composition of the deposition flux equal to or enriched compared to the background 2 m vapor isotopic composition. For comparison, we calculated the isotopic composition of ice in equilibrium with the given 2 m vapor isotopic composition. We

used the observed mean surface temperature during deposition conditions (−14°C) and equilibrium fractionation factors of Majoube (1971), Merlivat and Nief (1967) and Ellehoj et al. (2013) for the calculations.

5. Discussion

5.1. System Performance

Our measurement system has proven to produce reliable flux measurements of all three water isotopologues (Section 4.1, Table 1). Despite small differences in molecular characteristics between the different isotopologues, we found no differentiation by the measurement system. This agrees with assumptions made by Good et al. (2012) following Griffis et al. (2010), who found similar behavior for $H_2^{18}O$ and $H_2^{16}O$, and an only slightly dampened signal of HDO in their power spectra analysis.

5.1.1. Correction Coefficients for the EC Method

The lower sampling resolution of the CRDS made corrections necessary to account for high-frequency flux contributions that could not be resolved by the instrument. Specifically, the CRDS' low sampling resolution can be regarded as a low-pass-filter. As the CRDS' sampling frequency is only a fraction of the IRGA's sampling frequency and tube attenuation likely dampened the high-frequency signal additionally, the calculated $^{cc}_{Og}$-values were high. However, this should be regarded as an inevitable characteristic, rather than a deficiency of the method. Despite high maximum values of $^{cc}_{Og}$ up to 15 during moderately stable conditions, and even higher values for a strong atmospheric stability, the coefficients showed to be systematically dependent on turbulence parameters and can be explained as follows:

Depending on the state of the atmospheric boundary layer, relatively more or less energy is transported at higher frequencies, corresponding to a higher or lower correction coefficient, respectively. The stronger the stable stratification, that is, the higher the ζ-value, the smaller the dominant eddies with corresponding higher frequencies. This means that the cospectral peak shifts to higher frequencies with increasing atmospheric stability. Due to the lower sampling frequency, the CRDS system cannot resolve this progressively bigger high-frequency share of the flux and the correction factor therefore becomes larger.

The lowest $^{cc}_{Og}$-values were observed in unstable stratification. Here, the system was able to resolve most of the lower frequencies, at which transport is occurring under these conditions. Although generally lower, the cospectral peak under unstable conditions likewise shifts to higher frequencies with increasing wind speeds. This explains the increasing $^{cc}_{Og}$ with increasing friction velocities under unstable or near neutral conditions. In stable regimes, this dependency is masked by the pronounced effect of stratification on the cospectral peak (Massman, 2000), and the reason why stability regimes of $\zeta > 0.01$ were excluded in the analysis. A linear dependency of correction factors on wind speed, was previously observed by Ferrara et al. (2012) for empirical and analytical frequency correction approaches of CH_4-fluxes. However, it is important to note, that this behavior is intrinsic to closed-path analyzers like the CRDS. Massman (2000) indeed, found a slight decrease of correction factors with higher wind speeds for open-path instruments that suffer merely from high-pass-filters like block averaging.

Despite the reasonable justification for high $^{cc}_{Og}$-values during stable atmospheric conditions, it needs to be emphasized that stable stratification is likewise the biggest hindrance for this type of flux measurements. Most EC-periods that did not pass the ogive-quality test were periods during stable and very stable conditions. Previous studies have therefore often excluded stable stratification periods completely (Good et al., 2012). However, with our site of interest being predominantly stably stratified, we included stable conditions in our analysis and applied the same quality criteria to both, stable and unstable conditions. In doing so, we were able to identify reliable data to draw conclusions on the vapor isotopologue exchange through sublimation and deposition during polar day conditions, even in nonconvective regimes. Based on this, it needs to be mentioned that instruments with a higher temporal resolution will be necessary to measure isotopologue fluxes during polar night conditions. Strong atmospheric stability, as observed during polar night conditions, likely requires shorter integration times of seconds to minutes. Combined with the low resolution, closed-path analyzers, this limits the available frequency range, from which flux information can be gained. Furthermore, it needs to be kept in mind that the EC method is developed for direct

measurements of turbulent transport. However, under a strong stable stratification, transport might not comply with the turbulence theory alone but might also include submeso-motion-like transport (Acevedo et al., 2016; Mahrt, 2009). The general discussion of transport and its measurement in stably stratified conditions lies, however, beyond the scope of this work.

5.1.2. Comparison of δ_F Between Methods

Our EC estimates of the isotopic composition of the flux compared well to the more established FG and KP methods. During sublimation conditions, when uncertainties of EC estimates are smallest, FG and EC showed a correlation of >0.7. Correlation coefficients between the EC and KP methods were slightly smaller which could be due to the timing offset between the 25 min EC-period and the subsequent 35 min KP period. The steady-state assumption, necessary to compare the estimates of the two methods within one hour, might not be valid which could explain the difference in the estimates. For a more direct comparison, simultaneous measurements at several heights with multiple instruments would be needed which was not feasible with the available system set-up. In order to bypass the time offset, we interpolated the measurements of all levels to the midpoint of the EC period for the FG approach. This way, we introduced the uncertainty of interpolation but satisfied the steady-state assumption. This could be the reason why the FG results agreed better with the EC results. We point out, that if the exact same data were used for FG and KP estimates, both methods would yield the same result as noted by Good et al. (2012).

The FG and KP pitfalls outlined earlier become apparent when looking at the number of available periods for the comparison. Over half of the periods that passed the EC ogive quality screening did not pass the KP R^2 and FG humidity range (Δq) quality screening. This alone might speak for the EC method. However, as we have only evaluated available EC-periods for the comparison, FG and KP methods might be eligible at times when the EC quality criteria were not met. Nevertheless, the EC is a direct method, which allows measurements of fluxes without relying on simplified conceptual theories. As the stable water isotopologue analyzer development proceeds, an increased sampling frequency combined with reduced memory effect and smoothing will allow for the use of the full potential of the EC method when measuring isotopologue fluxes. Besides the high sampling frequency, an additional instrument requirement is the very low instrument drift. One quality criterion for EC-period rejection was defined as a high noise level on the low-frequency end of the cospectrum ($RMSE_{norm} > 0.1$). Since the ogive end-value is the critical parameter for correction factor calculation, this value needs to be accurate. Mammarella et al. (2010) argue that the low-frequency noise stems from instrument drift. Hence, it is important that instruments used for this kind of flux measurements have minimum drift in their readings. As CRDS instruments have shown to have a high degree of stability despite the harsh polar conditions, we have thus used a CRDS analyzer in our study.

5.2. Error Estimation

We used three different methods to quantify and characterize the error on the EC isotopologue flux measurements. The MC method was used to inform about the random error contribution as it only takes into account instrument noise. When comparing the median of the MC distribution with the other two median values, it becomes obvious that instrument noise accounts for only a fraction of the total uncertainty. The MC median is several times smaller than the ML or FS median. Both ML and FS error estimations are methods, that calculate the variance of the covariance and therefore account for stochastic sampling errors (Businger, 1986).

Stochastic sampling errors are directly related to the amount of available independent observations. Averaged covariances need significantly more independent observations (i.e., longer integration times) to yield a specific low uncertainty compared to regular scalar averages. According to Businger (1986), this is due to the intermittent character of second-order moments which seem especially related to large eddies. The CRDS instrument predominantly measures these large eddies with low frequencies. It is therefore not surprising that we find such high error estimations for the covariances computed from CRDS time series. By computing the cross- and autocovariances using different lags, the FS method specifically quantifies the influence of the number of independent observations. The ML approach approximates, instead, the number of independent observations by the integral length scale. This is likewise a possible explanation why the FS method yields higher error values than the ML method. That said, total uncertainties obtained with both

the ML and FS method, lie in a range commonly reported for scalar-flux measurements (e.g., Kessomkiat et al., 2013, Table 5).

If we interpret the random noise contribution as a precision estimate of our method, it becomes clear why prominent diurnal cycle structures can be observed in our measurements despite the high uncertainty estimates of FS (∼50%) and ML (∼30%). The bigger share of the overall uncertainty would then be attributed to sampling errors, and the FS and ML uncertainties can be interpreted as the combined uncertainty of the flux values due to precision and accuracy. Since the system set-up was not modified during the campaign and all measurements were post-processed following the same protocol, we argue that this systematic sampling error does not change during the observation period and we can therefore compare measurement values from different periods within the observation period. The direct comparison of data from a second measurement system, however, has to be done with care, accepting potential differences within the range given by ML or FS uncertainty estimates.

5.3. The Surface Isotopologue Flux at EastGRIP

We concentrate here on three examples of clear sky conditions in the interior of the GrIS. Other clear sky period observations were similar to the ones shown. We chose these time periods for our focus as they represent idealized conditions when the diurnal cycle is the dominant mode of variability for the meteorological parameters and influences of more complex drivers, such as clouds and snowfall, are reduced. At the same time, clear sky conditions allow for an unstable regime of the lower atmosphere with a negative temperature gradient close to the surface. Such convective boundary layers have been observed previously on ice sheets (Anderson & Neff, 2008). Our method has shown to be more reliable during such unstable atmospheric stratification.

Those ideal clear sky conditions show a signal of isotopologue surface fluxes that follow the diurnal cycle of the net surface radiation but are limited in amplitude by the saturation water vapor deficit. With warming conditions, the saturation vapor pressure becomes higher and the air can hold more moisture, which likewise allows for higher latent heat and isotopologue flux values. Indeed, the isotopologue fluxes mirror the latent heat flux behavior and all fluxes increase after the May period. However, wind conditions do not change substantially which points toward a stronger buoyancy effect that enhances turbulence in the June and July period and can explain the increased fluxes.

In all three example periods, the net isotopologue fluxes and latent heat flux are directed away from the surface, which implies a net sublimation flux in accordance with observations from other locations in the accumulation zone of the GrIS (Box & Steffen, 2001; Cullen et al., 2014; van den Broeke et al., 2011), but contrary to some modeling studies (Box et al., 2006; Franco et al., 2013).

For identifying model biases, the isotopic composition of the water vapor flux is the parameter of interest. We find that the isotopic composition of the humidity flux during sublimation and deposition shows a dependency on the snow surface and vapor isotopic composition, respectively. The observed isotopic enrichment of the sublimation flux throughout the season can thus be explained by enrichment in the surface snow isotopic composition as new snow is deposited. Furthermore, recent process model studies (Madsen et al., 2019; Ritter et al., 2016) as well as laboratory experimental studies (Hughes et al., 2021) have suggested changes in snow isotopic composition due to isotopically fractionating exchange-processes. Our measurements of the isotopic composition of the sublimation flux support the hypothesis of sublimation induced fractionation. The calculated linear regression models fitted to observations do not follow a one-to-one line with the snow isotopic composition, which would be expected if sublimation did not cause fractionation as stated by Dansgaard et al. (1973). Instead, we observe a depleted isotopic composition in the humidity flux compared to the snow surface isotopic composition. The regression models for δD and δ^{18}O are close to the theoretical equilibrium vapor lines that we calculated assuming established vapor-ice fractionation factors (Ellehoj et al., 2013; Majoube, 1971; Merlivat & Nief, 1967). This suggests that the isotopic composition of the sublimation flux can, to a first order, be calculated from the snow isotopic composition assuming equilibrium fractionation. Depending on the ratio between the sublimation and snowfall amount, the sublimation flux modifying the snow surface layer, might influence the snow isotopic signal that is later buried and stored in the snow column. Consequently, and determined by the meteorological conditions and pre-

cipitation seasonality at ice core drilling sites, the fractionation surface processes could have implications for paleoclimate proxy interpretation of ice core records. It has to be investigated to which extend the sublimation signal overprints the precipitation climate signal and which meteorological parameters are critical for controlling the magnitude of shifts in the snow isotopic composition. Establishing an understanding of the exact mechanisms and influencing parameters will be the subject of future studies.

For deposition conditions, the isotopic composition of the humidity flux becomes relatively more depleted with the decreasing isotopic composition of the vapor. Under the assumption of steady-state, we expect that the isotopic composition of the deposition flux is essentially the same as the isotopic composition of the frost forming during deposition. Yet the regression models for both isotopologue species are not consistent with the expected equilibrium fractionation vapor-solid values. First, this is because we calculate the solid isotopic composition with regard to the 2 m-level although we expect a substantial gradient between the 2 m-level and the vapor very close to the surface. Casado et al. (2016) found steep gradients of the isotopic composition in the centimeter range near the surface suggesting a more depleted vapor close to the ground compared to the 2 m observations. This would in general lead to the observed δ_F being more depleted than what would be expected from equilibrium fractionation of the 2 m water vapor level. Second, differences between the slopes of the regression and equilibrium lines can be explained by influences of kinetic fractionation processes during deposition conditions. During these periods, as shown in Figure 8, the air is frequently saturated and, with respect to the surface temperature, at times supersaturated. Supersaturation, as shown by Jouzel and Merlivat (1984), introduces a humidity gradient at the condensation interface and therefore causes kinetic fractionation influences. Since supersaturation and the vapor isotopic composition very close to the ground are difficult to measure, parameterizations of δ_F are challenging to establish. The observed dependency between the 2 m vapor isotopic composition and δ_F could serve as an empirical benchmark in future surface exchange studies and for quantifying the role of supersaturation on kinetic fractionation.

From our observations, we can conclude that isotopic fractionation during sublimation and deposition alters the snow surface isotopic composition. Whether this atmosphere-snow exchange affects the long-term mean isotopic composition of the surface snow, and its implications for paleoclimate ice core proxy interpretations requires further analysis.

6. Conclusions

The combination of a high-frequency sonic anemometer with a high-precision slow sensor for isotopologue measurements allowed direct measurements of in-situ surface fluxes of stable water isotopologues using the eddy-covariance method. This has previously not been conducted in such low humidity conditions as found in the interior of the Greenland Ice Sheet. We make use of the available high-frequency cospectrum of a co-located humidity sensor to correct for the high-frequency-flux loss, which does not require any kind of similarity assumption. Our method allows for the quantification of the stable water isotopologue exchange between the snowpack and the atmosphere with the commonly known limitations of eddy-covariance flux estimations. In particular, strong atmospheric stability was identified as a hindrance to isotopologue flux measurements since correction factors of over 15 are needed in very stable conditions. In addition, calculated flux errors were found to be higher in stable conditions. This implies that the application of the presented method and instrumental set-up is most applicable during dominantly unstable to slightly stable conditions. When evaluating other possible instruments as a substitute to the slow sensor used in this study, we highlight the need for very low drift of the analyzer to minimize the low-frequency noise.

Surface isotopologue fluxes during clear sky conditions were readily observable and allowed a quantification of the isotopologue exchange at the surface. During polar day, the net flux of isotopologues was directed away from the surface, that is, sublimation outweighed deposition and the snowpack lost heavy isotopologues to the vapor. The isotopic composition of the sublimation flux showed to be dependent on the surface snow isotopic composition and was, when compared to the snow, isotopically depleted. This depletion can, to a first order, be approximated assuming equilibrium fractionation during sublimation. Furthermore, the observed isotopic composition of the humidity flux during deposition conditions was dependent on the vapor isotopic composition. Our findings imply that, depending on the strength of vapor-snow exchange, the surface fluxes can modify the precipitation-weighted climate signal in snow with implications for ice core

records. Thus, the presented observations of the exchange of stable water isotopologues between the snow surface and lower atmosphere can serve as the basis for improved parameterizations of surface exchange processes in climate models and as an important component for snow isotopologue studies.

Conflict of Interest

The authors declare no conflicts of interest relevant to this study.

Data Availability Statement

Data sets for this research are available from PANGAEA: Wahl and Steen-Larsen (2021) [CC BY], Steen-Larsen and Wahl (2021a) [CC BY], Steen-Larsen and Wahl (2021c) [CC BY], Steen-Larsen and Wahl (2021d) [CC BY], Steen-Larsen and Wahl (2021b) [CC BY]. Data from the Program for Monitoring of the Greenland Ice Sheet (PROMICE) were provided by the Geological Survey of Denmark and Greenland (GEUS) at https://doi.org/10.22008/promice/data/aws and the corresponding reference which includes a link is Fausto and van As (2019).

Acknowledgments
The authors would like to thank Dr. Wei and two anonymous reviewers for their valuable comments which have greatly improved this article. The authors also thank N. Stoll and L. Dietrich for their helpful proofreading efforts. We thank the stable water isotope laboratory of the Alfred-Wegener-Institute in Bremerhaven, Germany for analyzing the snow samples for this project. We also thank INSTAAR, University of Colorado, Boulder for providing the water standards that were used for CRDS calibrations. We further thank everyone that supported the field campaign for this study. This project has received funding from the European Research Council (ERC) under the European Union's Horizon 2020 research and innovation program: Starting Grant-SNOWISO (grant agreement 759526). EastGRIP is directed and organized by the Centre for Ice and Climate at the Niels Bohr Institute, University of Copenhagen. It is supported by funding agencies and institutions in Denmark (A. P. Møller Foundation, University of Copenhagen), USA (US National Science Foundation, Office of Polar Programs), Germany (Alfred Wegener Institute, Helmholtz Centre for Polar and Marine Research), Japan (National Institute of Polar Research and Arctic Challenge for Sustainability), Norway (University of Bergen and Bergen Research Foundation), Switzerland (Swiss National Science Foundation), France (French Polar Institute Paul-Emile Victor, Institute for Geosciences and Environmental research), and China (Chinese Academy of Sciences and Beijing Normal University).

References

Acevedo, O. C., Mahrt, L., Puhales, F. S., Costa, F. D., Medeiros, L. E., & Degrazia, G. A. (2016). Contrasting structures between the decoupled and coupled states of the stable boundary layer. *Quarterly Journal of the Royal Meteorological Society*, *142*(695), 693–702. https://doi.org/10.1002/qj.2693

Ahlstrøm, A. P., Gravesen, P., Andersen, S. B., van As, D., Citterio, M., Fausto, R. S., & Petersen, D. (2008). A new programme for monitoring the mass loss of the Greenland ice sheet. *Geological Survey of Denmark and Greenland Bulletin*, *15*, 61–64.

Anderson, P. S., & Neff, W. D. (2008). Boundary layer physics over snow and ice. *Atmospheric Chemistry and Physics*, *8*(13), 3563–3582. https://doi.org/10.5194/acp-8-3563-2008

Baldocchi, D. (2014). Measuring fluxes of trace gases and energy between ecosystems and the atmosphere–The state and future of the eddy covariance method. *Global Change Biology*, *20*(12), 3600–3609. https://doi.org/10.1111/gcb.12649

Benetti, M., Lacour, J. L., Sveinbjörnsdóttir, A. E., Aloisi, G., Reverdin, G., Risi, C., et al. (2018). A framework to study mixing processes in the marine boundary layer using water vapor isotope measurements. *Geophysical Research Letters*, *45*(5), 2524–2532. https://doi.org/10.1002/2018GL077167

Bengtsson, L. (2010). The global atmospheric water cycle. *Environmental Research Letters*, *5*(2), 025202. https://doi.org/10.1088/1748-9326/5/2/025002

Benson, L. V., Hostetler, S. W., & Benson, L. V. (1994). Stable isotopes of oxygen and hydrogen in the Truckee River-Pyramid Lake surface-water system. *Limnology & Oceanography*, *39*(2), 344–355. https://doi.org/10.4319/lo.1994.39.8.1945

Berkelhammer, M., Noone, D. C., Steen-Larsen, H. C., Bailey, A., Cox, C. J., O'Neill, M. S., et al. (2016). Surface-atmosphere decoupling limits accumulation at Summit, Greenland. *Science Advances*, *2*(4), e1501704. https://doi.org/10.1126/sciadv.1501704

Bonne, J. L., Masson-Delmotte, V., Cattani, O., Delmotte, M., Risi, C., Sodemann, H., & Steen-Larsen, H. C. (2014). The isotopic composition of water vapour and precipitation in Ivittuut, southern Greenland. *Atmospheric Chemistry and Physics*, *14*(9), 4419–4439. https://doi.org/10.5194/acp-14-4419-2014

Box, J. E., Bromwich, D. H., Veenhuis, B. A., Bai, L. S., Stroeve, J. C., Rogers, J. C., et al. (2006). Greenland ice sheet surface mass balance variability (1988–2004) from calibrated polar MM5 output. *Journal of Climate*, *19*(12), 2783–2800. https://doi.org/10.1175/JCLI3738.1

Box, J. E., & Steffen, K. (2001). Sublimation on the Greenland ice sheet from automated weather station observations. *Journal of Geophysical Research*, *106*(D24), 33965–33981. https://doi.org/10.1029/2001JD900219

Braden-Behrens, J., Markwitz, C., & Knohl, A. (2019). Eddy covariance measurements of the dual-isotope composition of evapotranspiration. *Agricultural and Forest Meteorology*, *269–270*, 203–219. https://doi.org/10.1016/j.agrformet.2019.01.035

Businger, J. A. (1986). Evaluation of the accuracy with which dry deposition can be measured with current micrometeorological techniques. *Journal of Climate and Applied Meteorology*, *25*(8), 1100–1124. https://doi.org/10.1175/1520-0450(1986)025(1100:EOTAWW)2.0.CO;2

Casado, M., Landais, A., Masson-Delmotte, V., Genthon, C., Kerstel, E., Kassi, S., et al. (2016). Continuous measurements of isotopic composition of water vapour on the East Antarctic Plateau. *Atmospheric Chemistry and Physics*, *16*(13), 8521–8538. https://doi.org/10.5194/acp-16-8521-2016

Craig, H. (1961). Standards for reporting concentration of deuterium and oxygen-18 in natural water. *Science*, *133*, 1833–1834. https://doi.org/10.1126/science.133.3467.1833

Cullen, N. J., Mölg, T., Conway, J., & Steffen, K. (2014). Assessing the role of sublimation in the dry snow zone of the Greenland ice sheet in a warming world. *Journal of Geophysical Research: Atmosphere*, *119*(11), 6563–6577. https://doi.org/10.1002/2014JD021557

Dansgaard, W., Johnsen, S. J., Clausen, H. B., & Gundestrup, N. (1973). Stable isotope glaciology. *Meddelelser om Gronland Geoscience*, *197*, 2.

de Laeter, J. R., Böhlke, J. K., De Bièvre, P., Hidaka, H., Peiser, H. S., Rosman, K. J. R., & Taylor, P. D. P. (2003). Atomic weights of the elements. Review 2000 (IUPAC Technical Report). *Pure and Applied Chemistry*, *75*(6), 683–800. https://doi.org/10.1351/pac200375060683

Desjardins, R. L., MacPherson, J. I., Schuepp, P. H., & Karanja, F. (1989). An evaluation of aircraft flux measurements of CO_2, water vapor and sensible heat. *Boundary-Layer Meteorology*, *47*(1–4), 55–69. https://doi.org/10.1007/BF00122322

Ellehoj, M. D., Steen-Larsen, H. C., Johnsen, S. J., & Madsen, M. B. (2013). Ice-vapor equilibrium fractionation factor of hydrogen and oxygen isotopes: Experimental investigations and implications for stable water isotope studies. *Rapid Communications in Mass Spectrometry*, *27*(19), 2149–2158. https://doi.org/10.1002/rcm.6668

Fausto, R. S., As, D., Box, J. E., Colgan, W., Langen, P. L., & Mottram, R. H. (2016). The implication of nonradiative energy fluxes dominating Greenland ice sheet exceptional ablation area surface melt in 2012. *Geophysical Research Letters*, *43*(6), 2649–2658. https://doi.org/10.1002/2016GL067720

Fausto, R. S., & van As, D. (2019). Programme for monitoring of the Greenland ice sheet (PROMICE): Automatic weather station data Version: v03. *Geological Survey of Denmark and Greenland*. https://doi.org/10.22008/promice/data/aws

Ferrara, R., Loubet, B., Tommasi, Di, P., Bertolini, T., Magliulo, V., Cellier, P., et al. (2012). Eddy covariance measurement of ammonia fluxes: Comparison of high frequency correction methodologies. *Agricultural and Forest Meteorology*, *158–159*, 30–42. https://doi.org/10.1016/j.agrformet.2012.02.001

Fettweis, X. (2007). Reconstruction of the 1979–2006 Greenland ice sheet surface mass balance using the regional climate model MAR. *The Cryosphere*, *1*(1), 21–40. https://doi.org/10.5194/tc-1-21-2007

Finkelstein, P. L., & Sims, P. F. (2001). Sampling error in eddy correlation flux measurements. *Journal of Geophysical Research*, *106*(D4), 3503–3509. https://doi.org/10.1029/2000JD900731

Foken, T., Aubinet, M., & Leuning, R. (2012). The Eddy Covariance Method. In *Eddy covariance* (pp. 1–19). Dordrecht: Springer Netherlands. https://doi.org/10.1007/978-94-007-2351-1_110.1007/978-94-007-2351-1_1

Foken, T., & Wichura, B. (1996). Tools for quality assessment of surface-based flux measurements. *Agricultural and Forest Meteorology*, *78*(1–2), 83–105. https://doi.org/10.1016/0168-1923(95)02248-1

Foken, T., Wimmer, F., Mauder, M., Thomas, C., & Liebethal, C. (2006). Some aspects of the energy balance closure problem. *Atmospheric Chemistry and Physics*, *6*(1), 4395–4402. https://doi.org/10.5194/acp-6-4395-2006

Franco, B., Fettweis, X., & Erpicum, M. (2013). Future projections of the Greenland ice sheet energy balance driving the surface melt. *The Cryosphere*, *7*(1), 1–18. https://doi.org/10.5194/tc-7-1-2013

Fuller, W. (1976). *Introduction to statistical time series analysis*. New York: John Wiley. https://doi.org/10.2307/2344931

Galewsky, J., Steen-Larsen, H. C., Field, R. D., Worden, J., Risi, C., & Schneider, M. (2016). Stable isotopes in atmospheric water vapor and applications to the hydrologic cycle. *Reviews of Geophysics*, *54*(4), 809–865. https://doi.org/10.1002/2015RG000512

Good, S. P., Soderberg, K., Guan, K., King, E. G., Scanlon, T. M., & Caylor, K. K. (2014). δ 2 H isotopic flux partitioning of evapotranspiration over a grass field following a water pulse and subsequent dry down. *Water Resources Research*, *50*(2), 1410–1432. https://doi.org/10.1002/2013WR014333

Good, S. P., Soderberg, K., Wang, L., & Caylor, K. K. (2012). Uncertainties in the assessment of the isotopic composition of surface fluxes: A direct comparison of techniques using laser-based water vapor isotope analyzers. *Journal of Geophysical Research*, *117*(D15), D15301. https://doi.org/10.1029/2011JD017168

Grachev, A. A., Andreas, E. L., Fairall, C. W., Guest, P. S., & Persson, P. O. G. (2013). The critical Richardson number and limits of applicability of local similarity theory in the stable boundary layer. *Boundary-Layer Meteorology*, *147*(1), 51–82. https://doi.org/10.1007/s10546-012-9771-0

Griffis, T. J., Lee, X., Baker, J., Sargent, S., & King, J. (2005). Feasibility of quantifying ecosystem–atmosphere C18O16O exchange using laser spectroscopy and the flux-gradient method. *Agricultural and Forest Meteorology*, *135*(1–4), 44–60. https://doi.org/10.1016/j.agrformet.2005.10.002

Griffis, T. J., Sargent, S. D., Baker, J. M., Lee, X., Tanner, B. D., Greene, J., et al. (2008). Direct measurement of biosphere-atmosphere isotopic CO_2 exchange using the eddy covariance technique. *Journal of Geophysical Research*, *113*(D8), D08304. https://doi.org/10.1029/2007JD009297

Griffis, T. J., Sargent, S. D., Lee, X., Baker, J. M., Greene, J., Erickson, M., et al. (2010). Determining the oxygen isotope composition of evapotranspiration using eddy covariance. *Boundary-Layer Meteorology*, *137*(2), 307–326. https://doi.org/10.1007/s10546-010-9529-5

Gryazin, V., Risi, C., Jouzel, J., Kurita, N., Worden, J., Frankenberg, C., et al. (2014). To what extent could water isotopic measurements help us understand model biases in the water cycle over Western Siberia. *Atmospheric Chemistry and Physics*, *14*(18), 9807–9830. https://doi.org/10.5194/acp-14-9807-2014

Howat, I., Negrete, A., & Smith, B. (2015). *MEaSUREs Greenland ice mapping project (GIMP) digital elevation model Version 1, [90m], [03-07-2020]*. Boulder, CO: NASA National Snow and Ice Data Center Distributed Active Archive Center. https://doi.org/10.5067/NV34YUIXLP9W

Howat, I. M., Negrete, A., & Smith, B. E. (2014). The Greenland Ice Mapping Project (GIMP) land classification and surface elevation data sets. *The Cryosphere*, *8*(4), 1509–1518. https://doi.org/10.5194/tc-8-1509-2014

Hughes, A. G., Wahl, S., Jones, T. R., Zuhr, A., Hörhold, M., White, J. W. C., & Steen-Larsen, H. C. (2021). *The role of sublimation as a driver of climate signals in the water isotope content of surface snow: Laboratory and field experimental results*[preprint]. The Cryosphere Discussions. https://doi.org/10.5194/tc-2021-87

Jouzel, J., & Merlivat, L. (1984). Deuterium and oxygen 18 in precipitation' modeling of the isotopic effects during snow formation. *Journal of Geophysical Research*, *89*, 749–757. https://doi.org/10.1029/jd089id07p11749

Kaimal, J. C., Wyngaard, J. C., Izumi, Y., & Coté, O. R. (1972). Spectral characteristics of surface-layer turbulence. *Quarterly Journal of the Royal Meteorological Society*, *98*(417), 563–589. https://doi.org/10.1002/qj.49709841707

Keeling, C. D. (1958). The concentration and isotopic abundances of atmospheric carbon dioxide in rural areas. *Geochimica et Cosmochimica Acta*, *13*, 322–334. https://doi.org/10.1016/0016-7037(58)90033-4

Kessomkiat, W., Franssen, H.-J. H., Graf, A., & Vereecken, H. (2013). Estimating random errors of eddy covariance data: An extended two-tower approach. *Agricultural and Forest Meteorology*, *171–172*, 203–219. https://doi.org/10.1016/j.agrformet.2012.11.019

Kolmogorov, A. N. (1991). Dissipation of energy in the locally isotropic turbulence. *Proceedings of the Royal Society of London - Series A: Mathematical and Physical Sciences*, *434*(1890), 15–17. https://doi.org/10.1098/rspa.1991.0076

Lee, X., Griffis, T. J., Baker, J. M., Billmark, K. A., Kim, K., & Welp, L. R. (2009). Canopy-scale kinetic fractionation of atmospheric carbon dioxide and water vapor isotopes. *Global Biogeochemical Cycles*, *23*(1), GB1002. https://doi.org/10.1029/2008GB003331

Lee, X., Kim, K., & Smith, R. (2007). Temporal variations of the 18 O/16 O signal of the whole-canopy transpiration in a temperate forest. *Global Biogeochemical Cycles*, *21*(3), GB3013. https://doi.org/10.1029/2006GB002871

Lee, X., Massman, W., & Law, B. (2005). Handbook of Micrometeorology. In Lee, X., Massman, W., & Law, B. (Eds.), Handbook of Micrometeorology (Vol. 29). Dordrecht: Springer Netherlands. https://doi.org/10.1007/1-4020-2265-4

Lenaerts, J. T., Medley, B., van den Broeke, M. R., & Wouters, B. (2019). Observing and modeling ice sheet surface mass balance. *Reviews of Geophysics*, *57*(2), 376–420. https://doi.org/10.1029/2018RG000622

Madsen, M. V., Steen-Larsen, H. C., Hörhold, M., Box, J., Berben, S. M. P., Capron, E., et al. (2019). Evidence of Isotopic fractionation during vapor exchange between the atmosphere and the snow surface in greenland. *Journal of Geophysical Research: Atmosphere*, *124*(6), 2932–2945. https://doi.org/10.1029/2018JD029619

Mahrt, L. (1998). Stratified atmospheric boundary layers and breakdown of models. *Theoretical and Computational Fluid Dynamics*, *11*(3–4), 263–279. https://doi.org/10.1007/s001620050093

Mahrt, L. (2008). Bulk formulation of surface fluxes extended to weak-wind stable conditions. *Quarterly Journal of the Royal Meteorological Society*, *134*(630), 1–10. https://doi.org/10.1002/qj.197

Mahrt, L. (2009). Characteristics of Submeso Winds in the Stable Boundary Layer. *Boundary-Layer Meteorology*, *130*(1), 1–14. https://doi.org/10.1007/s10546-008-9336-4

Majoube, M. (1971). Fractionnement en 18O entre la glace et la vapeur d'eau. *Journal de Chimie Physique*, *68*(4), 625–636. https://doi.org/10.1051/jcp/1971680625

Mammarella, I., Werle, P., Pihlatie, M., Eugster, W., Haapanala, S., Kiese, R., et al. (2010). A case study of eddy covariance flux of N_2O measured within forest ecosystems: Quality control and flux error analysis. *Biogeosciences*, *7*(2), 427–440. https://doi.org/10.5194/bg-7-427-2010

Mann, J., & Lenschow, D. H. (1994). Errors in airborne flux measurements. *Journal of Geophysical Research*, *99*(D7), 14519. https://doi.org/10.1029/94JD00737

Massman, W. (2000). A simple method for estimating frequency response corrections for eddy covariance systems. *Agricultural and Forest Meteorology*, *104*(3), 185–198. https://doi.org/10.1016/S0168-1923(00)00164-7

Mauder, M., Liebethal, C., Göckede, M., Leps, J.-P., Beyrich, F., & Foken, T. (2006). Processing and quality control of flux data during LITFASS-2003. *Boundary-Layer Meteorology*, *121*(1), 67–88. https://doi.org/10.1007/s10546-006-9094-0

Merlivat, L., & Nief, G. (1967). *Fractionnement isotopique lors des changements d'etat solide-vapeur et liquide-vapeur de l'eau a des temperatures inferieures a 0C*. Tellus.

Moore, C. J. (1986). Frequency response corrections for eddy correlation systems. *Boundary-Layer Meteorology*, *37*(1–2), 17–35. https://doi.org/10.1007/BF00122754

Noël, B., Van De Berg, W. J., Van Meijgaard, E., Kuipers Munneke, P., Van De Wal, R. S., & Van Den Broeke, M. R. (2015). Evaluation of the updated regional climate model RACMO2.3: Summer snowfall impact on the Greenland Ice Sheet. *The Cryosphere*, *9*(5), 1831–1844. https://doi.org/10.5194/tc-9-1831-2015

Obukhov, A. M. (1946). 'Turbulentnost' v temperaturnoj – Neodnorodnoj atmosfere (Turbu- lence in an Atmosphere with a Non-uniform Temperature). *Trudy Inst. Theor. Geofiz. AN SSSR*, *1*, 95–115.

Ritter, F., Christian Steen-Larsen, H., Werner, M., Masson-Delmotte, V., Orsi, A., Behrens, M., et al. (2016). Isotopic exchange on the diurnal scale between near-surface snow and lower atmospheric water vapor at Kohnen station, East Antarctica. *The Cryosphere*, *10*(4), 1647–1663. https://doi.org/10.5194/tc-10-1647-2016

Santos, E., Wagner-Riddle, C., Lee, X., Warland, J., Brown, S., Staebler, R., et al. (2012). Use of the isotope flux ratio approach to investigate the $C^{18}O^{16}O$ and $^{13}CO_2$ exchange near the floor of a temperate deciduous forest. *Biogeosciences*, *9*(7), 2385–2399. https://doi.org/10.5194/bg-9-2385-2012

Schmid, H. P., Grimmond, C. S. B., Cropley, F., Offerle, B., & Su, H. B. (2000). Measurements of CO_2 and energy fluxes over a mixed hardwood forest in the mid-western United States. *Agricultural and Forest Meteorology*, *103*, 357–374. https://doi.org/10.1016/S0168-1923(00)00140-4

Sorbjan, Z., & Grachev, A. A. (2010). An evaluation of the flux–gradient relationship in the stable boundary layer. *Boundary-Layer Meteorology*, *135*(3), 385–405. https://doi.org/10.1007/s10546-010-9482-3

Spank, U., & Bernhofer, C. (2008). Another simple method of spectral correction to obtain robust eddy-covariance results. *Boundary-Layer Meteorology*, *128*(3), 403–422. https://doi.org/10.1007/s10546-008-9295-9

Steen-Larsen, H. C., Johnsen, S. J., Masson-Delmotte, V., Stenni, B., Risi, C., Sodemann, H., et al. (2013). Continuous monitoring of summer surface water vapor isotopic composition above the Greenland Ice Sheet. *Atmospheric Chemistry and Physics*, *13*(9), 4815–4828. https://doi.org/10.5194/acp-13-4815-2013

Steen-Larsen, H. C., Risi, C., Werner, M., Yoshimura, K., & Masson-Delmotte, V. (2017). Evaluating the skills of isotope-enabled general circulation models against in situ atmospheric water vapor isotope observations. *Journal of Geophysical Research: Atmosphere*, *122*(1), 246–263. https://doi.org/10.1002/2016JD025443

Steen-Larsen, H. C., Sveinbjörnsdottir, A. E., Peters, A. J., Masson-Delmotte, V., Guishard, M. P., Hsiao, G., et al. (2014). Climatic controls on water vapor deuterium excess in the marine boundary layer of the North Atlantic based on 500 days of in situ, continuous measurements. *Atmospheric Chemistry and Physics*, *14*(15), 7741–7756. https://doi.org/10.5194/acp-14-7741-2014

Steen-Larsen, H. C., & Wahl, S. (2021a). *2m processed sensible and latent heat flux, friction velocity and stability at EastGRIP site on Greenland Ice Sheet, summer 2019*. PANGAEA. https://doi.org/10.1594/PANGAEA.928827

Steen-Larsen, H. C., & Wahl, S. (2021b). *2m, raw 20Hz data of wind, sonic temperature and humidity at EastGRIP site on Greenland Ice Sheet, summer 2019*. PANGAEA. https://doi.org/10.1594/PANGAEA.931439

Steen-Larsen, H. C., & Wahl, S. (2021c). *2m wind speed, wind direction and air temperature at EastGRIP site on Greenland Ice Sheet, summer 2019*. PANGAEA. https://doi.org/10.1594/PANGAEA.925618

Steen-Larsen, H. C., & Wahl, S. (2021d). *Calibrated 2m stable water vapor isotope data from EastGRIP, Greenland Ice Sheet summer 2019*. PANGAEA. https://doi.org/10.1594/PANGAEA.928823

Swinbank, W. C. (1951). The measurement of vertical transfer of heat and water vapor by eddies in the lower atmosphere. *Journal of Meteorology*, *8*(3), 135–145. https://doi.org/10.1175/1520-0469(1951)008⟨0135:TMOVTO⟩2.0.CO;2

Trenberth, K. E., Smith, L., Qian, T., Dai, A., & Fasullo, J. (2007). Estimates of the global water budget and its annual cycle using observational and model Data. *Journal of Hydrometeorology*, *8*(4), 758–769. https://doi.org/10.1175/JHM600.1

van den Broeke, M. R., Smeets, C. J. P. P., & van den Wal, R. S. W. (2011). The seasonal cycle and interannual variability of surface energy balance and melt in the ablation zone of the west Greenland ice sheet. *The Cryosphere*, *5*(2), 377–390. https://doi.org/10.5194/tc-5-377-2011

Van Dijk, A. (2002). Extension to 3D of "the effect of line averaging on scalar flux measurements with a sonic anemometer near the surface" by Kristensen and Fitzjarrald. *Journal of Atmospheric and Oceanic Technology*, *19*(1), 80–82. https://doi.org/10.1175/1520-0426(2002)019⟨0080:ETOTEO⟩2.0.CO;2

van Dijk, A., Moene, A. F., & de Bruin, H. A. R. (2004). The principles of surface flux physics: Theory, practice and description of the ECPACK library. In Internal, R. (Ed.), (No. 2004/1). Wageningen, The Netherlands: Meteorology and Air Quality Group, Wageningen University.

Van Geldern, R., & Barth, J. A. (2012). Optimization of instrument setup and post-run corrections for oxygen and hydrogen stable isotope measurements of water by isotope ratio infrared spectroscopy (IRIS). *Limnology and Oceanography: Methods*, *10*, 1024–1036. https://doi.org/10.4319/lom.2012.10.1024

Wahl, S., & Steen-Larsen, H. C. (2021). *2m isotopologue fluxes at EastGRIP site on Greenland Ice Sheet, summer 2019*. PANGAEA. https://doi.org/10.1594/PANGAEA.931425

Webb, E. K., Pearman, G. I., & Leuning, R. (1980). Correction of flux measurements for density effects due to heat and water vapour transfer. *Quarterly Journal of the Royal Meteorological Society*, *106*(447), 85–100. https://doi.org/10.1002/qj.49710644707

Wei, Z., Yoshimura, K., Okazaki, A., Kim, W., Liu, Z., & Yokoi, M. (2015). Partitioning of evapotranspiration using high-frequency water vapor isotopic measurement over a rice paddy field. *Water Resources Research*, *51*(5), 3716–3729. https://doi.org/10.1002/2014WR016737

Welp, L. R., Lee, X., Kim, K., GRriffis, T. J., Billmark, K. A., & Baker, J. M. (2008). δ^{18}O of water vapour, evapotranspiration and the sites of leaf water evaporation in a soybean canopy. *Plant, Cell & Environment*, *31*(9), 1214–1228. https://doi.org/10.1111/j.1365-3040.2008.01826.x

Weng, Y., Touzeau, A., & Sodemann, H. (2020). Correcting the impact of the isotope composition on the mixing ratio dependency of water vapour isotope measurements with cavity ring-down spectrometers. *Atmospheric Measurement Techniques*, *13*(6), 3167–3190. https://doi.org/10.5194/amt-13-3167-2020

Wohlfahrt, G., Hörtnagl, L., Hammerle, A., Graus, M., & Hansel, A. (2009). Measuring eddy covariance fluxes of ozone with a slow-response analyser. *Atmospheric Environment*, *43*(30), 4570–4576. https://doi.org/10.1016/j.atmosenv.2009.06.031

Yakir, D., & Wang, X.-F. (1996). Fluxes of CO_2 and water between terrestrial vegetation and the atmosphere estimated from isotope measurements. *Nature*, *380*. https://doi.org/10.1038/380515a0

Paper II

The role of sublimation as a driver of climate signals in the water isotope content of surface snow: Laboratory and field experimental results

Abigail G. Hughes, Sonja Wahl, Tyler R. Jones, Alexandra Zuhr, Maria Hörhold, James W. C. White, Hans Christian Steen-Larsen
The Cryosphere, **15** (2021)

The Cryosphere, 15, 4949–4974, 2021
https://doi.org/10.5194/tc-15-4949-2021

The Cryosphere Open Access EGU

The role of sublimation as a driver of climate signals in the water isotope content of surface snow: laboratory and field experimental results

Abigail G. Hughes[1], Sonja Wahl[2], Tyler R. Jones[1], Alexandra Zuhr[3,4], Maria Hörhold[5], James W. C. White[1], and Hans Christian Steen-Larsen[2]

[1]Institute of Arctic and Alpine Research, University of Colorado Boulder, Boulder, Colorado, USA
[2]Geophysical Institute, University of Bergen and Bjerknes Centre for Climate Research, Bergen, Norway
[3]Alfred-Wegener-Institut Helmholtz-Zentrum für Polar- und Meeresforschung,
Research Unit Potsdam, Telegrafenberg A45, 14473 Potsdam, Germany
[4]Institute of Geosciences, University of Potsdam, Karl-Liebknecht-Str. 24–25, 14476 Potsdam-Golm, Germany
[5]Alfred-Wegener-Institut Helmholtz-Zentrum für Polar- und Meeresforschung,
Research Unit Bremerhaven, 27568 Bremerhaven, Germany

Correspondence: Abigail G. Hughes (abigail.hughes@colorado.edu)

Received: 11 March 2021 – Discussion started: 14 April 2021
Revised: 28 August 2021 – Accepted: 8 September 2021 – Published: 25 October 2021

Abstract. Ice core water isotope records from Greenland and Antarctica are a valuable proxy for paleoclimate reconstruction, yet the processes influencing the climate signal stored in the isotopic composition of the snow are being challenged and revisited. Apart from precipitation input, post-depositional processes such as wind-driven redistribution and vapor–snow exchange processes at and below the surface are hypothesized to contribute to the isotope climate signal subsequently stored in the ice. Recent field studies have shown that surface snow isotopes vary between precipitation events and co-vary with vapor isotopes, which demonstrates that vapor–snow exchange is an important driving mechanism. Here we investigate how vapor–snow exchange processes influence the isotopic composition of the snowpack. Controlled laboratory experiments under forced sublimation show an increase in snow isotopic composition of up to 8 ‰ δ^{18}O in the uppermost layer due to sublimation, with an attenuated signal down to 3 cm snow depth over the course of 4–6 d. This enrichment is accompanied by a decrease in the second-order parameter d-excess, indicating kinetic fractionation processes. Our observations confirm that sublimation alone can lead to a strong enrichment of stable water isotopes in surface snow and subsequent enrichment in the layers below. To compare laboratory experiments with realistic polar conditions, we completed four 2–3 d field experiments at the East Greenland Ice Core Project site (northeast Greenland) in summer 2019. High-resolution temporal sampling of both natural and isolated snow was conducted under clear-sky conditions and demonstrated that the snow isotopic composition changes on hourly timescales. A change of snow isotope content associated with sublimation is currently not implemented in isotope-enabled climate models and is not taken into account when interpreting ice core isotopic records. However, our results demonstrate that post-depositional processes such as sublimation contribute to the climate signal recorded in the water isotopes in surface snow, in both laboratory and field settings. This suggests that the ice core water isotope signal may effectively integrate across multiple parameters, and the ice core climate record should be interpreted as such, particularly in regions of low accumulation.

1 Introduction

Water isotope records in polar ice cores have been used as a proxy to reconstruct local temperature and evaporation source conditions dating back hundreds of thousands of

years. The isotope–paleothermometer relationship used to interpret ice core water isotope records is based on the assumption that the observed stable water isotope signal is primarily composed of the input signals from individual precipitation events (Johnsen et al., 2001; Werner et al., 2011; Sime et al., 2019). However, this approach does not take into account the effects of post-depositional surface exchange processes such as vapor exchange and wind-driven redistribution. Recent field studies have shown that the isotopic composition of surface snow varies in parallel with atmospheric water vapor without occurrence of newly precipitated snow (Steen-Larsen et al., 2014) and can change on sub-diurnal timescales (Ritter et al., 2016; Casado et al., 2018), suggesting a coupling between the atmospheric water vapor and surface snow through isotope exchange.

The primary water isotope signal (i.e., δ^{18}O, δD) in polar precipitation closely reflects the temperature gradient experienced by an air mass from source to deposition and ultimately the temperature of condensation in the cloud (Dansgaard, 1964; Dansgaard et al., 1973; Jouzel and Merlivat, 1984; Jouzel et al., 1997). Therefore, seasonal differences in the isotopic composition of the precipitation have historically been assumed to be the primary contributor to observed annual cycles in the ice core. In addition, the second-order parameter deuterium excess (d-excess $= \delta\mathrm{D} - 8 \cdot \delta^{18}\mathrm{O}$) results from kinetic fractionation due to molecular differences between the movement of oxygen and hydrogen in the hydrologic cycle. Traditionally, it is thought that the ice core d-excess signal is driven by the evaporation conditions at the moisture source to an ice core site (Merlivat and Jouzel, 1979).

There are several processes known to influence the climate signal recorded in ice core water isotopes. First, precipitation may not take place continuously throughout the year, and precipitation intermittency and seasonal bias influence the isotope record (Werner et al., 2000; Casado et al., 2018; Münch et al., 2017; Münch and Laepple, 2018; Zuhr et al., 2021). Second, surface processes such as snowdrift erosion and redistribution may hamper the consecutive deposition and burial of snow layers through time, leading to a lack of a continuous time record. For example, wind-drifted snow can form large persistent surface features/dunes with variations in the snow density and height, altering the isotope signal spatially and vertically. This issue has been approached by stacking multiple cores or snow pit profiles in order to resolve the climate signal (Casado et al., 2018; Münch et al., 2017; Münch and Laepple, 2018; Zuhr et al., 2021). Third, after deposition the snow and firn undergo vapor diffusion. Unconsolidated snow grains have open pathways between pore spaces, allowing for vapor transport and mixing. Diffusion attenuates the seasonal signal and acts as a smoothing function, and is well-constrained (Whillans and Grootes, 1985; Cuffey and Steig, 1998; Johnsen et al., 2000; Jones et al., 2017a). It has been shown that diffusion may smooth across noise and gaps from intermittent precipitation events, leading to the observed isotope records that imply continuous seasonal temperature changes (Laepple et al., 2016, 2018). However, a remaining missing link between the accumulated signal and the ice core record is a well-defined understanding of snow–air exchange. Continuous isotope exchange between the snow surface and water vapor is known to influence the recorded climate signal, yet the effects are still not fully resolved.

While it was previously assumed that sublimation of snow and ice occurs layer by layer and does not cause isotopic fractionation of remaining ice (Dansgaard, 1964), recent studies have shown this is not the case and that snow is subjected to isotopic fractionation due to sublimation (Ekaykin et al., 2009; Sokratov and Golubev, 2009; Ebner et al., 2017; Madsen et al., 2019). In the accumulation zone of ice sheets, the typical region for ice core drill sites, the snow surface and lower atmosphere are coupled through the continuous humidity exchange in the form of sublimation and deposition of water molecules and isotopologues (Wahl et al., 2021). This interaction continuously imprints on the snow surface δ^{18}O and δD isotopic composition and suggests an interpretation of snow isotopes as an integrated climate record, rather than a precipitation signal only (Steen-Larsen et al., 2014). As sublimation is a non-equilibrium process comparable to evaporation, it likewise influences the surface snow d-excess, questioning the interpretation of d-excess as a source region signal.

In this study, we investigated how the isotope signal of surface snow is altered over multiple days via post-depositional exchange between the snow and the near-surface atmospheric water vapor. We utilized multiple types of experiments including both controlled laboratory experiments and in situ field observations. First, we performed a simple laboratory experiment to observe the effects of sublimation under dry air in a controlled environment. Next, we performed two field experiments in northeast Greenland to (1) analyze the change of snow of known isotopic composition under characteristic polar conditions and (2) document the isotope signal evolution of undisturbed snow as it naturally exists at the ice sheet surface. For all experiments, continuous atmospheric vapor measurements were made above the snow surface to complement the snow sampling and allow us to observe ongoing snow–vapor isotope exchange. Thus, these laboratory and field experiments are the first to measure both δ^{18}O and δD at fine vertical and temporal resolution for multiple depths across several multi-day experimental periods under differing environmental conditions, with simultaneous continuous measurements of atmospheric vapor δ^{18}O and δD. In the case of the laboratory experiments presented, the vapor isotopic composition can directly be interpreted as the isotopic composition of the flux, since the experimental set-up fulfills the closure assumption and therefore allows a direct comparison of flux and snow isotopic composition. With these data we demonstrate the importance of post-depositional processes on the snow surface water isotope sig-

Table 1. Overview of all experiments conducted. Eight laboratory experiments were completed, with L1–L5 completed at the University of Colorado Boulder and L6–L8 completed at the University of Copenhagen. Four field experiments (F1–F4) were completed at the East Greenland Ice Core Project field site. Field experiments included associated field box samples (FB2–FB4) and field surface samples (FS1–FS4). For L experiments, the controlled settings of the individual experiment runs are given, whereas for the field experiments, the environmental conditions are listed. The mean sublimation rate for field (F–FB/FS) experiments was calculated for all observations in which the latent heat flux (LHF) was positive (i.e., directed away from the surface). The median peak sublimation rate in June and July 2019 was 250 $\mathrm{g\,m^{-2}\,d^{-1}}$, and maximum observed peak sublimation rates were 600–700 $\mathrm{g\,m^{-2}\,d^{-1}}$.

Experiment type	Experiment name	Mean flow rate (liters per minute)	Mean temperature (°C)	Mean sublimation rate (LHF > 0) ($\mathrm{g\,m^{-2}\,d^{-1}}$)	Peak sublimation rate (LHF > 0) ($\mathrm{g\,m^{-2}\,d^{-1}}$)	Starting snow δ^{18}O (‰)	Duration
Laboratory	L1*	2	−12	428.4	–	−20	5 d
	L2	3	−12	428.4	–	−20	5 d
	L3	3	−12	508.4	–	−20	5 d
	L4	4	−12	568.8	–	−20	5 d
	L5*	5	−12	692.3	–	−20	5 d
	L6*	5	−9	779.9	–	−28	6 d
	L7	5	−8	965.0	–	−28	4 d
	L8	5	−5	1329.3	–	−28	5 d
Field box	F2–FB2	–	−7.5	157.5	386.1	−26.1	41 h
	F3–FB3	–	−10.5	218.5	712.9	−25.2	39 h
	F4–FB4	–	−12.7	130.3	279.7	−25.1	51 h
Field surface	F1–FS1	–	−7.6	171.6	619.6	–	57 h
	F2–FS2	–	−7.5	157.5	386.1	–	41 h
	F3–FS3	–	−10.5	218.5	712.9	–	39 h
	F4–FS4	–	−12.7	130.3	279.7	–	51 h

* Stars denote the subset of laboratory experiments selected for further discussion.

nal, and we provide better constraints on transfer functions between the atmospheric conditions including water vapor isotopic composition and the climate signal recorded in the surface snow, with implications for interpretation of ice core records.

2 Methods

We investigated through a combination of laboratory and field experiments (Table 1) the influence of phase changes (i.e., sublimation and vapor deposition) on the snow surface isotopic composition. Laboratory experiments were run in a controlled environment, which allowed us to isolate the effects of idealized sublimation conditions. The sublimation rate was varied between different experiment runs through adjusting temperature and the flow rate of dry air. Complementary field experiments provided greater insight as to how laboratory findings are consistent with field observations occurring at the surface of the ice sheet. The field experiments were run under close-to-ideal conditions, which limited the duration of the experiments to intervals of time with clear-sky conditions. In return, the sampling resolution was increased for the field experiments.

Throughout this work, water isotope measurements are reported in standard delta notation given in per mil (‰) (Craig, 1961):

$$\delta_i = \left(\frac{R_i}{R_{\mathrm{VSMOW}}} - 1\right), \tag{1}$$

where i refers to δD or δ^{18}O, and R is the ratio of heavy to light isotopes, such that $R_{^{18}\mathrm{O}} = [^1\mathrm{H}_2^{18}\mathrm{O}]/[^1\mathrm{H}_2^{16}\mathrm{O}]$ and $R_{\mathrm{D}} = [^2\mathrm{H}^1\mathrm{H}^{16}\mathrm{O}]/[^1\mathrm{H}_2^{16}\mathrm{O}]$, where ^{2}H is referred to as D. Samples were referenced to Vienna Standard Mean Ocean Water (VSMOW).

2.1 Laboratory experimental methods (L experiments)

For the laboratory experiments (L1–L8), dry air was circulated over boxes containing isotopically homogeneous snow samples that were kept at fixed temperatures (Fig. 1a). An experimental chamber was designed that consisted of an inner plexiglass box, which sat inside an outer plywood box (2.7 cm thick) used for temperature regulation. The entire setup was placed in a large freezer, with the inner temperature moderated by a PID-controlled (Omega CN7800; 50 W) cable heater wrapped around the inside of the plywood box. Dry air was produced with a generator (Puregas CDA-10) and run through Drierite desiccant, resulting in humidity < 100 ppm (i.e., < 5 % RH). The amount of dry air

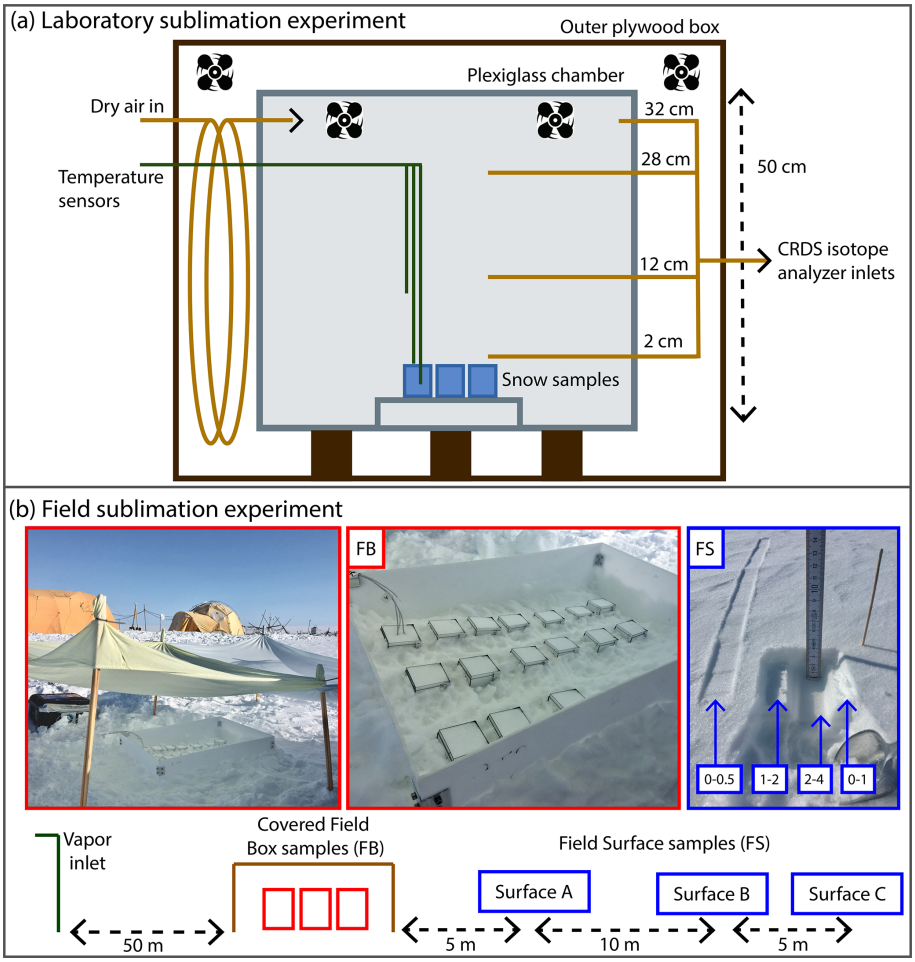

Figure 1. **(a)** Diagram of laboratory experiment setup. A plexiglass chamber was placed within an outer plywood box in a freezer, and dry air regulated by a mass flow controller was pumped into the inner box above four to six homogeneous snow samples, placed on a small shelf to allow airflow. Fans inside the box maintained air circulation. Three temperature sensors were placed at different heights, and continuous CRDS measurements of the vapor were made at four inlet heights (2, 12, 28, 32 cm above the snow surface). **(b)** Schematic diagram of the field sampling setup at EastGRIP. From left to right: atmospheric vapor at 10 cm above the snow surface was continuously measured by a CRDS. Homogenous box samples (FB; red) were partially buried and covered, and temperature sensors were placed in the atmosphere, snow surface, and below the surface. Three surface sampling locations (FS A, B, C; blue) were spaced 5–10 m apart, with samples taken at every time interval at each location. A photo example of one sample is shown, in which the left-most sample is the 0–0.5 cm sample, while the intervals for 0–1, 1–2, and 2–4 cm can be seen in the small pit.

circulated in the box was regulated by a HORIBA SEC-4400 mass flow controller, and two continuously running computer fans at the top of the chamber maintained mixed air. In order to maintain positive pressure in the box, flow rates less than $2\,\mathrm{L\,min^{-1}}$ could not be used. Four to six small plastic boxes ($5.7 \times 5.7 \times 7.6$ cm) were filled with snow that was well-mixed and sifted so that the snow grain size (1–2 mm) and isotope value were homogenous, and the initial mass of each sample was measured. The samples were placed at the bottom of the inner box, on a shelf with underlying airflow to prevent a temperature gradient within the samples. Every 24 h, one sample was removed, and the mass of that sample was measured. The boxes could be opened on one side, and a metal spatula was used to collect snow samples with 5 mm resolution to obtain a vertical isotope profile. Snow samples were transferred to 20 mL HDPE scintillation vials for storage and kept frozen until analysis, at which time they were melted and immediately transferred to 2 mL vials. Liquid samples were then analyzed using a Picarro L2130-*i* cavity ring-down spectrometer (CRDS), in conjunction with a CTC Analytics HTC PAL autosampler injection system and Picarro V1102-*i* vaporization module. Each sample was measured with six injections, and the reported value is based on the average of the last three injections to remove memory effects (Schauer et al., 2016). Every analysis run of 40 samples also included three known water isotope standards bracketing the sample isotope values for calibration (e.g., as done

in Jones et al., 2017b). The resulting discrete measurements have uncertainties of 0.1 ‰ δ^{18}O and 1 ‰ δD.

For the duration of all experiments, several additional parameters were monitored. A Picarro L2130-*i* CRDS was continuously measuring ($\sim$ 1 Hz) vapor (humidity, δ^{18}O, δD) from four heights above the snow surface (2, 12, 28, 36 cm), cycling between each level every hour. The second-order parameter d-excess (d-excess $= \delta D - 8 \cdot \delta^{18}O$) was also calculated from those measurements. Three Pico Technologies PT-104 data logger temperature sensors were placed in the box to record continuously: one 10 cm above the snow surface, one on the surface of the snow, and one $\sim$ 4 cm below the snow surface.

Two sets of experiments were conducted with varying sublimation rates controlled by adjusting temperature and dry air flow rate (Table 1). For five experiment runs, the temperature was held steady at -12 °C while the dry air flow rate was changed between a constant flow rate of 2, 3, 4, and 5 L min^{-1} (L1–L5, respectively). These experiments used snow from Boulder, Colorado, with a starting value of approximately -20 ‰ δ^{18}O, and they were carried out at the Institute of Arctic and Alpine Research at the University of Colorado Boulder. Three additional experiment runs had the temperature of the inner box held constant at -9, -8, or -5 °C (L6–L8, respectively), and the flow rate of dry air above the snow samples was held steady at 5 L min^{-1}. These experiments used snow from the East Greenland Ice Core Project field site with a starting δ^{18}O value of approximately -28 ‰ and were completed at the section for Physics of Ice, Climate and Earth at the University of Copenhagen. In total, eight experiments were completed.

2.2 Field experimental methods (F experiments)

Field experiments were conducted at the East Greenland Ice Core Project (EastGRIP) field camp in July 2019. EastGRIP is located at 75.6268° N, 35.9915° W in the accumulation zone of the Greenland Ice Sheet. In July 2019, the meteorological conditions at the site were characterized by low temperatures (mean -9.0 °C, measured at 2 m above the snow surface) and high relative humidities (mean 91 % RH with respect to ice), leading to an average specific humidity of 2.3 g kg^{-1}. Positive temperatures (> 0 °C) were very rare, and we observed a positive change in snow height of about 2 cm during July.

The goal of in situ field experiments was to characterize interactions between the snow surface and near-surface atmospheric vapor on short timescales and to monitor the evolution of the isotopic signal in the snow. To do so, we selected four 2–3 d experimental periods (field experiments, F1–F4) during which changes in water isotopes in the snow surface and atmospheric vapor were measured simultaneously through three sample types (Fig. 1b): (1) discrete box samples (field box, FB2–FB4), (2) discrete surface samples (field surface, FS1–FS4), and (3) continuous vapor measurements at 10 cm above the snow surface. Each experiment was conducted during a period of good weather, such that precipitation or windblown snow would not bias results. This required air temperatures below freezing, sustained wind speeds below 5–6 m s^{-1}, and no precipitation.

2.2.1 Discrete box samples (FB experiments)

At the beginning of each period, 14–16 boxes ($5.7 \times 5.7 \times 7.6$ cm) were filled with well-mixed surface snow. Sampling boxes were partially buried in the snow surface, with the top of the sample box 1–2 cm above the surrounding snow surface to minimize any risk of contamination from windblown snow. Samples were also protected from direct overhead sunlight using a light-colored thin cloth covering. Although this deviates from natural conditions in which the snow surface is exposed and not covered, this modification was necessary to prevent solar heating of the sample boxes which may have led to melt of the snow samples. A Pico Technologies PT-104 data logger was used to measure temperature during the experimental period, with four sensors placed in an additional snow-filled box. The logger continuously recorded temperatures of the ambient air, snow surface, 3 cm below surface, and 6 cm below surface.

One box was collected every 3 h; each box was equipped with one removable side so that a vertical profile of the snow was accessible. Snow samples were taken at intervals 0–0.5, 0.5–1, 1–1.5, 1.5–2.5, and 2.5–4.5 cm from the surface using a spatula. The snow samples were transferred to a 20 mL HDPE scintillation vial for storage. Discrete samples are referred to as field box (FB) samples, with each experiment designated FB2, FB3, and FB4 (Table 1).

2.2.2 Discrete surface samples (FS experiments)

In addition to the isolated boxes, every 3 h we collected samples from a clean, undisturbed surface snow area at the same time as the boxes were sampled. Because wind effects can lead to variability in snow surface density and isotopic value, surface samples were collected from three locations, designated sites A, B, and C. The distance from A to B was 10 m and from B to C was 5 m (Fig. A1). At each surface location, samples were collected from 0–0.5, 0–1, 1–2, and 2–4 cm below the surface (Fig. 1b). The snow samples were transferred to a 20 mL HDPE scintillation vial for storage. Discrete surface samples are referred to as field surface (FS) samples, with each experiment designated FS1, FS2, FS3, and FS4 (Table 1).

All snow samples (both field box (FB) and field surface (FS)) were kept frozen after collection and were measured at the Stable Isotope Lab at the University of Colorado Boulder. Samples were analyzed using a Picarro L2130-*i*, in conjunction with a CTC Analytics HTC PAL autosampler injection system and Picarro V1102-*i* vaporization module. The same measurement protocol was used as described in Sect. 2.1.

2.2.3 Continuous vapor measurements

Continuous atmospheric water vapor isotope measurements were made at 10 cm above the snow surface, ∼ 50 m away from the FS sampling site so as not to be contaminated by snow sampling activity. The measurements were made with a Picarro L2130-*i* CRDS, which was kept in a temperature-controlled tent and measured humidity, δ^{18}O, and δD. Using a diaphragm pump (KNF model DC-B 12V UNMP850), air was pumped through a ∼ 12 m long heated copper tube to the analyzer (similar to the setup described in Madsen et al., 2019).

Four types of calibrations were performed on the water vapor isotope measurements of the CRDS, similar to the calibration protocol described in Steen-Larsen et al. (2013): (1) humidity calibration, (2) humidity-isotope response calibration, (3) VSMOW-VSLAP scale calibration, and (4) drift calibration. All calibrations are applied to water vapor isotope measurements in both laboratory and field experiments. Details of the calibration setup specific to laboratory and field experiments are described in Appendix B.

Latent heat flux (LHF) was also continuously measured during the field campaign using a Campbell Scientific IRGASON eddy-covariance (EC) system. The two-in-one EC system measured humidity and three-dimensional wind at a sampling frequency of 20 Hz in the same sample volume at 2.15 m above the snow surface. LHF values were computed for 30 min intervals using Campbell Scientific's software EasyFlux™ adjusted for sublimation conditions and accounting for wind rotation and frequency corrections. Latent heat flux is related to sublimation: LHF = sublimation rate $\cdot\,\lambda$, where λ is the latent heat of sublimation at 0 °C, 2834 kJ kg^{-1}; a positive LHF indicates sublimation, and negative LHF indicates vapor deposition.

3 Results

3.1 Laboratory experiments

3.1.1 Sublimation rate

The mean sublimation rate for each laboratory experiment is calculated based on mass loss with time and surface area, reported in Table 1. Sublimation rate does not significantly change with time and is shown for each experiment in Fig. A8. The mass of each box was measured at the onset of the experiment and immediately before each sampling. Since we only push dry air into the chamber, the experiment relates only to sublimation processes. We find that the LHF associated with sublimation varies from approximately 15 W m^{-2} (Experiment L1 at 2 L min^{-1} and −12 °C) to 44 W m^{-2} (Experiment L8 at 5 L min^{-1} and −3 °C).

Latent heat flux values in laboratory experiments are comparable to the peak daytime sublimation fluxes observed during the field campaign, albeit the average LHF during the sublimation period in the field was substantially smaller than observed during the laboratory experiments (Table 1). The mean daytime positive LHF was ∼ 5 W m^{-2}, and the maximum LHF observed was ∼ 23 W m^{-2}. Therefore, laboratory experiments can be considered representative of processes occurring during peak daytime conditions in the field.

3.1.2 Snow measurements

Eight laboratory experiments (L1–L8) were completed, with temperature, dry air flow rate, and sublimation rate documented in Table 1. In all experiments, the surface snow experiences substantial isotopic changes, with δ^{18}O increasing by up to 8 ‰ and d-excess decreasing by over 25 ‰. δ^{18}O and d-excess signals for all experiments are shown in Fig. A10, with a subset of experiments shown in Fig. 2. Changes in the isotope signal are observed to propagate several centimeters into the snowpack due to diffusion over 4–6 d, driven by the induced sublimate-related isotope change at the surface. The rate of change is calculated for the mean isotope value for each day of sampling, ranging from 0.25–0.70 ‰ d^{-1} for δ^{18}O and 0.66–2.64 ‰ d^{-1} for d-excess (Fig. A11a and b). There is a strong relationship between mass loss and isotope values, with an average $R^2 = 0.90$ for daily mean box δ^{18}O vs. mass loss for experiments L1–L8. The relationship between sublimation rate and δ^{18}O rate of change has $R^2 = 0.13$, and sublimation rate vs. d-excess rate of change has $R^2 = 0.54$ (Fig. A11c).

Because δ^{18}O reflects equilibrium fractionation and d-excess is influenced by kinetic fractionation, a comparison of these variables provides insight into the extent of fractionation effects occurring during sublimation. The slope of d-excess vs. δ^{18}O is calculated for samples within each box (Fig. 3a), and the slope with time over the duration of each experiment is shown in Fig. 3b. The slope ranges from −0.91 ‰ to −3.57 ‰ d-excess/‰ δ^{18}O and decreases over the course of all experiments. In general, there is a decrease in slope associated with an increase in sublimation rate, as indicated by the color scale reflecting sublimation rate in Fig. 3b and as shown in Fig. A9.

3.1.3 Vapor measurements

During all laboratory experiments, a Picarro L2130-*i* CRDS was used to continuously measure vapor in the chamber at 2, 12, 28, and 36 cm, cycling through each height for 1 h measurement periods. We exclude the first 20 min of each measurement period to remove memory effects from valve changes. Figure 4 shows an example of temperature and vapor data for experiment L5, including the 28 and 32 cm levels, which represent sublimated vapor which is more well-mixed than that immediately above the snow surface. Dry air pumped into the top of the box is mixed using a set of fans creating turbulence above the snow surface. The vertical differences in humidity and isotopic composition of the air

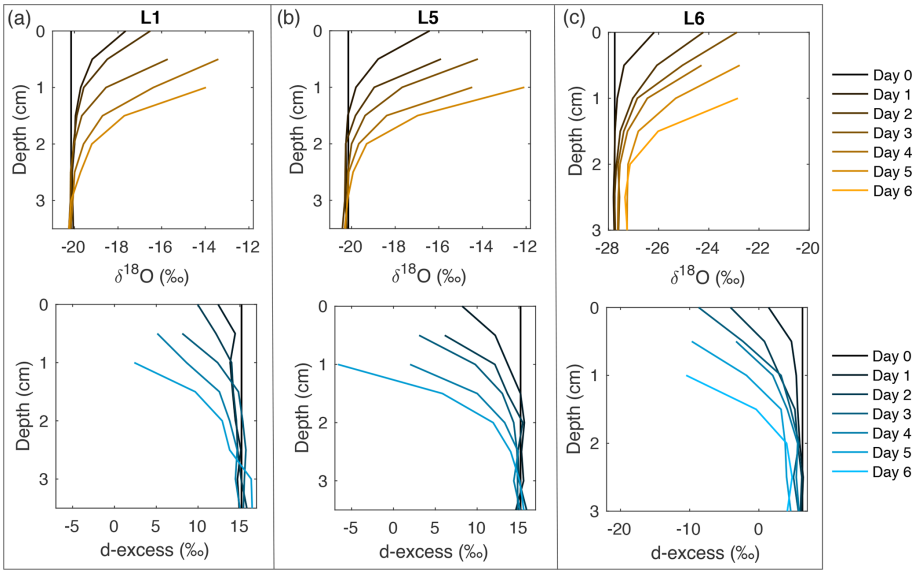

Figure 2. Snow δ^{18}O (top) and d-excess (bottom) vertical profiles from three of the laboratory experiments: **(a)** L1 ($-12\,^{\circ}$C, $2\,\mathrm{L\,min^{-1}}$), **(b)** L5 ($-12\,^{\circ}$C, $5\,\mathrm{L\,min^{-1}}$), and **(c)** L6 ($-9\,^{\circ}$C, $5\,\mathrm{L\,min^{-1}}$). Day 0 (black) represents the initial homogeneous snow sample, with colors progressively moving towards orange (δ^{18}O) and blue (d-excess) with each day of sampling. As each experiment progresses from Day 0 to Day 6, sublimation drives an increase in δ^{18}O and decrease in d-excess, with the greatest change at the snow surface. Similar figures for all laboratory experiments (L1–L8) can be found in Fig. A10.

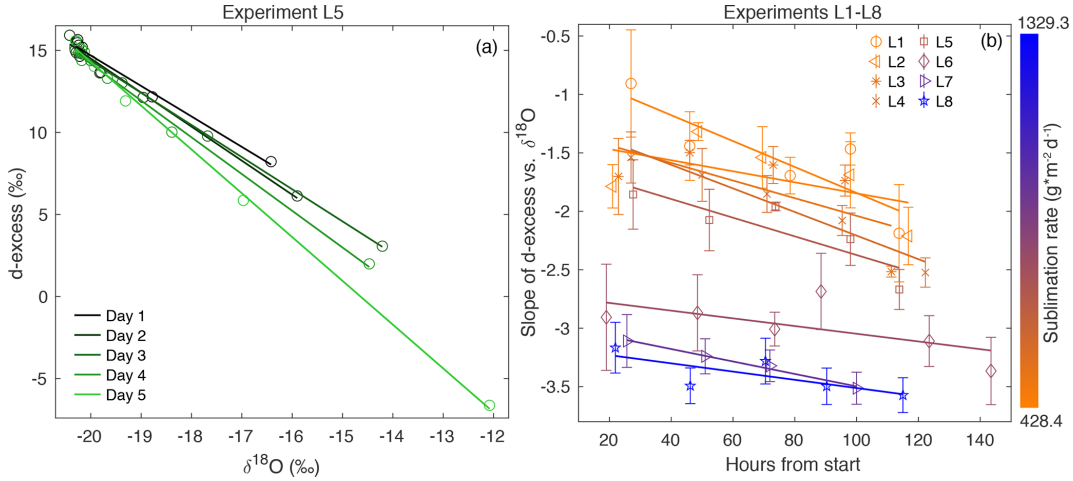

Figure 3. **(a)** d-excess vs. δ^{18}O is shown for the vertical snow profile at each day of sampling in Experiment L5, with a linear regression calculated for each day. This gives a slope of d-excess vs. δ^{18}O, which evolves with time. **(b)** The slope of d-excess vs. δ^{18}O with time is shown for each experiment L1–L8, demonstrating an inverse relationship between sublimation rate and slope of d-excess vs. δ^{18}O. Error bars indicate 95 % confidence intervals for each slope.

in the box (i.e., differences between 28 and 32 cm as seen in Fig. 4) likely indicate that the ventilation is not strong enough to maintain a fully homogeneous air mass in the box, allowing for a slight vertical gradient.

Over the course of each 4–6 d experimental period, we observe several trends in vapor measurements consistent across all laboratory experiments. Humidity decreases with time, due to a reduction in the sublimating surface area each time a snow sample box is removed. Vapor δ^{18}O increases with time, consistent with the increase in δ^{18}O observed in the snow surface. Similarly, d-excess decreases with time in both vapor measurements and the snow surface.

3.2 Field experiments

Four experiments (F1, F2, F3, F4) were carried out during the 2019 EastGRIP field season, with surface samples (FS1, FS2, FS3, FS4) collected for all experiments and box

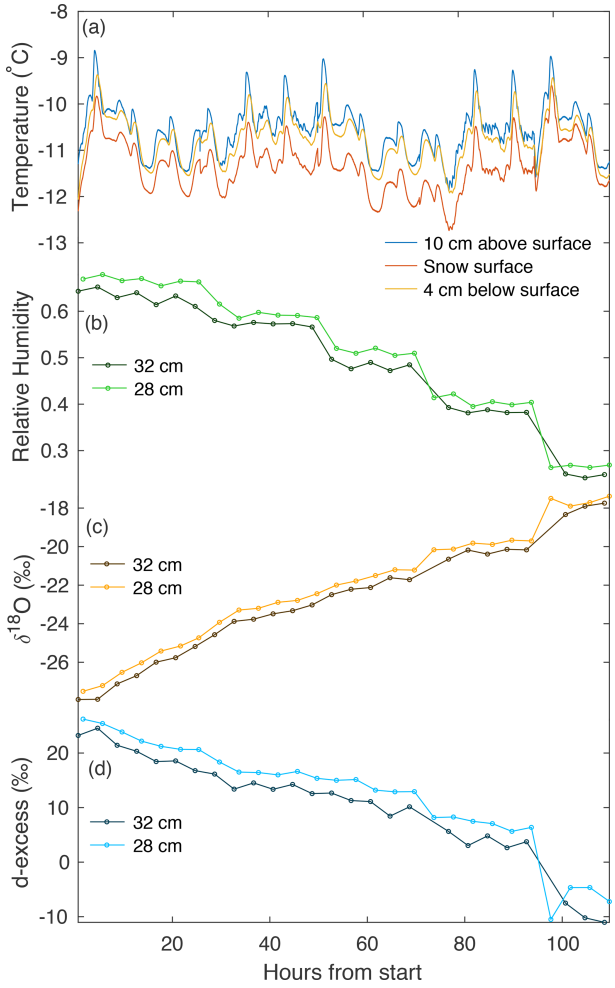

Figure 4. An example of continuous temperature and vapor measurements from experiment L5. **(a)** Three temperature sensors continuously measure at different heights with respect to the snow surface (10 cm above, on the surface, and ∼ 4 cm below the surface). A CRDS measured **(b)** humidity, **(c)** δ^{18}O, and **(d)** d-excess in vapor, continuously cycling at four heights. Panels **(b–d)** show vapor measurements at 28 and 32 cm above the snow surface. We document the average of each measurement period, with the first 20 min excluded to remove memory effects.

samples (FB2, FB3, FB4) collected for three experiments. Each of the four experiments lasted 40–60 h and is supported by continuous measurements of near-surface (10 cm) atmospheric vapor (δ^{18}O, δD, d-excess, humidity), temperature (snow and atmosphere), and LHF. Within each experiment, surface snow and box samples are collected every 3 h. The duration and average environmental conditions of each experiment are reported in Table 1. A compilation of results for measurements of FS, FB, and atmospheric vapor is shown in Fig. 5 and discussed in the next section. All FS and FB samples are shown in Figs. A12 and A13, respectively, with additional vapor measurements shown in Fig. A14.

Table 2. The maximum range of isotope measurements is shown for the mean value of the top (0–0.5 cm) sample for all FS experiments.

Experiment	Range δ^{18}O (‰)	Range d-excess (‰)
FS1	1.44	4.00
FS2	3.00	4.37
FS3	1.84	4.12
FS4	2.06	2.62
Mean	2.09	3.78

3.2.1 Variability in δ^{18}O and d-excess of surface snow

In order to account for horizontal and vertical spatial variability as a result of redistribution of snow in sastrugi and snow dunes, we averaged isotope values across the three surface locations (A, B, C) for each time of sampling and for each depth interval (i.e., one averaged value each for 0–0.5, 0–1, 1–2, and 2–4 cm at every time sampled). In the following figures and tables we focus on the location-averaged values for each sampling time and depth, referred to as FS1, FS2, FS3, and FS4 for each FS surface experiment. Isotope values for all surface locations (A, B, C) are shown together with the averages in Fig. A12. Location-averaged surface snow measurements at all depths across FS1, FS2, FS3, and FS4 range from approximately −30.3 ‰ to −20.7 ‰ δ^{18}O and 4.6 ‰ to 14.3 ‰ d-excess. In all experiments, we consistently observe changes in surface snow isotopic composition on an hourly timescale (Fig. 5). The maximum change in average δ^{18}O of the top surface sample (0–0.5 cm) during a single experiment occurred during FS2, which experienced an enrichment of 3 ‰ δ^{18}O and decrease of 4.37 ‰ in d-excess. This evolution is substantially smaller than the isotopic change observed in vapor measurements, which has ranges of 5 ‰–12 ‰ δ^{18}O over individual experiment periods and ranges for d-excess of 15 ‰–24 ‰. The maximum change in δ^{18}O and d-excess observed within the top surface sample (0.0–5 cm) during each experiment is reported in Table 2.

3.2.2 Relationship between vapor and surface snow

Over the course of all experiments, the minimum atmospheric vapor δ^{18}O value observed is −50 ‰, while the maximum observed value is −33 ‰ (a range of 17 ‰). Within each 40–60 h long experiment, the minimum range of variability observed is about 5 ‰ (F4), and the maximum is about 12 ‰ (F3). Vapor δ^{18}O co-varies with humidity and temperature (Fig. A14), with the lowest δ^{18}O measurements observed during cold, dry conditions. A clear diurnal cycle is observed in vapor measurements for experiments F3 and F4, while experiments F1 and F2 are more variable. The change in atmospheric δ^{18}O associated with the diurnal cycle is much smaller than that observed during synoptic weather changes, similar to the pattern previously observed at the northwest Greenland site NEEM (Steen-Larsen et al.,

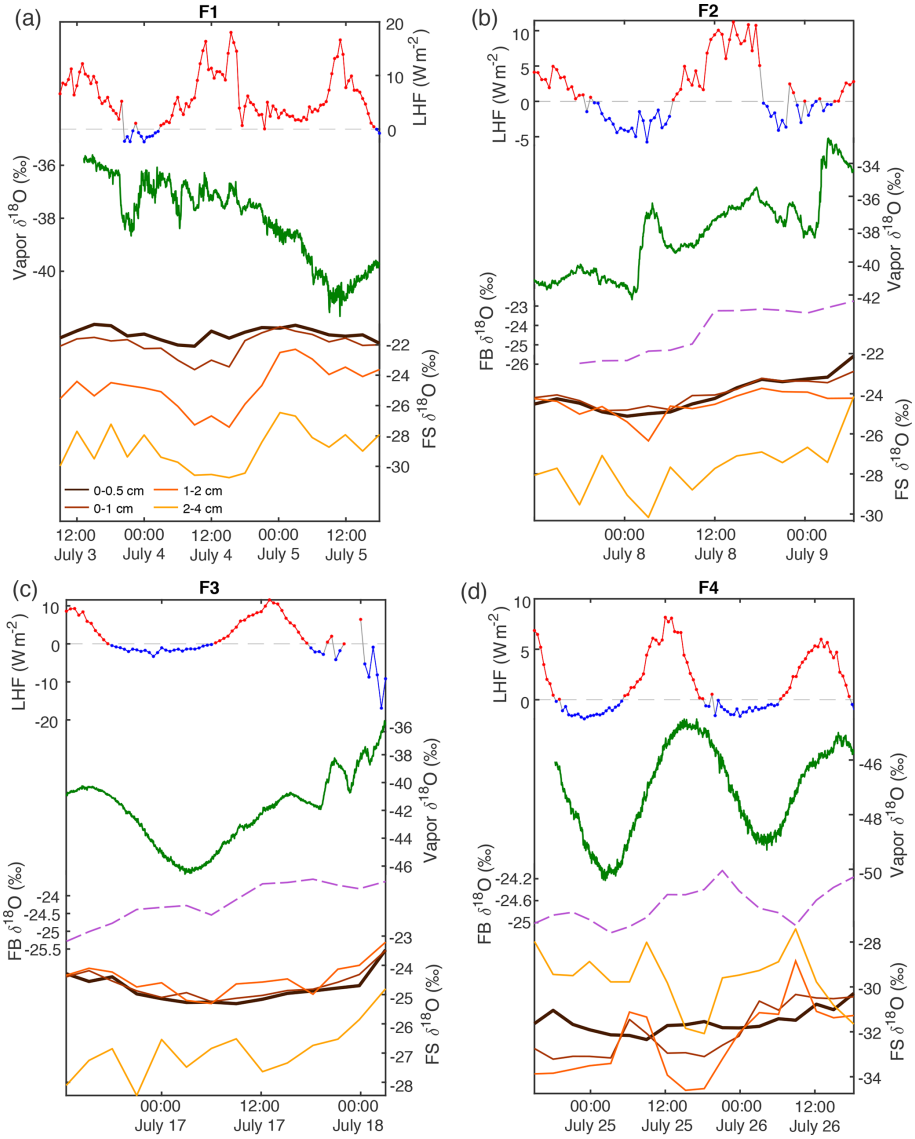

Figure 5. A compilation of data from the 2019 field season shows atmospheric measurements and surface snow samples; from top: latent heat flux (red, positive values; blue, negative values; dashed gray line at 0), δ^{18}O (green) of atmospheric vapor (2 min average) measured at 10 cm, δ^{18}O of the top sample (0–0.5 cm) of the FB box sample (pink dashed), and δ^{18}O of FS snow surface samples. Each snow surface sampling interval shown represents the average of three surface sampling locations (A, B, C) for four different depth intervals: 0–0.5 cm (black), 0–1 cm (red), 1–2 cm (orange), and 2–4 cm (yellow). δ^{18}O of FS samples tends to reflect δ^{18}O in atmospheric vapor, with the relationship strongest in the upper surface samples (Table 3). Additional data including temperature and vapor humidity are shown in Fig. A14.

2014). For example, we observe a strong diurnal cycle in F4 and the first half of F3, both of which have an amplitude of approximately 5 ‰–6 ‰ δ^{18}O; the change between experiments with different synoptic-scale atmospheric conditions is much greater (i.e., a 17 ‰ δ^{18}O range is observed between the maximum value during F2 and the minimum value during F4).

Over clear-sky experimental periods with no precipitation, we observe the δ^{18}O value of surface snow increasing and decreasing on an hourly timescale, corresponding to changes in vapor δ^{18}O (Fig. 5). To compare the evolution of the isotope signal in vapor and snow measurements, the vapor δ^{18}O is downsampled to 3 h resolution to match snow sampling resolution. A statistically significant ($p \leq 0.05$) relationship is observed between δ^{18}O of 0–0.5 cm snow surface samples and atmospheric vapor measurements for experiments FS2, FS3, and FS4, but not FS1 (Fig. A15, Table 3). The lack of a significant correlation in FS1 may be a result of some synoptic-scale weather difference, as it is the only experiment period in which there is a sustained decrease in vapor δ^{18}O, and a diurnal cycle in temperature, LHF, and vapor δ^{18}O is least distinguishable.

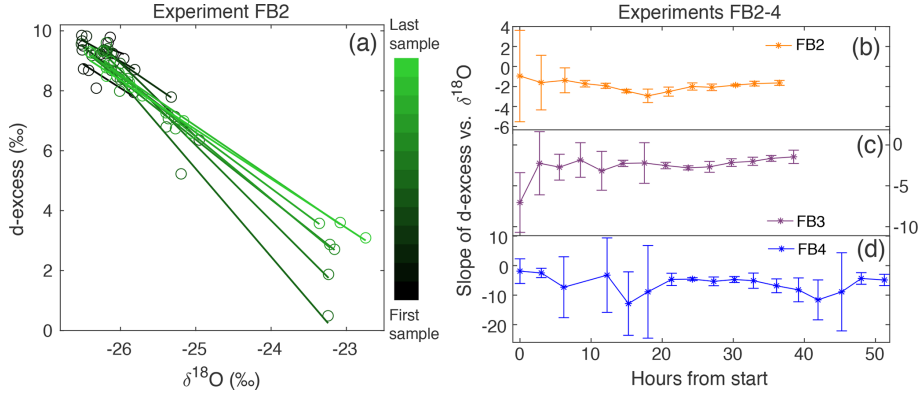

Figure 6. **(a)** d-excess vs. δ^{18}O is shown for the vertical snow profile at each time of sampling in Experiment FB2, with a linear regression calculated for each day. This gives a slope of d-excess vs. δ^{18}O, which evolves with time. The sampling time is indicated by the color scale from black (first sample taken) to light green (last sample taken). The slope of d-excess vs. δ^{18}O with time is shown for experiments **(b)** FB2, **(c)** FB3, and **(d)** FB4. Error bars indicate the 95 % confidence interval for each slope.

Table 3. The R value, P value, and root-mean-square error (RMSE) are documented for the relationship between the top (0–0.5 cm) FS sample δ^{18}O and interpolated vapor δ^{18}O. Significance is determined by $p \leq 0.05$. δ^{18}O of vapor vs. surface samples is shown in Fig. A15.

Experiment	Slope	R value	P value	Significance	RMSE
FS1	0.84	0.22	0.374	No	1.62
FS2	2.16	0.73	0.002	Yes	1.67
FS3	4.73	0.82	0.000	Yes	1.60
FS4	1.56	0.49	0.043	Yes	1.39

4 Discussion

In the laboratory experiments, the snow was sublimating under dry air, resulting in a higher LHF than was observed in a typical field setting. For this reason, laboratory experiments are considered an extreme example of natural processes and can be used to identify and understand the physical processes associated with sublimation which would occur on a slower timescale in nature. Laboratory results show a strong signal of enrichment in the snow surface δ^{18}O, as light isotopes preferentially sublimate from the surface due to fractionation. In addition we observe a strong decrease in the snow surface d-excess. Decreasing d-excess driven by kinetic fractionation is also observed when a body of water evaporates into a sub-saturated atmosphere (Benson and White, 1994; Merlivat and Jouzel, 1979). As a similar effect is observed during sublimation in laboratory experiments, we draw the analogy that this is due to kinetic fractionation. This aligns with previous experimental and modeling studies (Ritter et al., 2016; Ebner et al., 2017) and confirms our hypothesis that the upper several centimeters of the snow surface are rapidly (i.e., on a sub-daily timescale) influenced by equilibrium and kinetic fractionation during sublimation. This contradicts the traditional theory of sublimation, which states that sublimation occurs layer by layer and does not alter the snow isotopic composition, on which ice core paleoclimate water isotope research has been resting (Dansgaard et al., 1973).

In order to interpret these results in the context of natural processes, we consider the results of the field experiments. Previous studies have shown that significant isotopic changes of surface snow are observed (using daily sampling resolution) over periods of time without precipitation, and this is associated with snow metamorphism (Steen-Larsen et al., 2014; Casado et al., 2018). We expand on these findings with higher-resolution field sampling, showing that snow surface δ^{18}O and d-excess change on an hourly basis, which was hypothesized by Madsen et al. (2019); this demonstrates that similar processes to the lab experiments are occurring in a natural environment, albeit less extreme.

To interpret the driving factors in snow isotope changes, we consider differences between the FB box and FS surface samples. The FB samples were covered to shield from direct sunlight and windblown snow and therefore were less likely to experience vapor deposition or frost. Figure 7 shows a comparison of the top 0–0.5 cm sample for all FB and FS experiments with LHF. Over the course of the field experiments, we observe several 6–12 h periods of increasing δ^{18}O in 0–0.5 cm FB and FS samples, primarily during periods of positive LHF and decreasing d-excess; this is indicative of sublimation as suggested by laboratory experiments and model results. We also observe several 6–12 h periods in which the FS δ^{18}O decreases, despite experiments taking place during time periods with no precipitation and minimal wind-drifted snow. Periods of decreasing FS δ^{18}O occur primarily during nighttime hours with negative or low LHF measurements (Fig. 7; negative LHF indicated by shading) and increasing d-excess. There is no significant decrease in δ^{18}O in FB2 and FB3 associated with these periods, while there is a simultaneous decrease in δ^{18}O in FB4 and FS4.

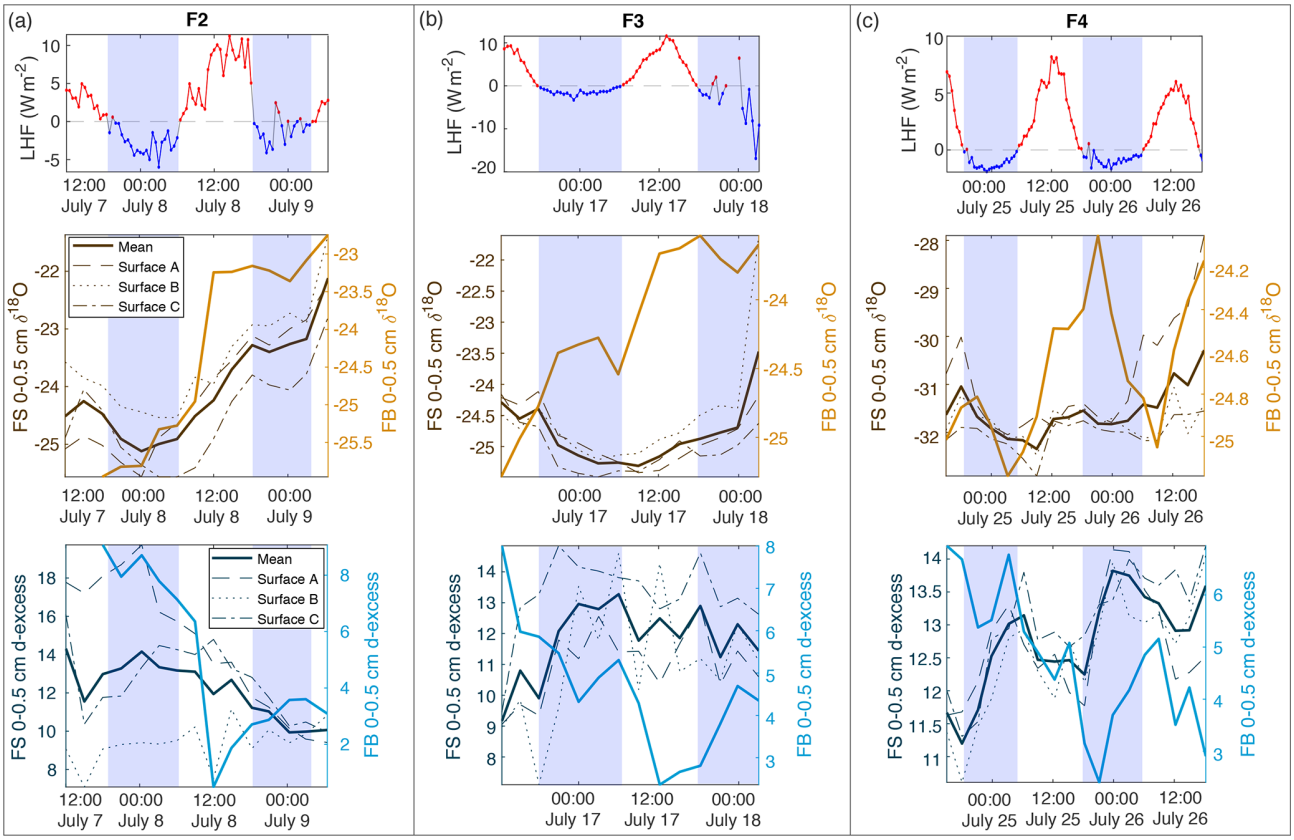

Figure 7. Comparison of latent heat flux (LHF) and 0–0.5 cm samples for mean FS surface samples and FB box samples for **(a)** F2, **(b)** F3, and **(c)** F4. Positive LHF values are indicated in red, and negative LHF values are marked blue with associated shading in all subplots (LHF, δ^{18}O, and d-excess). FS surface snow 0–0.5 cm values are shown in brown (δ^{18}O) and dark blue (d-excess), with each location (A, B, C) designated by dashed lines and the mean of all locations as the bold solid line. FB box snow 0–0.5 cm values are shown in light orange (δ^{18}O) and light blue (d-excess) bold lines.

Additionally, the 0–0.5 cm d-excess decreases substantially in all FB experiments, similar to the signal that was observed due to kinetic fractionation during sublimation in laboratory experiments. In general, the box samples experience less decrease in δ^{18}O than associated FS samples due to minimized vapor deposition during periods of negative LHF and greater total decrease in d-excess due to increased total sublimation across the entire experimental period. This demonstrates that vapor deposition of preferentially isotopically heavy water molecules in the form of frost significantly contributes to the surface snow signal on a rapid timescale (Casado et al., 2018).

There are still several factors in the field experiments which could complicate interpretation of the results. While it is clear in the laboratory experiments that any changes in the snow composition are a direct result of sublimation, we cannot isolate individual processes occurring in field experiments. For example, atmospheric vapor δ^{18}O measurements often vary in phase with LHF, but during some periods (most notably the latter half of F1 and F3) vapor δ^{18}O deviates from the LHF trend. At this stage it is unclear whether LHF, vapor δ^{18}O, or another factor is influencing the snow surface, or whether the snow surface composition is driving vapor δ^{18}O. Additionally, the isotopic composition of deeper snow layers could influence the surface snow due to diffusion. We note a general trend observed in Experiments FS1, FS2, and FS3 in which the deepest surface sample (2–4 cm) has the lowest values for both δ^{18}O and d-excess. However, throughout the duration of FS4, the upper samples (0–0.5, 0–1, and 1–2 cm) have a lower δ^{18}O value than the 2–4 cm sample, likely due to a precipitation event preceding FS4 which may have deposited surface snow with anomalously low δ^{18}O. If there are significant differences between the composition of adjacent snow layers, the surface snow could be influenced by a combination of interstitial diffusion and atmospheric driving forces (i.e., LHF and vapor δ^{18}O). This may also explain some isotope inter-experiment differences between FB and FS results, as FB samples are homogeneous and FS samples have vertical variability in snow isotopic composition.

A key finding from field experiments is that both sublimation and vapor deposition influence the surface snow on an hourly timescale; this is supported by laboratory experi-

ments, demonstrating that sublimation has the ability to influence the mean surface snow isotopic composition in the top 1–2 cm of the snowpack during precipitation-free periods. These changes are occurring faster than the average recurrence of precipitation events and could produce substantial changes in the mean isotopic composition of the upper several centimeters of the snowpack over a long precipitation-free period. This suggests that effects from sublimation and vapor deposition may be superimposed on the precipitation signal, resulting in a snowpack record indicative of multiple parameters including atmospheric conditions, water vapor isotopic composition, condensation temperature (i.e., δ^{18}O), and precipitation source region conditions (i.e., d-excess). The extent to which this occurs is dependent on the accumulation rate at the ice core site, as these processes primarily influence the top few centimeters of the snow column. A site such as SE-Dome (southeast Greenland), which receives 102 cm yr^{-1} of ice equivalent precipitation (Furukawa et al., 2017) (i.e., several meters of snowfall), will be less affected than a drier location with significantly less annual accumulation, such as Antarctic sites like WAIS Divide (24 cm annual accumulation) (Fudge et al., 2016) or South Pole (7.4 cm annual accumulation) (Mosley-Thompson et al., 1999).

To assess the relevance of our results on longer timescales, we make use of a simple mass balance calculation and an observed mean LHF in July of 3.1 W m^{-2}, indicating a net removal of snow from the surface due to sublimation. By assuming equilibrium fractionation during sublimation (Wahl et al., 2021), we can calculate the isotopic composition of the humidity flux and the associated removal of isotopologues. When considering reasonable values of a 5 cm layer of snow, a snow density of 300 kg m^{-3}, an initial isotopic composition of -20 ‰ δ^{18}O, and a surface temperature of -9 °C for the month of July, the snow would be enriched by ~ 4 ‰ δ^{18}O due to the net humidity flux, which is substantial. For comparison, the seasonal amplitude (i.e., summer peak to winter trough) at the Renland Ice Cap, for example, is about 8 ‰ in δ^{18}O (Hughes et al., 2020). We acknowledge that this is a highly simplified mass balance calculation without taking into account the vapor isotopic composition or precipitation inputs. However, since vapor exchange is a continuous process, it will continuously affect the layer of snow that is in contact with the atmosphere and will therefore imprint on the snow isotopic composition with a general net daily sublimation signal during months with a net sublimation flux.

Which months show a net sublimation flux is dependent on the geographical location and general climatology of the area. Especially in the context of paleoclimatological interpretation of ice cores, this cannot be assumed to be constant in time. If the vapor–snow exchange imprints on the seasonal snow isotopic composition as indicated in the result of the mass balance calculation, one would need to take changes in sublimation seasonality into account when making assumptions about vapor-exchange effects on paleo timescales, as has been previously demonstrated for precipitation seasonality (Werner et al., 2000).

On shorter timescales in our laboratory experiments we observe changes of up to 8 ‰ δ^{18}O and 20 ‰ d-excess over time periods of several days, and in FS field experiments we find an average change of 2.09 ‰ δ^{18}O and 3.78 ‰ d-excess on very short (sub-diurnal) timescales. This observation, in combination with our mass balance calculation of 4 ‰ change in δ^{18}O over the month of July, suggests that under typical natural conditions, changes in the surface isotope value occurring on a short timescale may have an impact on the mean seasonally recorded isotope signal. Previous studies have addressed the effect of seasonally biased accumulation rate on diffusion and the recorded δ^{18}O isotope signal (Persson et al., 2011; Casado et al., 2020; Hughes et al., 2020) and the effect of physical modifications and snow redistribution of the snow surface on the accumulation intermittency (Zuhr et al., 2021), but the effect of sublimation-driven changes in surface snow isotopic composition between precipitation events has not been quantified previously. Whether the magnitude of the mean isotope change due to sublimation and snow–vapor exchange outweighs the effects of snow redistribution, accumulation bias, and diffusion has yet to be determined. This could be further explored through future experiments which account for additional variables or are completed at a larger scale. For example, the effect of snow specific surface area (SSA) could be determined by making simultaneous SSA and isotope measurements. Additionally, to remove the effect of wind redistribution and snow dunes on snow isotope spatial variability, a large pit could be filled with homogeneous snow for continuous sampling. In this case, the snow would have a known starting isotopic composition, similar to the FB experiments completed here but be subject to more natural conditions as in the FS experiments. Finally, as weather conditions would allow, it would be beneficial to have multiple experimental periods greater than 48 h.

In order to fully understand the implications of sublimation and vapor deposition on the ice core record, it is necessary to quantify the effects of these processes over the course of a full year. While not in the scope of this paper, this problem can first be approached through mass and isotope flux measurements throughout the summer field season (Wahl et al., 2021). Subsequent modeling of these processes throughout the annual climate cycle will provide insight as to what magnitude snow–vapor exchange influences surface snow on longer timescales (i.e., months to years), and how it may be recorded in the ice core isotope record. This could inform us to what extent changes in frequency of precipitation events, accumulation rate, and LHF could influence the isotope signal recorded in ice cores on decadal to millennial scales. Our findings suggest that these variables contribute to a combined isotope signal, in which δ^{18}O and d-excess in ice core records likely incorporate individual precipitation events (i.e., condensation temperature and moisture source

region conditions, respectively), surface redistribution (i.e., wind drift and erosion), and a post-depositional alteration signal reflecting atmospheric conditions at the ice core site. Snow isotope models such as CROCUSiso (Touzeau et al., 2018), the Community Firn Model (Stevens et al., 2020), and isotope-enabled climate models would therefore be updated through the incorporation of isotope fractionation during sublimation, snow–vapor isotope exchange, and snow metamorphosis.

5 Conclusions

In this study, we have combined controlled laboratory experiments with field measurements in an effort to constrain the effects of sublimation on surface snow isotopic composition. Experiments in a controlled laboratory setting demonstrate isotopic enrichment due to fractionation occurring during sublimation. In experimental results, δ^{18}O increases as light isotopes preferentially sublimate due to fractionation, and d-excess decreases due to kinetic fractionation. These changes occur rapidly, substantially changing the isotopic composition of the top 2–3 cm of snow over a 4–6 d period. Field experiments included continuous measurements of atmospheric vapor and latent heat flux during periods of high-resolution surface snow sampling, during which we observed significant changes in the top 1–2 cm of snow surface isotopes on a sub-diurnal timescale. We observed periods of increasing and decreasing δ^{18}O, indicating that both sublimation and vapor deposition influence the surface snow on an hourly basis. This supports our hypothesis that rapid change occurs in a natural setting and propagates into the snowpack, moderately altering the initial precipitation isotope signal.

Post-depositional effects have implications for the interpretation of ice core data, which traditionally is assumed to only record isotopic variability from precipitation. Our results complement previous studies demonstrating spatial and temporal variability in snow surface isotopes, further strengthening the idea that the ice core record not only integrates the climate signal of condensation temperature (i.e., δ^{18}O and δD) and moisture source conditions (i.e., d-excess) during precipitation, but also may integrate the atmospheric conditions between precipitation events (in both δ^{18}O and d-excess). These factors should in the future be included in isotope-enabled climate models, which may include estimates of synoptic-scale patterns across annual cycles that would influence latent heat flux, vapor composition, and the resulting influence on surface snow isotopes. This will improve future interpretations of ice core data and may be the missing link in the transfer function between climate and an uninterrupted isotope record, strengthening our interpretation of ice core water isotopes as a proxy for a continuous integrated climate record.

Appendix A: Figures and tables

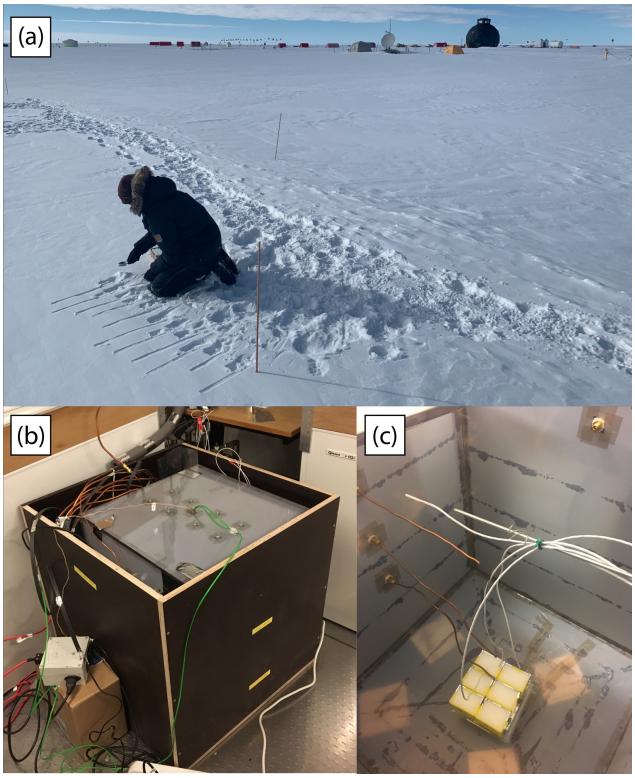

Figure A1. (a) A photo of the FS sampling location shows the proximity between individual samples and sites. In the foreground is FS site A being sampled, with sites B and C seen in the background. The full laboratory experimental setup, with the top of the outer plywood box removed, is shown in **(b)**, with the inside of the plexiglass chamber shown in **(c)**.

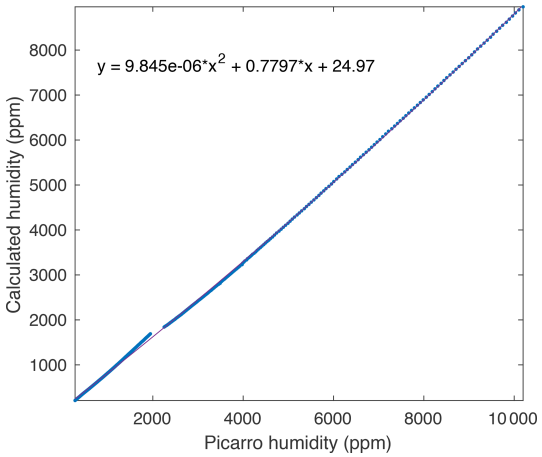

Figure A2. A comparison between measured and true humidity (determined from saturation temperature) yields a quadratic response, which is used to calibrate the measured humidity.

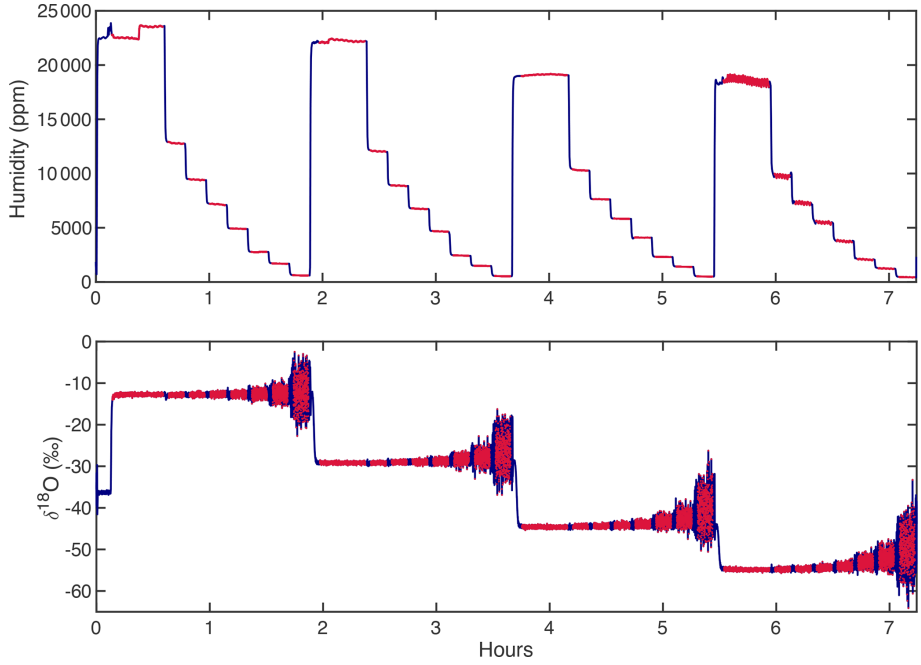

Figure A3. An example of a calibration sequence shows each standard (i.e., KBW −14.15 ‰, KAW −30.30 ‰, KPW −45.41 ‰, SPGW −55.18 ‰ δ^{18}O) measured at multiple humidity levels for 12–20 min. The full calibration sequence (blue) is trimmed (red) such that the transition periods between humidity intervals and isotopic standards are ignored, and the average value of each trimmed period is calculated.

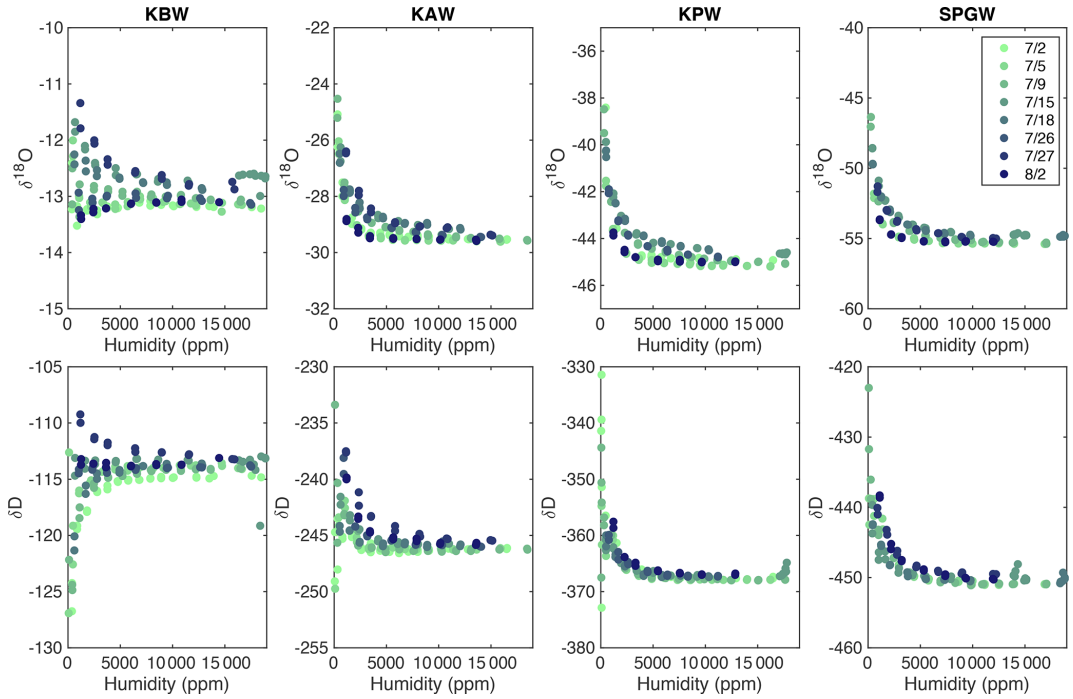

Figure A4. A compilation of all calibration runs from the 2019 EastGRIP field season demonstrates slight drift in the isotopic values, particularly at water concentrations less than 5000 ppm. In total, eight calibration runs were completed (indicated by color) for four isotope standards (standard values can be found in Table A1).

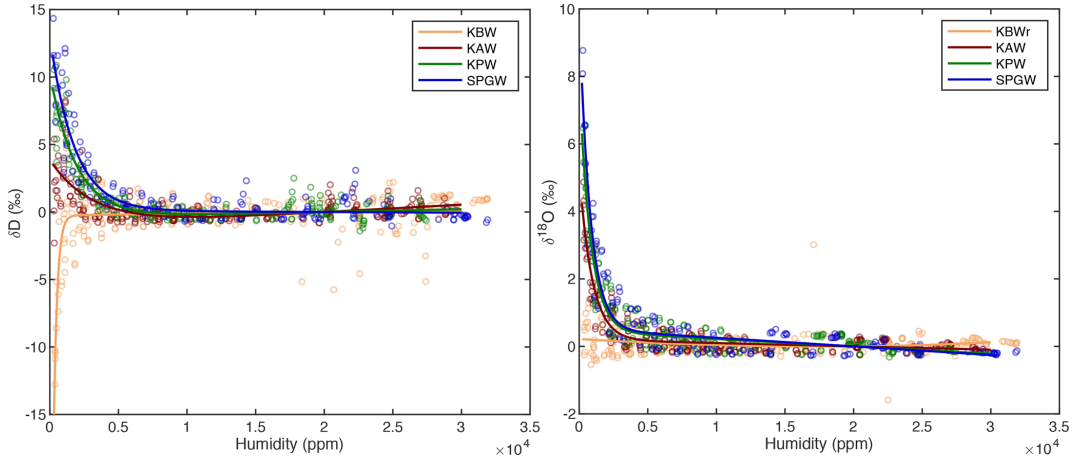

Figure A5. A double exponential curve is fit to the compiled calibration data for each standard for both δ^{18}O and δD, characterizing the instrumental humidity-isotope response. This curve, normalized to the isotope value at 20 000 ppm, is used to correct the measured isotope data for bias at low humidity values.

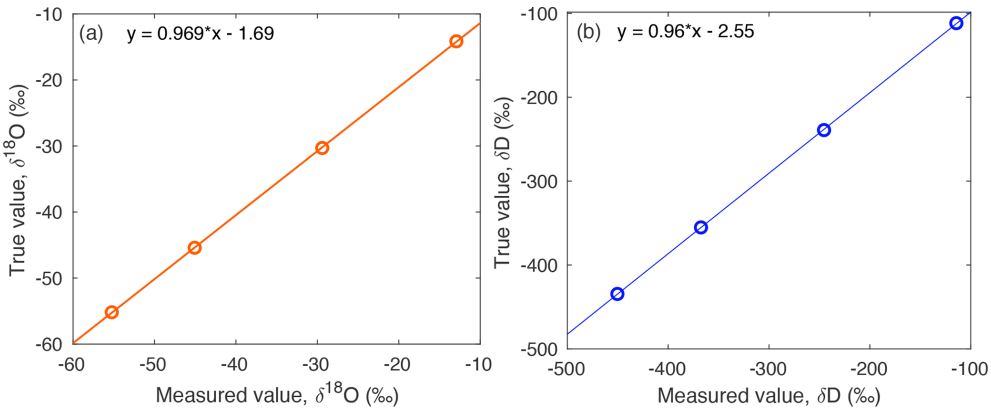

Figure A6. The true values of standards on the VSMOW-SLAP scale are compared to a compilation of standards measured across the field season, to yield a linear relationship for **(a)** δ^{18}O and **(b)** d-excess. This correction is applied to measured isotope data.

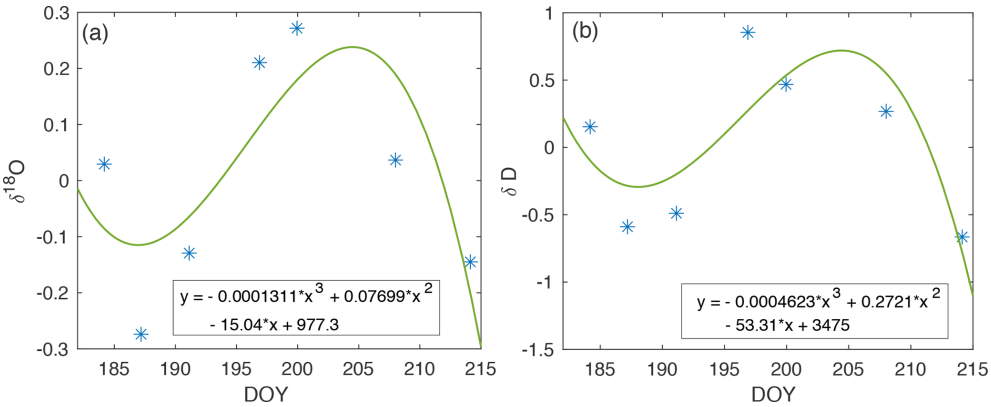

Figure A7. Drift in isotope measurements across the 2019 EGRIP field season (blue). The cubic polynomial curve fit (green) is used to correct experimental vapor measurements for the associated periods of time.

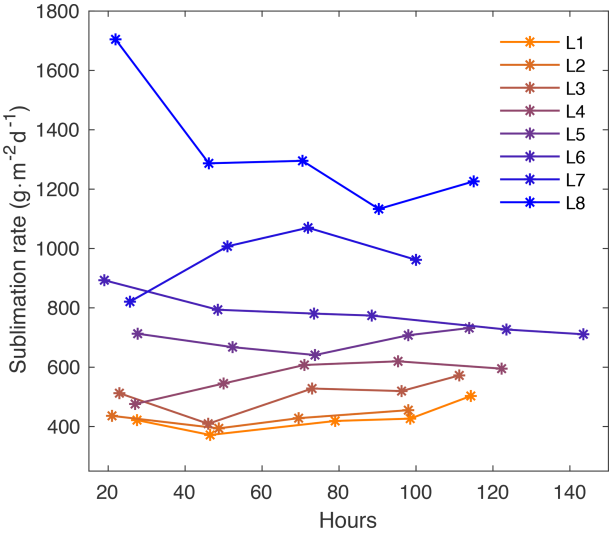

Figure A8. Sublimation rate with time for each laboratory experiment (L1–L8). The sublimation rate varies with temperature and dry air flow rate and is relatively constant with time throughout each experiment.

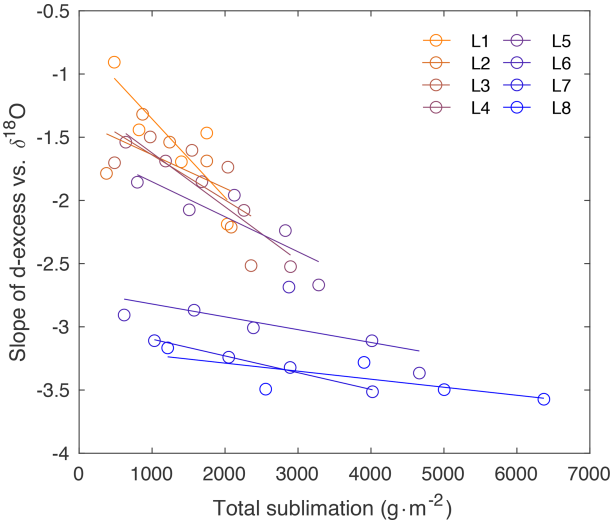

Figure A9. Slope of d-excess vs. δ^{18}O (as shown in Fig. 3) in comparison to total sublimation (sublimation rate times hours).

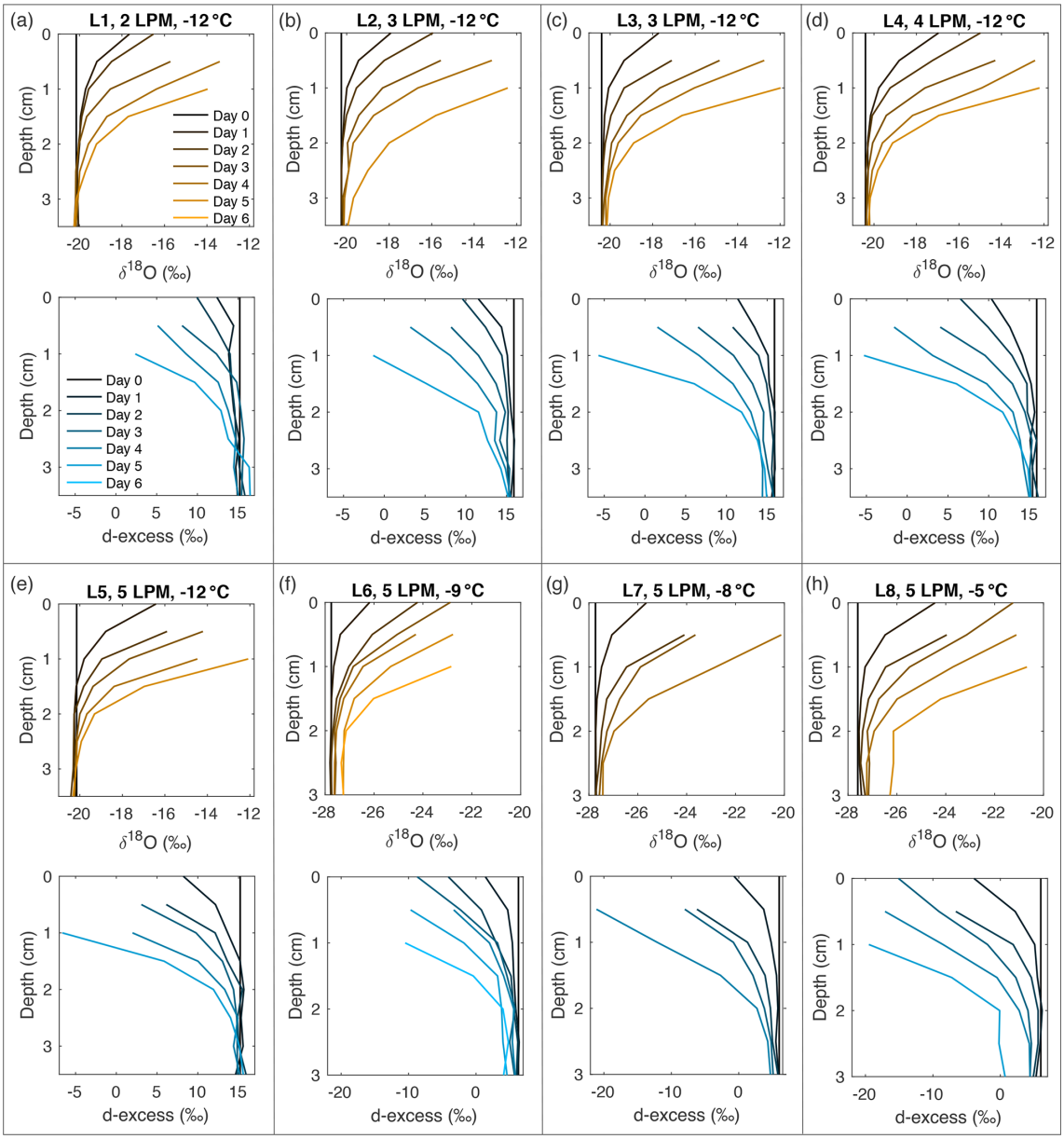

Figure A10. Snow $\delta^{18}O$ (orange) and d-excess (blue) vertical profiles from all laboratory experiments (L1–L8, **(a–h)**, respectively). Conditions for each experiment are indicated in each subplot. Day 0 (black) represents the initial homogeneous snow sample, with colors progressively moving towards orange ($\delta^{18}O$) and blue (d-excess) with each day of sampling. As each experiment progresses from Day 1 to Day 6, sublimation drives an increase in $\delta^{18}O$ and decrease in d-excess, with the greatest change at the snow surface.

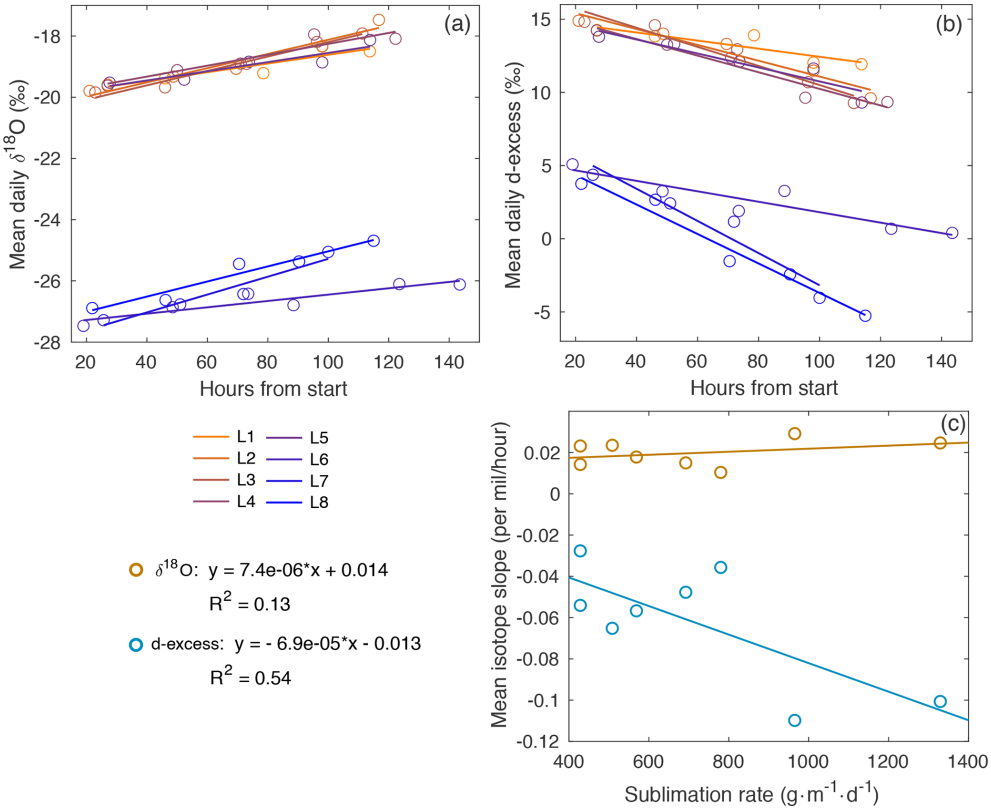

Figure A11. Mean daily **(a)** δ^{18}O and **(b)** d-excess with time for laboratory experiments L1–L8. The slope of the line for each experiment is represented in **(c)**, compared to sublimation rate. There is a slight increase in δ^{18}O slope vs. sublimation rate ($R^2 = 0.13$), with a stronger relationship observed in the decrease in d-excess vs. sublimation rate ($R^2 = 0.54$).

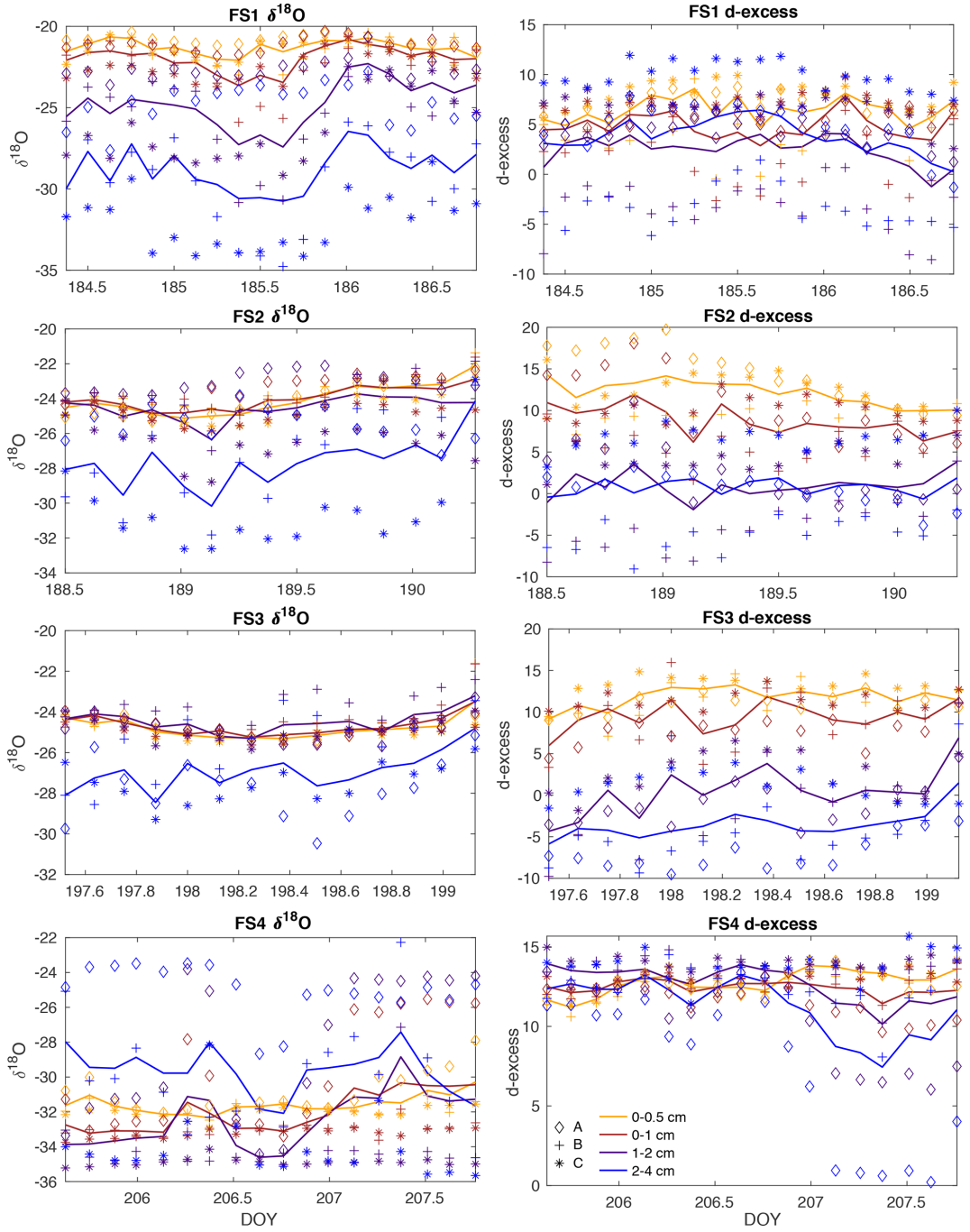

Figure A12. All surface samples are shown for field experiments FS1–FS4 (top to bottom, respectively), including δ^{18}O (left column) and d-excess (right column). Symbols represent sampling locations (diamond, Site A; plus, Site B; asterisk, Site C), and colors indicate sampling height (yellow, 0–0.5 cm from surface; red, 0–1 cm; purple, 1–2 cm; blue, 2–4 cm). Solid lines are the average of the three sampling locations (A, B, C).

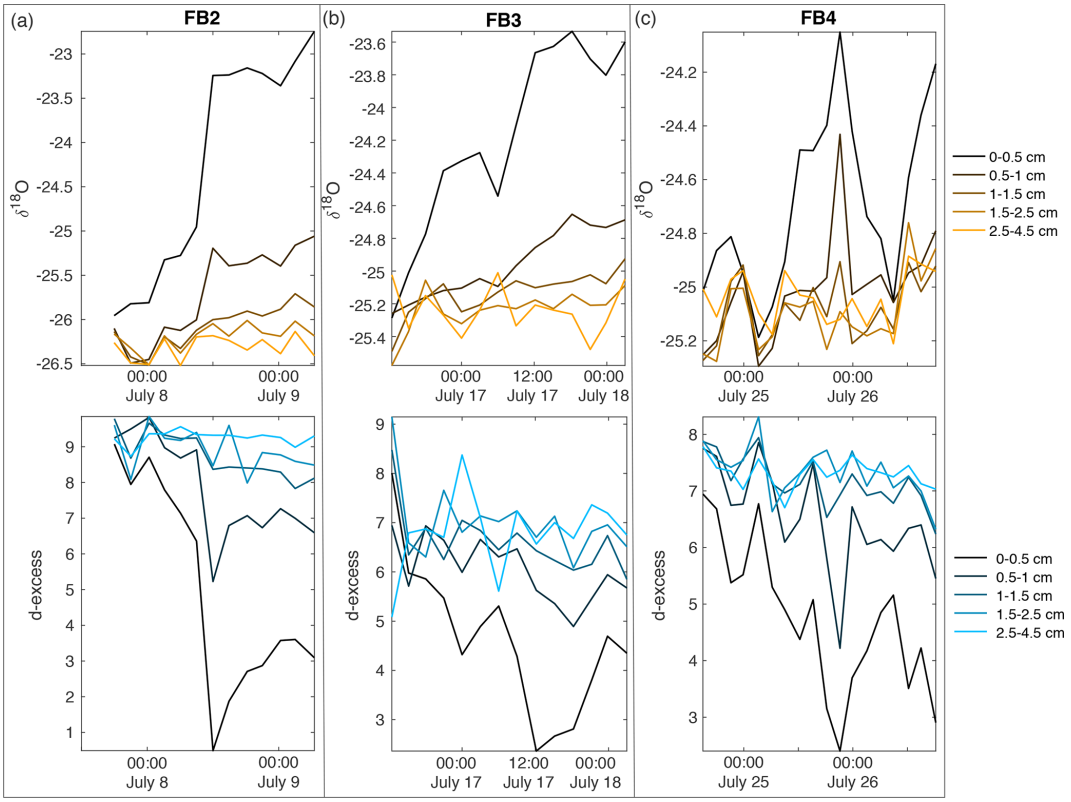

Figure A13. Field box samples are shown for **(a)** FB2, **(b)** FB3, and **(c)** FB4, including δ^{18}O (top row) and d-excess (bottom row). Colors indicate sampling depth from surface; black is the surface sample from 0–0.5 cm, progressing with depth towards light orange (δ^{18}O) and light blue (d-excess) at 2.5–4.5 cm below the surface.

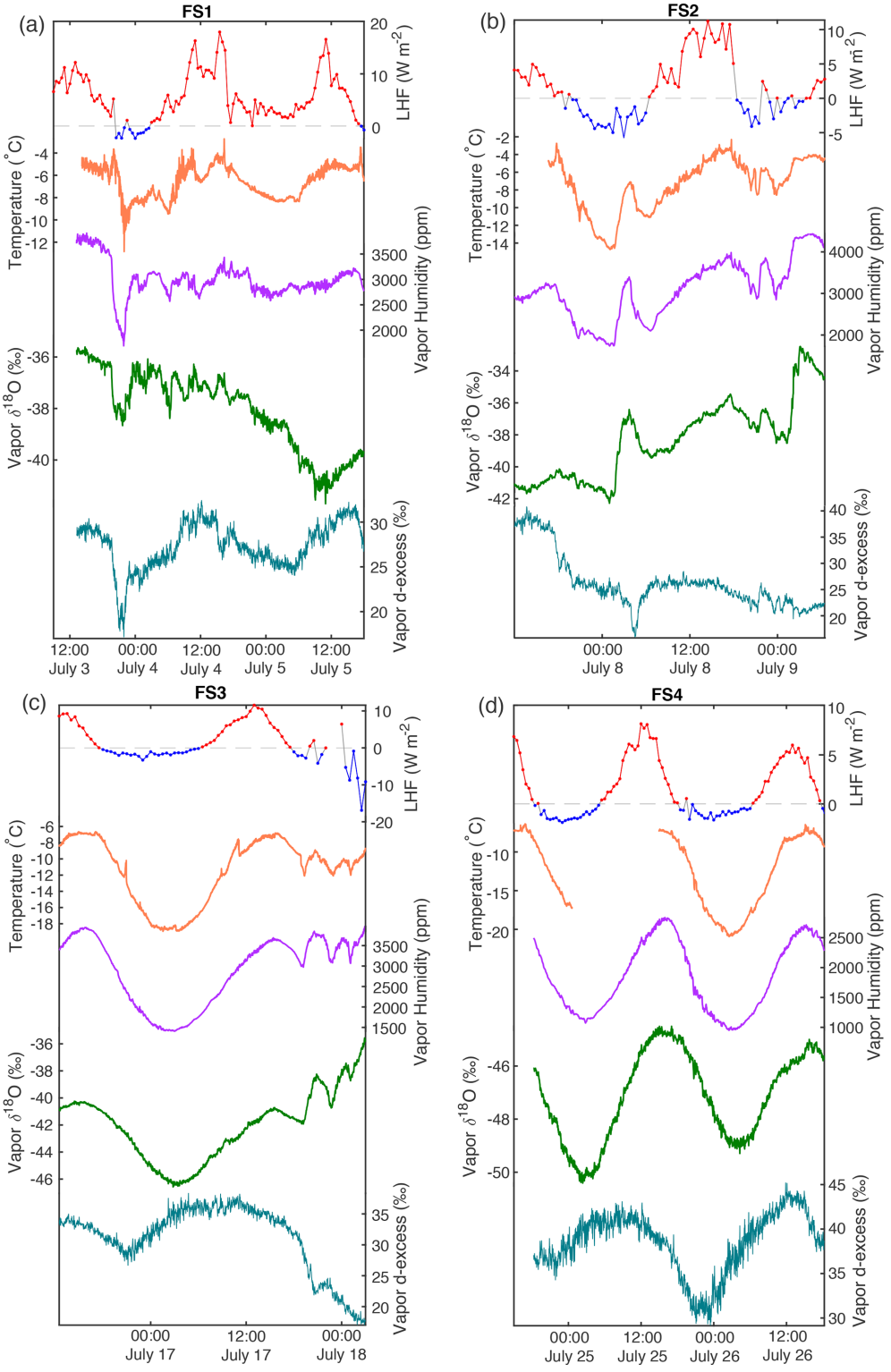

Figure A14. Additional atmospheric conditions are shown for all field experiments F1–F4 (**a**–**d**, respectively). From top: latent heat flux (red, positive values; blue, negative values; dashed gray line at 0), temperature (orange), and atmospheric vapor measurements at 10 cm above the snow surface. Humidity (purple), δ^{18}O (green), and d-excess (teal).

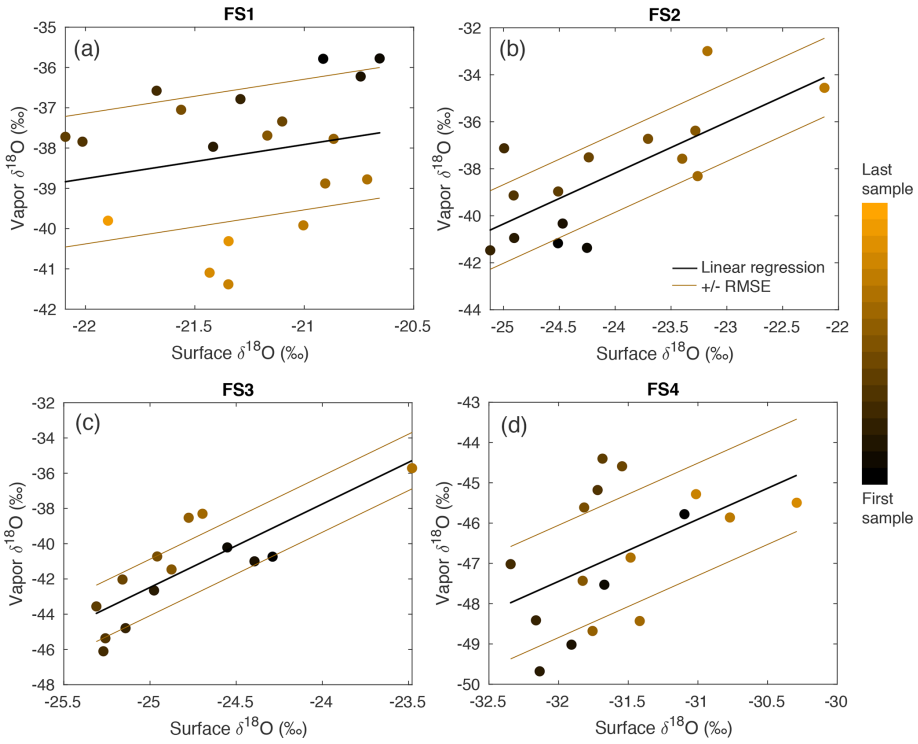

Figure A15. A comparison between δ^{18}O of vapor and the top (0–0.5 cm) FS sample shows a significant relationship in FS2, FS3, and FS4, determined by P values ≤ 0.05. The sampling time is indicated by a color scale from black (first sample taken) to orange (last sample taken), and a linear regression (black line) is calculated for each experiment. The linear regression $+/-$ the root-mean-square error is shown as brown lines.

Table A1. Standards used in field and laboratory experiments.

Standard	δ^{18}O (‰)	δD (‰)
Boulder (KBW)	−14.15	−111.65
Antarctic (KAW)	−30.30	−239.13
Polar (KPW)	−45.41	−355.18
South Pole Glacial (SPGW)	−55.18	−434.47
Bermuda	−0.25	2.1
NEEM	−33.50	−257.1
−40	−39.93	−310.7
DC02	−54.07	−428.2

Appendix B: Vapor calibrations

The following four types of calibrations were performed to calibrate the water vapor isotope measurements of the CRDS, similar to the calibration protocol described in Steen-Larsen et al. (2013): (1) humidity, (2) humidity-isotope, (3) VSMOW-VSLAP, and (4) drift. For all isotope calibrations in both laboratory and field setups, the liquid standard was first vaporized using a nebulizer system, which produced vapor at 20 000–25 000 ppm. This vapor was combined with a dry air source using an open split, and a mass flow controller regulated the flow of dry air ranging from 10–21 cc min^{-1}. The CRDS inlet constantly pulled a vacuum at 30 cc min^{-1}; therefore, the remaining air flow is pulled from the humidified nebulizer source. This allowed for a constant stream of vapor at a controlled isotopic value and humidity level.

The calibration runs performed before and after each field experiment consisted of a 7 h cycle with each of the four standards (Table A1) measured for 12 min at eight different humidity levels from 500–12000 ppm, as well as a half-hour measurement at $>$ 20 000 ppm (Fig. A3). This calibration was performed before and after each field experiment run (Fig. A4). Vapor measurements have uncertainty of 0.23 ‰ δ^{18}O and 1.4 ‰ δD (Steen-Larsen et al., 2013). Details of each laboratory and field calibration type are as follows.

1. *Humidity calibration*. The measured humidity was corrected to the true humidity using a polynomial relationship, which was determined by calibration to a range of known humidity levels (Fig. A2). This instrument-specific relationship was not expected to significantly drift with time.

    a. *Laboratory*. A laboratory humidity calibration was carried out by drawing humid air through a chilled ethanol bath, calculating the true humidity based on the saturation vapor pressure of the bath temperature (Fig. A2).

    b. *Field*. The humidity calibration required a full laboratory setup, which was not available in the field. Due to instrument damage during shipping, the calibration could not be performed after the field season. Therefore, the humidity measurements were calibrated to a second Picarro L2130-*i* CRDS instrument which was continuously measuring atmospheric vapor $\sim$ 30 m away and was calibrated for humidity. Simultaneous humidity measurements were matched and used to calibrate the CRDS instrument measurements reported here.

2. *Humidity-isotope response calibrations*. Isotopic bias occurs at a lower humidity level (i.e., less than 10 000 ppm) and is sensitive to isotope concentration (Weng et al., 2020). Because experimental vapor measurements are typically below 5000 ppm, it is important to perform a rigorous calibration of multiple isotopic standards (Table A1) at varying humidity levels (Figs. A3, A4). A double-exponential curve is fit to the isotope response with respect to humidity (Fig. A5) and is used to correct deviations in low-humidity experimental data.

    a. *Laboratory*. The humidity-isotope response was determined by a full calibration of four isotopic standards (Table A1) measured for 20–30 min at a range of humidity levels from $\sim$ 500–10 000 ppm. For experiments L1–L5, vapor measurements were calibrated to KAW, and vapor measurements in experiments L6–L8 were calibrated to NEEM. These standards were closest to the isotopic values of the vapor measurements, which differed between experiments due to different starting snow isotopic composition.

    b. *Field*. All calibration runs performed before and after each experiment run were compiled for the full field season. A double-exponential curve was fit to the compilation of data for each standard to determine the mean instrument response to humidity (Fig. A5). The vapor measurements were calibrated using the mean curve for KPW, which has the closest isotope value to average vapor measurements.

3. *VSMOW-SLAP scale calibration*. The calibration to the VSMOW-SLAP scale was established using standards (Table A1) which bracketed the measured water vapor isotope data (Fig. A6). A linear relationship is calculated between the "True value", or the established isotopic standard value, and the "Measured value", which is calculated from standard measurements.

    a. *Laboratory*. The "Measured values" for the VSMOW-VSLAP scale were taken from the isotopic values at $\sim$ 6000–8000 ppm measured in the full calibration used for the humidity-isotope response curve.

    b. *Field*. The "Measured values" were derived from the mean value of each standard measured for $>$ 10 min at 20 000–35 000 ppm over the course of the field season.

4. *Drift calibration*. While points (2) and (3) above account for mean instrument isotope deviations from standard values, instrument drift with time has also been observed in CRDS. For this reason, we calculated a best fit with respect to time for the isotope values at higher humidities from each calibration performed (Fig. A7). Deviations from the mean are then corrected for within each experiment period.

    a. *Laboratory*. A short calibration of three to four standards at three to four humidity levels was completed before and after each experiment run. Instru-

ment drift was calculated from the variability in KAW (L1–L5) and NEEM (L6–L8) at 2000 ppm.

b. *Field*. The isotope drift with respect to time was calculated from the mean value of measurements at 20 000 ppm for each calibration.

Data availability. Latent heat flux data are available on the PANGAEA data archive at https://doi.org/10.1594/PANGAEA.928827 (Steen-Larsen and Wahl, 2021). Laboratory and field experimental data are available at https://doi.pangaea.de/10.1594/PANGAEA.937355 (Hughes, 2021).

Author contributions. AGH and HCSL designed the laboratory and field setup and experiments. AGH carried out the experiments with significant contributions from HCSL. SW and AZ assisted with field snow sampling, and MH assisted with materials and production ideas of the laboratory experimental chamber. AGH wrote the article with significant contributions from HCSL, TRJ, and SW and edits from all authors.

Competing interests. The authors declare that they have no conflict of interest.

Disclaimer. Publisher's note: Copernicus Publications remains neutral with regard to jurisdictional claims in published maps and institutional affiliations.

Acknowledgements. Abigail Hughes acknowledges support from the National Science Foundation through the Graduate Research Fellowship Program (grant no. DGE 1650115). This paper has received funding from the European Research Council (ERC) under the European Union's Horizon 2020 research and innovation program: Starting Grant SNOWISO (grant agreement no. 759526). EGRIP is directed and organized by the Centre for Ice and Climate at the Niels Bohr Institute, University of Copenhagen. It is supported by funding agencies and institutions in Denmark (A. P. Møller Foundation, University of Copenhagen), USA (US National Science Foundation, Office of Polar Programs), Germany (Alfred Wegener Institute, Helmholtz Centre for Polar and Marine Research), Japan (National Institute of Polar Research and Arctic Challenge for Sustainability), Norway (University of Bergen and Trond Mohn Foundation), Switzerland (Swiss National Science Foundation), France (French Polar Institute Paul-Emile Victor, Institute for Geosciences and Environmental research), Canada (University of Manitoba) and China (Chinese Academy of Sciences and Beijing Normal University). Funding has also been provided by the National Science Foundation program of Arctic Natural Sciences (grant no. 1804098). The authors also thank the Stable Isotope Lab at the University of Colorado Boulder for facility and instrument use, and Bruce Vaughn and Valerie Morris for assistance.

Financial support. This research has been supported by the Horizon 2020 (grant no. SNOWISO (759526)) and the National Science Foundation (grant nos. 1804098 and 1650115).

Review statement. This paper was edited by Joel Savarino and reviewed by three anonymous referees.

References

Benson, L. V. and White, J. W. C.: Stable isotopes of oxygen and hydrogen in the Truckee River-Pyramid Lake surface-water system, 3. Source of water vapor overlying Pyramid Lake, Limnol. Oceanogr., 39, 1945–1958, 1994.

Casado, M., Landais, A., Picard, G., Münch, T., Laepple, T., Stenni, B., Dreossi, G., Ekaykin, A., Arnaud, L., Genthon, C., Touzeau, A., Masson-Delmotte, V., and Jouzel, J.: Archival processes of the water stable isotope signal in East Antarctic ice cores, The Cryosphere, 12, 1745–1766, https://doi.org/10.5194/tc-12-1745-2018, 2018.

Casado, M., Münch, T., and Laepple, T.: Climatic information archived in ice cores: impact of intermittency and diffusion on the recorded isotopic signal in Antarctica, Clim. Past, 16, 1581–1598, https://doi.org/10.5194/cp-16-1581-2020, 2020.

Craig, H.: Isotopic variations in meteoric waters, Science, 133, 1702–1703, https://doi.org/10.1126/science.133.3465.1702, 1961.

Cuffey, K. M. and Steig, E. J.: Isotopic diffusion in polar firn: implications for interpretation of seasonal climate parameters in ice-core records, with emphasis on central Greenland, J. Glaciol., 44, 273–284, 1998.

Dansgaard, W.: Stable isotopes in precipitation, Tellus, 16, 436–468, https://doi.org/10.3402/tellusa.v16i4.8993, 1964.

Dansgaard, W., Johnsen, S., Clausen, H., and Gundestrup, N.: Stable isotope glaciology, Meddelelser om Gronland, 197, 1–53, 1973.

Ebner, P. P., Steen-Larsen, H. C., Stenni, B., Schneebeli, M., and Steinfeld, A.: Experimental observation of transient δ^{18}O interaction between snow and advective airflow under various temperature gradient conditions, The Cryosphere, 11, 1733–1743, https://doi.org/10.5194/tc-11-1733-2017, 2017.

Ekaykin, A. A., Hondoh, T., Lipenkov, V. Y., and Miyamoto, A.: Post-depositional changes in snow isotope content: preliminary results of laboratory experiments, Clim. Past Discuss., 5, 2239–2267, https://doi.org/10.5194/cpd-5-2239-2009, 2009.

Fudge, T. J., Markle, B. R., Cuffey, K. M., Buizert, C., Taylor, K. C., Steig, E. J., Waddington, E. D., Conway, H., and Koutnik, M.: Variable relationship between accumulation and temperature in West Antarctica for the past 31,000 years, Geophys. Res. Lett., 43, 3795–3803, https://doi.org/10.1002/2016GL068356, 2016.

Furukawa, R., Uemura, R., Fujita, K., Sjolte, J., Yoshimura, K., Matoba, S., and Iizuka, Y.: Seasonal-Scale Dating of a Shallow Ice Core From Greenland Using Oxygen Isotope Matching Between Data and Simulation, J. Geophys. Res.-Atmos., 122, 10873–10887, https://doi.org/10.1002/2017JD026716, 2017.

Thayer, A.: Snow experiments EGRIP lab and field experiment data, PANGAEA [data set], https://doi.pangaea.de/10.1594/PANGAEA.937355, 2021.

Hughes, A. G., Jones, T. R., Vinther, B. M., Gkinis, V., Stevens, C. M., Morris, V., Vaughn, B. H., Holme, C., Markle, B. R., and White, J. W. C.: High-frequency climate variability in the Holocene from a coastal-dome ice core in east-central Greenland, Clim. Past, 16, 1369–1386, https://doi.org/10.5194/cp-16-1369-2020, 2020.

Johnsen, S. J., Clausen, H. B., Cuffey, K. M., Hoffmann, G., Schwander, J., and Creyts, T.: Diffusion of stable isotopes in polar firn and ice: the isotope effect in firn diffusion, Physics of Ice Core Records, 121–140, 2000.

Johnsen, S. J., Dahl-jensen, D., Gundestrup, N., Steffensen, J. P., Clausen, H. B., Miller, H., Masson-Delmotte, V., Sveinbjo, A. E., Sveinbjörnsdóttir, Á. E., and White, J.: Oxygen isotope and palaeotemperature records from six Greenland ice-core stations: Camp Century, Dye-3, GRIP, GISP2, Renland and NorthGRIP, J. Quaternary Sci., 16, 299–307, https://doi.org/10.1002/jqs.622, 2001.

Jones, T., Cuffey, K., White, J., Steig, E., Buizert, C., Markle, B., McConnell, J., and Sigl, M.: Water isotope diffusion in the WAIS Divide ice core during the Holocene and last glacial, J. Geophys. Res.-Earth, 122, 290–309, https://doi.org/10.1002/2016JF003938, 2017a.

Jones, T. R., White, J. W. C., Steig, E. J., Vaughn, B. H., Morris, V., Gkinis, V., Markle, B. R., and Schoenemann, S. W.: Improved methodologies for continuous-flow analysis of stable water isotopes in ice cores, Atmos. Meas. Tech., 10, 617–632, https://doi.org/10.5194/amt-10-617-2017, 2017b.

Jouzel, J. and Merlivat, L.: Deuterium and Oxygen 18 in Precipitation: Modeling of the Isotopic Effects During Snow Formation, J. Geophys. Res., 89, 11749–11757, 1984.

Jouzel, J., Alley, R. B., Cuffey, K. M., Dansgaard, W., Grootes, G., Hoffmann, P., Johnsen, S. J., Koster, R. D., Peel, D., Shuman, C. A., Stievenard, M., Stuiver, M., and White, J.: Validity of the temperature reconstruction from water isotopes in ice cores, J. Geophys. Res., 102, 26471–26487, 1997.

Laepple, T., Hörhold, M., Münch, T., Freitag, J., Wegner, A., and Kipfstuhl, S.: Layering of surface snow and firn at Kohnen Station, Antarctica: Noise or seasonal signal?, J. Geophys. Res.-Earth, 121, 1849–1860, https://doi.org/10.1002/2016JF003919, 2016.

Laepple, T., Münch, T., Casado, M., Hoerhold, M., Landais, A., and Kipfstuhl, S.: On the similarity and apparent cycles of isotopic variations in East Antarctic snow pits, The Cryosphere, 12, 169–187, https://doi.org/10.5194/tc-12-169-2018, 2018.

Madsen, M. V., Steen-Larsen, H. C., Hörhold, M., Box, J., Berben, S. M., Capron, E., Faber, A.-K., Hubbard, A., Jensen, M. F., Jones, T. R., Kipfstuhl, S., Koldtoft, I., Pillar, H. R., Vaughn, B. H., Vladimirova, D., and Dahl-Jensen, D.: Evidence of Isotopic Fractionation During Vapor Exchange Between the Atmosphere and the Snow Surface in Greenland, J. Geophys. Res.-Atmos., 124, 2932–2945, https://doi.org/10.1029/2018JD029619, 2019.

Merlivat, L. and Jouzel, J.: Global Climatic Interpretation of the Deuterium-Oxygen 18 Relationship for Precipitation, J. Geophys. Res., 84, 5029–5033, 1979.

Mosley-Thompson, E., Paskievitch, J. F., Gow, A. J., and Thompson, L. G.: Late 20th Century increase in South Pole snow accumulation, J. Geophys. Res.-Atmos., 104, 3877–3886, https://doi.org/10.1029/1998JD200092, 1999.

Münch, T. and Laepple, T.: What climate signal is contained in decadal- to centennial-scale isotope variations from Antarctic ice cores?, Clim. Past, 14, 2053–2070, https://doi.org/10.5194/cp-14-2053-2018, 2018.

Münch, T., Kipfstuhl, S., Freitag, J., Meyer, H., and Laepple, T.: Constraints on post-depositional isotope modifications in East Antarctic firn from analysing temporal changes of isotope profiles, The Cryosphere, 11, 2175–2188, https://doi.org/10.5194/tc-11-2175-2017, 2017.

Persson, A., Langen, P. L., Ditlevsen, P., and Vinther, B. M.: The influence of precipitation weighting on interannual variability of stable water isotopes in Greenland, J. Geophys. Res.-Atmos., 116, D20120, https://doi.org/10.1029/2010JD015517, 2011.

Ritter, F., Steen-Larsen, H. C., Werner, M., Masson-Delmotte, V., Orsi, A., Behrens, M., Birnbaum, G., Freitag, J., Risi, C., and Kipfstuhl, S.: Isotopic exchange on the diurnal scale between near-surface snow and lower atmospheric water vapor at Kohnen station, East Antarctica, The Cryosphere, 10, 1647–1663, https://doi.org/10.5194/tc-10-1647-2016, 2016.

Schauer, A. J., Schoenemann, S. W., and Steig, E. J.: Routine high-precision analysis of triple water-isotope ratios using cavity ring-down spectroscopy, Rapid Commun. Mass. Sp., 30, 2059–2069, https://doi.org/10.1002/rcm.7682, 2016.

Sime, L. C., Hopcroft, P. O., and Rhodes, R. H.: Impact of abrupt sea ice loss on Greenland water isotopes during the last glacial period, P. Natl. Acad. Sci. USA, 116, 4099–4104, https://doi.org/10.1073/pnas.1807261116, 2019.

Sokratov, S. A. and Golubev, V. N.: Snow isotopic content change by sublimation, J. Glaciol., 55, 823–828, 2009.

Steen-Larsen, H. C. and Wahl, S.: 2 m processed sensible and latent heat flux, friction velocity and stability at EastGRIP site on Greenland Ice Sheet, summer 2019, PANGAEA [data set], https://doi.org/10.1594/PANGAEA.928827, 2021.

Steen-Larsen, H. C., Johnsen, S. J., Masson-Delmotte, V., Stenni, B., Risi, C., Sodemann, H., Balslev-Clausen, D., Blunier, T., Dahl-Jensen, D., Ellehøj, M. D., Falourd, S., Grindsted, A., Gkinis, V., Jouzel, J., Popp, T., Sheldon, S., Simonsen, S. B., Sjolte, J., Steffensen, J. P., Sperlich, P., Sveinbjörnsdóttir, A. E., Vinther, B. M., and White, J. W. C.: Continuous monitoring of summer surface water vapor isotopic composition above the Greenland Ice Sheet, Atmos. Chem. Phys., 13, 4815–4828, https://doi.org/10.5194/acp-13-4815-2013, 2013.

Steen-Larsen, H. C., Masson-Delmotte, V., Hirabayashi, M., Winkler, R., Satow, K., Prié, F., Bayou, N., Brun, E., Cuffey, K. M., Dahl-Jensen, D., Dumont, M., Guillevic, M., Kipfstuhl, S., Landais, A., Popp, T., Risi, C., Steffen, K., Stenni, B., and Sveinbjörnsdottír, A. E.: What controls the isotopic composition of Greenland surface snow?, Clim. Past, 10, 377–392, https://doi.org/10.5194/cp-10-377-2014, 2014.

Stevens, C. M., Verjans, V., Lundin, J. M. D., Kahle, E. C., Horlings, A. N., Horlings, B. I., and Waddington, E. D.: The Community Firn Model (CFM) v1.0, Geosci. Model Dev., 13, 4355–4377, https://doi.org/10.5194/gmd-13-4355-2020, 2020.

Touzeau, A., Landais, A., Morin, S., Arnaud, L., and Picard, G.: Numerical experiments on vapor diffusion in polar snow and firn and its impact on isotopes using the multi-layer energy balance model Crocus in SURFEX v8.0, Geosci. Model Dev., 11, 2393–2418, https://doi.org/10.5194/gmd-11-2393-2018, 2018.

Wahl, S., Steen-Larsen, H. C., Reuder, J., and Hörhold, M.: Quantifying the Stable Water Isotopologue Exchange Between the Snow Surface and Lower Atmosphere by Direct Flux Measurements, J. Geophys. Res.-Atmos., 126, e2020JD034400, https://doi.org/10.1029/2020JD034400, 2021.

Weng, Y., Touzeau, A., and Sodemann, H.: Correcting the impact of the isotope composition on the mixing ratio dependency of water vapour isotope measurements with cavity ring-down spectrometers, Atmos. Meas. Tech., 13, 3167–3190, https://doi.org/10.5194/amt-13-3167-2020, 2020.

Werner, M., Mikolajewicz, U., Heimann, M., and Hoffmann, G.: Borehole versus isotope temperatures on Greenland: Seasonality does matter, Geophys. Res. Lett., 27, 723–726, 2000.

Werner, M., Langebroek, P. M., Carlsen, T., Herold, M., and Lohmann, G.: Stable water isotopes in the ECHAM5 general circulation model: Toward high-resolution isotope modeling on a global scale, J. Geophys. Res.-Atmos., 116, D15109, https://doi.org/10.1029/2011JD015681, 2011.

Whillans, I. and Grootes, P.: Isotopic diffusion in cold snow and firn, J. Geophys. Res., 90, 3910–3918, https://doi.org/10.1029/JD090iD02p03910, 1985.

Zuhr, A. M., Münch, T., Steen-Larsen, H. C., Hörhold, M., and Laepple, T.: Local scale depositional processes of surface snow on the Greenland ice sheet, The Cryosphere Discuss. [preprint], https://doi.org/10.5194/tc-2021-36, in review, 2021.

Paper III

Challenging Old Axioms: Interpretations of Water Isotopes in Ice Cores

Sonja Wahl, Hans Christian Steen-Larsen, Abigail Hughes, Laura J. Dietrich, Alexandra Zuhr, Melanie Behrens, Anne-Katrine Faber, Maria Hörhold
submitted to *Nature Geoscience*

Bibliography

Albert, M. R., and R. L. Hawley (2002), Seasonal changes in snow surface roughness characteristics at Summit, Greenland: Implications for snow and firn ventilation, *Annals of Glaciology*, *35*, 510–514, doi:10.3189/172756402781816591. 16

Alley, R. B. (2000), The Younger Dryas cold interval as viewed from central Greenland, *Quaternary Science Reviews*, *19*(1-5), 213–226, doi:10.1016/S0277-3791(99)00062-1. 1

Amory, C., H. Gallée, F. Naaim-Bouvet, V. Favier, E. Vignon, G. Picard, A. Trouvilliez, L. Piard, C. Genthon, and H. Bellot (2017), Seasonal Variations in Drag Coefficient over a Sastrugi-Covered Snowfield in Coastal East Antarctica, *Boundary-Layer Meteorology*, *164*(1), 107–133, doi:10.1007/s10546-017-0242-5. 16

Anderson, P. S., and W. D. Neff (2008), Boundary layer physics over snow and ice, *Atmospheric Chemistry and Physics*, *8*(13), 3563–3582, doi:10.5194/acp-8-3563-2008. 15

Andreas, E. L. (1987), A theory for the scalar roughness and the scalar transfer coefficients over snow and sea ice, *Boundary-Layer Meteorology*, *38*(1-2), 159–184, doi:10.1007/BF00121562. 22

Bagheri Dastgerdi, S., M. Behrens, J.-L. Bonne, M. Hörhold, G. Lohmann, E. Schlosser, and M. Werner (2021), Continuous monitoring of surface water vapour isotopic compositions at Neumayer Station III, East Antarctica, *The Cryosphere*, *15*(10), 4745–4767, doi:10.5194/tc-15-4745-2021. 37

Bamber, J. L., R. M. Westaway, B. Marzeion, and B. Wouters (2018), The land ice contribution to sea level during the satellite era, *Environmental Research Letters*, *13*(6), 063,008, doi:10.1088/1748-9326/aac2f0. 42

Benson, L. V., S. W. Hostetler, and L. V. Benson (1994), Stable isotopes of oxygen and hydrogen in the Truckee River-Pyramid Lake surface-water system., *Limnology and Oceanography*, *39*(2), 344–355, doi:10.4319/lo.1994.39.8.1945. 38

Bentley, C. R., and B. R. Koci (2007), Drilling to the beds of the Greenland and Antarctic ice sheets: A review, *Annals of Glaciology*, *47*(November 2006), 1–9, doi:10.3189/172756407786857695. 13

Bigeleisen, J., M. L. Perlman, and H. C. Prosser (1952), Conversion of Hydrogenic Materials to Hydrogen for Isotopic Analysis, *Analytical Chemistry*, *24*(8), 1356–1357, doi:10.1021/ac60068a025. 17

Box, J. E., and K. Steffen (2001), Sublimation on the Greenland ice sheet from automated weather station observations, *Journal of Geophysical Research Atmospheres*, *106*(D24), 33,965–33,981, doi:10.1029/2001JD900219. 15, 16, 41

Brutsaert, W. (1975a), A Theory for Local Evaporation (or Heat Transfer) from Roufh and Smooth Surfaces at Ground Level, *Water Resources Research*, *11*(4), 543–550. 11, 12, 35

Brutsaert, W. (1975b), The Roughness Length for Water Vapor, Sensible heat, and other scalars, *J. Atmospherical Science*. 11, 12, 35

Buizert, C., V. Gkinis, J. P. Severinghaus, F. He, B. S. Lecavalier, P. Kindler, M. Leuenberger, A. E. Carlson, B. Vinther, V. Masson-Delmotte, J. W. White, Z. Liu, B. Otto-Bliesner, and E. J. Brook (2014), Greenland temperature response to climate forcing during the last deglaciation, *Science*, *345*(6201), 1177–1180, doi:10.1126/science.1254961. 1

Burkhart, J. F., M. Hutterli, R. C. Bales, and J. R. McConnell (2004), Seasonal accumulation timing and preservation of nitrate in firn at Summit, Greenland, *Journal of Geophysical Research: Atmospheres*, *109*(19), 1–9, doi:10.1029/2004JD004658. 16

Businger, J. A., J. C. Wyngaard, Y. Izumi, and E. F. Bradley (1971), Flux-Profile Relationships in the Atmospheric Surface Layer, *Journal of the Atmospheric Sciences*, *28*(2), 181–189, doi:10.1175/1520-0469(1971)028<0181:FPRITA>2.0.CO;2. 22

Cappa, C. D. (2003), Isotopic fractionation of water during evaporation, *Journal of Geophysical Research*, *108*(D16), 4525, doi:10.1029/2003JD003597. 12, 42

Capron, E., S. O. Rasmussen, T. J. Popp, T. Erhardt, H. Fischer, A. Landais, J. B. Pedro, G. Vettoretti, A. Grinsted, V. Gkinis, B. Vaughn, A. Svensson, B. M. Vinther, and J. W. C. White (2021), The anatomy of past abrupt warmings recorded in Greenland ice, *Nature Communications*, *12*(1), 2106, doi:10.1038/s41467-021-22241-w. 1

Casado, M. (2016), Water stable isotopic composition on the East Antarctic Plateau : measurements at low temperature of the vapour composition, utilisation as an atmospheric tracer and implication for paleoclimate studies, Ph.D. thesis, Universite Paris-Saclay. 18

Casado, M., A. Landais, V. Masson-Delmotte, C. Genthon, E. Kerstel, S. Kassi, L. Arnaud, G. Picard, F. Prie, O. Cattani, H. C. Steen-Larsen, E. Vignon, and P. Cermak (2016), Continuous measurements of isotopic composition of water vapour on the East Antarctic Plateau, *Atmospheric Chemistry and Physics*, *16*(13), 8521–8538, doi:10.5194/acp-16-8521-2016. 3, 15, 37

Casado, M., A. Landais, G. Picard, T. Münch, T. Laepple, B. Stenni, G. Dreossi, A. Ekaykin, L. Arnaud, C. Genthon, A. Touzeau, V. Masson-Delmotte, and J. Jouzel (2018), Archival processes of the water stable isotope signal in East Antarctic ice cores, *The Cryosphere*, *12*(5), 1745–1766, doi:10.5194/tc-12-1745-2018. 2

Casado, M., T. Münch, and T. Laepple (2020), Climatic information archived in ice cores: impact of intermittency and diffusion on the recorded isotopic signal in Antarctica, *Climate of the Past*, *16*(4), 1581–1598, doi:10.5194/cp-16-1581-2020. 3, 41

Casado, M., A. Landais, G. Picard, L. Arnaud, G. Dreossi, B. Stenni, and F. Prié (2021), Water Isotopic Signature of Surface Snow Metamorphism in Antarctica, *Geophysical Research Letters*, *48*(17), 1–11, doi:10.1029/2021gl093382. 41

Cauquoin, A., M. Werner, and G. Lohmann (2019), Water isotopes climate relationships for the mid-Holocene and preindustrial period simulated with an isotope-enabled version of MPI-ESM, *Climate of the Past*, *15*(6), 1913–1937, doi:10.5194/cp-15-1913-2019. 13, 14

Chazette, P., C. Flamant, H. Sodemann, J. Totems, A. Monod, E. Dieudonné, A. Baron, A. Seidl, H. C. Steen-Larsen, P. Doira, A. Durand, and S. Ravier (2021), Experimental investigation of the stable water isotope distribution in an Alpine lake environment (L-WAIVE), *Atmospheric Chemistry and Physics*, *21*(14), 10,911–10,937, doi:10.5194/acp-21-10911-2021. 42

Craig, H. (1961), Standard for Reporting Concentrations of Deuterium and Oxygen-18 in Natural Waters, *Science*, *133*(3467), 1833–1834, doi:10.1126/science.133.3467.1833. 6

Craig, H., and L. I. Gordon (1965), Deuterium and Oxygen 18 variations in the ocean and the marine atmosphere, in *Stable Isotopes in Oceanographic Studies and Paleotemperatures*, edited by E. Tongiorgi, pp. 9–130, Laboratorio di Geologia Nucleare, Pisa. 10, 12, 37

Cullen, N. J., and K. Steffen (2001), Unstable near-surface boundary conditions in summer on top of the Greenland ice sheet, *Geophysical Research Letters*, *28*(23), 4491–4493, doi:10.1029/2001GL013417. 15

Cullen, N. J., T. Mölg, J. Conway, and K. Steffen (2014), Assessing the role of sublimation in the dry snow zone of the Greenland ice sheet in a warming world, *Journal of Geophysical Research: Atmospheres*, *119*(11), 6563–6577, doi:10.1002/2014JD021557. 16, 41

Dansgaard, W. (1953), The Abundance of O 18 in Atmospheric Water and Water Vapour, *Tellus*, *5*(4), 461–469, doi:10.1111/j.2153-3490.1953.tb01076.x. 6

Dansgaard, W. (1954), Oxygen-18 Abundance in Fresh Water, *Nature*, *174*(4422), 234–235, doi:10.1038/174234a0. 6

Dansgaard, W. (1964), Stable isotopes in precipitation, *Tellus*, *16*(4), 436–468, doi:10.3402/tellusa.v16i4.8993. 1, 6, 12, 13

Dansgaard, W., and S. J. Johnsen (1969), A flow model and a time scale for the ice core from camp century, Greenland, *Journal of Glaciology*, *8*(53). 15

Dansgaard, W., S. J. Johnsen, J. Moller, and C. C. Langway (1969), One Thousand Centuries of Climatic Record from Camp Century on the Greenland Ice Sheet, *Science*, *166*(3903), 377–380, doi:10.1126/science.166.3903.377. 13

Dansgaard, W., S. J. Johnsen, H. B. Clausen, and N. Gundestrup (1973), *Stable isotope glaciology*, vol. 197, C.A. Reitzel, København. 3

de Laeter, J. R., J. K. Böhlke, P. De Bièvre, H. Hidaka, H. S. Peiser, K. J. R. Rosman, and P. D. P. Taylor (2003), Atomic weights of the elements. Review 2000 (IUPAC Technical Report), *Pure and Applied Chemistry*, *75*(6), 683–800, doi:10.1351/pac200375060683. 6

Dibb, J. E., and M. Fahnestock (2004), Snow accumulation, surface height change, and firn densification at Summit, Greenland: Insights from 2 years of in situ observation, *Journal of Geophysical Research*, *109*(D24), D24,113, doi:10.1029/2003JD004300. 16

Dütsch, M., S. Pfahl, and H. Sodemann (2017), The Impact of Nonequilibrium and Equilibrium Fractionation on Two Different Deuterium Excess Definitions, *Journal of Geophysical Research: Atmospheres*, *122*(23), doi:10.1002/2017JD027085. 7

Ebner, P. P., H. C. Steen-Larsen, B. Stenni, M. Schneebeli, and A. Steinfeld (2017), Experimental observation of transient δ18O interaction between snow and advective airflow under various temperature gradient conditions, *The Cryosphere*, *11*(4), 1733–1743, doi:10.5194/tc-11-1733-2017. 3

Ekaykin, A. A., V. Y. Lipenkov, I. N. Kuzmina, J. R. Petit, V. Masson-Delmotte, and S. J. Johnsen (2004), The changes in isotope composition and accumulation of snow at Vostok station, East Antarctica, over the past 200 years, *Annals of Glaciology*, *39*, 569–575, doi: 10.3189/172756404781814348. 16

Ellehoj, M. D., H. C. Steen-Larsen, S. J. Johnsen, and M. B. Madsen (2013), Ice-vapor equilibrium fractionation factor of hydrogen and oxygen isotopes: Experimental investigations and implications for stable water isotope studies, *Rapid Communications in Mass Spectrometry*, *27*(19), 2149–2158, doi:10.1002/rcm.6668. 7, 39, 40

EPICA community-members (2004), Eight glacial cycles from an Antarctic ice core, *Nature*, *429*(6992), 623–628, doi:10.1038/nature02599. 1

Epstein, S., and T. Mayeda (1953), Variation of O18 content of waters from natural sources, *Geochimica et Cosmochimica Acta*, *4*(5), 213–224, doi:10.1016/0016-7037(53)90051-9. 17

Fahnestock, M., R. Bindschadler, R. Kwok, and K. Jezek (1993), Greenland Ice Sheet Surface Properties and Ice Dynamics from ERS-1 SAR Imagery, *Science*, *262*(5139), 1530–1534, doi:10.1126/science.262.5139.1530. 24

Fausto, R. S., D. van As, K. D. Mankoff, B. Vandecrux, M. Citterio, A. P. Ahlstrom, S. B. Andersen, W. Colgan, N. B. Karlsson, K. K. Kjeldsen, N. J. Korsgaard, S. H. Larsen, S. Nielsen, A. O. Pedersen, C. L. Shields, A. M. Solgaard, and J. E. Box (2021), Programme for Monitoring of the Greenland Ice Sheet (PROMICE) automatic weather station data, *Earth System Science Data*, *13*(8), 3819–3845, doi:10.5194/essd-13-3819-2021. 25

Filhol, S., and M. Sturm (2015), Snow bedforms: A review, new data, and a formation model, *Journal of Geophysical Research: Earth Surface*, *120*(9), 1645–1669, doi: 10.1002/2015JF003529. 16

Fisher, D. A., N. Reeh, and H. Clausen (1985), Stratigraphic Noise in Time Series Derived from Ice Cores, *Annals of Glaciology*, *7*, 76–83, doi:10.3189/S0260305500005942. 3

Foken, T., and B. Wichura (1996), Tools for quality assessment of surface-based flux measurements, *Agricultural and Forest Meteorology*, *78*(1-2), 83–105, doi:10.1016/0168-1923(95)02248-1. 22, 23

Foken, T., F. Wimmer, M. Mauder, C. Thomas, and C. Liebethal (2006), Some aspects of the energy balance closure problem, *Atmospheric Chemistry and Physics*, *6*(12), 4395–4402, doi:10.5194/acp-6-4395-2006. 21

Friedman, I., C. Benson, and J. Gleason (1991), Isotopic changes during snow metaporphism, in *Stable Isotope Geochemistry: A Tribute to Samuel Epstein*, vol. 3, edited by H. Tayoir, J. O'Neill, and I. Kaplan, pp. 211–221, Geochemical Society. 3

Fujita, K., and O. Abe (2006), Stable isotopes in Daily precipitation at Dome Fuji, East Antarctica, *Geophysical Research Letters*, *33*(18), 6–9, doi:10.1029/2006GL026936. 3, 16

Gat, J. R. (1996), Oxygen and Hydrogen Isotopes in the Hydrologic Cycle, *Annual Review of Earth and Planetary Sciences*, *24*(1), 225–262, doi:10.1159/000088336. 12

Gehre, M., H. Geilmann, J. Richter, R. A. Werner, and W. A. Brand (2004), Continuous flow 2H/1H and 18O/ 16O analysis of water samples with dual inlet precision, *Rapid Communications in Mass Spectrometry*, *18*(22), 2650–2660, doi:10.1002/rcm.1672. 17

Genthon, C., L. Piard, E. Vignon, J. B. Madeleine, M. Casado, and H. Gallée (2017), Atmospheric moisture supersaturation in the near-surface atmosphere at Dome C, Antarctic Plateau, *Atmospheric Chemistry and Physics*, *17*(1), 691–704, doi:10.5194/acp-17-691-2017. 41

Ghosh, P., and W. A. Brand (2003), Stable isotope ratio mass spectrometry in global climate change research, *International Journal of Mass Spectrometry*, *228*(1), 1–33, doi:10.1016/S1387-3806(03)00289-6. 17

Gonfiantini, R., L. I. Wassenaar, and L. J. AraguasAraguas (2020), Stable isotope fractionations in the evaporation of water: The wind effect, *Hydrological Processes*, *34*(16), 3596–3607, doi:10.1002/hyp.13804. 42

Gromke, C., C. Manes, B. Walter, M. Lehning, and M. Guala (2011), Aerodynamic Roughness Length of Fresh Snow, *Boundary-Layer Meteorology*, *141*(1), 21–34, doi:10.1007/s10546-011-9623-3. 16

Grootes, P. M., and M. Stuiver (1997), Oxygen 18/16 variability in Greenland snow and ice with 10 3 - to 10 5 -year time resolution, *Journal of Geophysical Research: Oceans*, *102*(C12), 26,455–26,470, doi:10.1029/97JC00880. 14

Hanna, E., J. Cappelen, X. Fettweis, S. H. Mernild, T. L. Mote, R. Mottram, K. Steffen, T. J. Ballinger, and R. J. Hall (2021), Greenland surface air temperature changes from 1981 to 2019 and implications for ice-sheet melt and mass-balance change, *International Journal of Climatology*, *41*(S1), E1336–E1352, doi:10.1002/joc.6771. 15

Hoffmann, G., J. Jouzel, and V. Masson (2000), Stable water isotopes in atmospheric general circulation models, *Hydrological Processes*, *14*(8), 1385–1406, doi:10.1002/1099-1085(20000615)14:8<1385::AID-HYP989>3.0.CO;2-1. 13

Högström, U. (1988), Non-dimensional wind and temperature profiles in the atmospheric surface layer: A re-evaluation, *Boundary-Layer Meteorology*, *42*(1-2), 55–78, doi:10.1007/BF00119875. 22

Holtslag, A. A. M., and H. A. R. De Bruin (1988), Applied Modeling of the Nighttime Surface Energy Balance over Land, *Journal of Applied Meteorology*, *27*(6), 689–704, doi:10.1175/1520-0450(1988)027<0689:AMOTNS>2.0.CO;2. 22

Horita, J., K. Rozanski, and S. Cohen (2008), Isotope effects in the evaporation of water: a status report of the CraigGordon model, *Isotopes in Environmental and Health Studies*, *44*(1), 23–49, doi:10.1080/10256010801887174. 6, 12

Hughes, A. G., S. Wahl, T. R. Jones, A. Zuhr, M. Horhold, J. W. C. White, and H. C. Steen-Larsen (2021), The role of sublimation as a driver of climate signals in the water isotope content of surface snow: Laboratory and field experimental results, *The Cryosphere*, *15*, 4949–4974, doi:10.5194/tc-15-4949-2021. 31

Johnsen, S. J. (1977), Stable isotope profiles compared with temperature profiles in firn with historical temperature records, *Isotopes and Impurities in Snow and Ice - Symposium 118*, pp. 338–392. 3

Johnsen, S. J., W. Dansgaard, and J. W. White (1989), The origin of Arctic precipitation under present and glacial conditions, *Tellus, Series B*, *41 B*(4), 452–468, doi:10.3402/tellusb.v41i4.15100. 1, 12, 37

Johnsen, S. J., H. B. Clausen, K. M. Cuffey, G. Hoffmann, J. Schwander, and T. Creyts (2000), Diffusion of stable isotope in polar firn and ice: the isotope effect in firn diffusion, *Physics of Ice Core Records*, doi:10.7916/D8KW5D4X. 3

Jones, T. R., J. W. White, E. J. Steig, B. H. Vaughn, V. Morris, V. Gkinis, B. R. Markle, and S. W. Schoenemann (2017), Improved methodologies for continuous-flow analysis of stable water isotopes in ice cores, *Atmospheric Measurement Techniques*, *10*(2), 617–632, doi:10.5194/amt-10-617-2017. 13

Jones, T. R., W. H. Roberts, E. J. Steig, K. M. Cuffey, B. R. Markle, and J. W. White (2018), Southern Hemisphere climate variability forced by Northern Hemisphere ice-sheet topography, *Nature*, *554*(7692), 351–355, doi:10.1038/nature24669. 1

Joussaume, S., R. Sadourny, and J. Jouzel (1984), A general circulation model of water isotope cycles in the atmosphere, *Nature*, *311*(5981), 24–29, doi:10.1038/311024a0. 13

Jouzel, J., R. B. Alley, K. M. Cuffey, W. Dansgaard, P. Grootes, G. Hoffmann, S. J. Johnsen, R. D. Koster, D. Peel, C. A. Shuman, M. Stievenard, M. Stuiver, and J. White (1997), Validity of the temperature reconstruction from water isotopes in ice cores, *Journal of Geophysical Research: Oceans*, *102*(C12), 26,471–26,487, doi:10.1029/97JC01283. 2

Jouzel, J., V. Masson-Delmotte, O. Cattani, G. Dreyfus, S. Falourd, G. Hoffmann, B. Minster, J. Nouet, J. M. Barnola, J. Chappellaz, H. Fischer, J. C. Gallet, S. Johnsen, M. Leuenberger, L. Loulergue, D. Luethi, H. Oerter, F. Parrenin, G. Raisbeck, D. Raynaud, A. Schilt, J. Schwander, E. Selmo, R. Souchez, R. Spahni, B. Stauffer, J. P. Steffensen, B. Stenni, T. F. Stocker, J. L. Tison, M. Werner, and E. W. Wolff (2007), Orbital and Millennial Antarctic Climate Variability over the Past 800,000 Years, *Science*, *317*(5839), 793–796, doi:10.1126/science.1141038. 1

Jouzel, J., G. Delaygue, A. Landais, V. Masson-Delmotte, C. Risi, and F. Vimeux (2013), Water isotopes as tools to document oceanic sources of precipitation, *Water Resources Research*, *49*(11), 7469–7486, doi:10.1002/2013WR013508. 1

Karlsson, N. B., S. Razik, M. Hörhold, A. Winter, D. Steinhage, T. Binder, and O. Eisen (2020), Surface accumulation in Northern Central Greenland during the last 300 years, *Annals of Glaciology*, *61*(81), 214–224, doi:10.1017/aog.2020.30. 25

Kim, K., and X. Lee (2011), Isotopic enrichment of liquid water during evaporation from water surfaces, *Journal of Hydrology*, *399*(3-4), 364–375, doi:10.1016/j.jhydrol.2011.01.008. 12, 42

King, J. C., P. S. Anderson, M. C. Smith, and S. D. Mobbs (1996), The surface energy and mass balance at Halley, Antarctica during winter, *Journal of Geophysical Research: Atmospheres*, *101*(14), 19,119–19,128, doi:10.1029/96jd01714. 15, 16

Koenig, L. S., A. Ivanoff, P. M. Alexander, J. A. MacGregor, X. Fettweis, B. Panzer, J. D. Paden, R. R. Forster, I. Das, J. R. McConnell, M. Tedesco, C. Leuschen, and P. Gogineni (2016), Annual Greenland accumulation rates (20092012) from airborne snow radar, *The Cryosphere*, *10*(4), 1739–1752, doi:10.5194/tc-10-1739-2016. 16

Kohn, M. J., and J. M. Welker (2005), On the temperature correlation of δ18O in modern precipitation, *Earth and Planetary Science Letters*, *231*(1-2), 87–96, doi:10.1016/j.epsl.2004.12.004. 3

Krinner, G., and M. Werner (2003), Impact of precipitation seasonality changes on isotopic signals in polar ice cores: A multi-model analysis, *Earth and Planetary Science Letters*, *216*(4), 525–538, doi:10.1016/S0012-821X(03)00550-8. 3

Landais, A., E. Barkan, and B. Luz (2008), Record of δ18O and 17O-excess in ice from Vostok Antarctica during the last 150,000 years, *Geophysical Research Letters*, *35*(2), 1–5, doi:10.1029/2007GL032096. 2

Lenaerts, J. T., B. Medley, M. R. van den Broeke, and B. Wouters (2019), Observing and Modeling Ice Sheet Surface Mass Balance, *Reviews of Geophysics*, *57*(2), 376–420, doi:10.1029/2018RG000622. 15, 41

Madsen, M. V., H. C. SteenLarsen, M. Hörhold, J. Box, S. M. P. Berben, E. Capron, A. Faber, A. Hubbard, M. F. Jensen, T. R. Jones, S. Kipfstuhl, I. Koldtoft, H. R. Pillar, B. H. Vaughn, D. Vladimirova, and D. DahlJensen (2019), Evidence of Isotopic Fractionation During Vapor Exchange Between the Atmosphere and the Snow Surface in Greenland, *Journal of Geophysical Research: Atmospheres*, *124*(6), 2932–2945, doi:10.1029/2018JD029619. 3

Mahrt, L. (2009), Characteristics of Submeso Winds in the Stable Boundary Layer, *Boundary-Layer Meteorology*, *130*(1), 1–14, doi:10.1007/s10546-008-9336-4. 23

Majoube, M. (1970), Fractionation Factor of 18O between Water Vapour and Ice, *Nature*, *226*(5252), 1242–1242, doi:10.1038/2261242a0. 9

Majoube, M. (1971a), Fractionnement en oxygene 18 et en deuterium entre l'eau et sa vapeur, *Journal de Chimie Physique*, *68*, 1423–1436. 7, 9

Majoube, M. (1971b), Fractionnement en 18O entre la glace et la vapeur d'eau, *Journal de Chimie Physique*, *68*(4), 625. 7

Markle, B. R., E. J. Steig, C. Buizert, S. W. Schoenemann, C. M. Bitz, T. J. Fudge, J. B. Pedro, Q. Ding, T. R. Jones, J. W. White, and T. Sowers (2017), Global atmospheric teleconnections during Dansgaard-Oeschger events, *Nature Geoscience*, *10*(1), 36–40, doi:10.1038/ngeo2848. 1

Masson-Delmotte, V., J. Jouzel, A. Landais, M. Stievenard, S. J. Johnsen, J. W. C. White, M. Werner, A. Sveinbjornsdottir, and K. Fuhrer (2005), GRIP Deuterium Excess Reveals Rapid and Orbital-Scale Changes in Greenland Moisture Origin, *Science*, *309*(5731), 118–121, doi:10.1126/science.1108575. 1

Masson-Delmotte, V., D. Buiron, A. Ekaykin, M. Frezzotti, H. Gallée, J. Jouzel, G. Krinner, A. Landais, H. Motoyama, H. Oerter, K. Pol, D. Pollard, C. Ritz, E. Schlosser, L. C. Sime, H. Sodemann, B. Stenni, R. Uemura, and F. Vimeux (2011), A comparison of the present

and last interglacial periods in six Antarctic ice cores, *Climate of the Past*, *7*(2), 397–423, doi:10.5194/cp-7-397-2011. 2, 16

Merlivat, L. (1978), Molecular diffusivities of H216O, HD16O, and H218O in gases, *The Journal of Chemical Physics*, *69*(6), 2864–2871, doi:10.1063/1.436884. 12

Merlivat, L., and J. Jouzel (1979), Global Climatic interpretation of the deuterium excess-oxygen 18 relationship for precipitation, *Journal of Geophysical Research*, *84*(C8), 5029–5033, doi:10.29/JC084iC08p05029. 11, 12, 35, 38, 39

Merlivat, L., and G. Nief (1967), Fractionnement isotopique lors des changements d'etat solide-vapeur et liquide-vapeur de l'eau a des temperatures inferieures a 0°C, *Tellus*. 7, 9

Mernild, S. H., E. Hanna, J. R. Mcconnell, M. Sigl, A. P. Beckerman, J. C. Yde, J. Cappelen, J. K. Malmros, and K. Steffen (2015), Greenland precipitation trends in a long-term instrumental climate context (1890-2012): Evaluation of coastal and ice core records, *International Journal of Climatology*, *35*(2), 303–320, doi:10.1002/joc.3986. 16

Monin, A. S., and A. M. Obukhov (1954), Osnovnye zakonomernosti turbulentnogo peremeshivanija v prizemnom sloe atmosfery (Basic Laws of Turbulent Mixing in the Atmosphere Near the Ground), *Trudy geofiz. inst. AN SSSR*, *24*(151), 163–187. 22

Mosley-Thompson, E., J. R. McConnell, R. C. Bales, Z. Li, P.-N. Lin, K. Steffen, L. G. Thompson, R. Edwards, and D. Bathke (2001), Local to regional-scale variability of annual net accumulation on the Greenland ice sheet from PARCA cores, *Journal of Geophysical Research: Atmospheres*, *106*(D24), 33,839–33,851, doi:10.1029/2001JD900067. 16

Münch, T., S. Kipfstuhl, J. Freitag, H. Meyer, and T. Laepple (2017), Constraints on post-depositional isotope modifications in East Antarctic firn from analysing temporal changes of isotope profiles, *The Cryosphere*, *11*(5), 2175–2188, doi:10.5194/tc-11-2175-2017. 40

Münch, T., M. Werner, and T. Laepple (2021), How precipitation intermittency sets an optimal sampling distance for temperature reconstructions from Antarctic ice cores, *Climate of the Past*, *17*(4), 1587–1605, doi:10.5194/cp-17-1587-2021. 3

NEEM community-members (2013), Eemian interglacial reconstructed from a Greenland folded ice core, *Nature*, *493*(7433), 489–494, doi:10.1038/nature11789. 1, 13

Neumann, T. A., E. D. Waddington, E. J. Steig, and P. M. Grootes (2005), Non-climate influences on stable isotopes at Taylor Mouth, Antarctica, *Journal of Glaciology*, *51*(173), 248–258, doi:10.3189/172756505781829331. 3

Neumann, T. A., M. R. Albert, R. Lomonaco, C. Engel, Z. Courville, and F. Perron (2008), Experimental determination of snow sublimation rate and stable-isotopic exchange, *Annals of Glaciology*, *49*, 1–6, doi:10.3189/172756408787814825. 41

Optis, M., A. Monahan, and F. C. Bosveld (2016), Limitations and breakdown of Monin-Obukhov similarity theory for wind profile extrapolation under stable stratification, *Wind Energy*, *19*(6), 1053–1072, doi:10.1002/we.1883. 22

Palerme, C., J. E. Kay, C. Genthon, T. L'Ecuyer, N. B. Wood, and C. Claud (2014), How much snow falls on the Antarctic ice sheet?, *The Cryosphere*, *8*(4), 1577–1587, doi:10.5194/tc-8-1577-2014. 16

Pang, H., S. Hou, A. Landais, V. Masson-Delmotte, J. Jouzel, H. C. Steen-Larsen, C. Risi, W. Zhang, S. Wu, Y. Li, C. An, Y. Wang, F. Prie, B. Minster, S. Falourd, B. Stenni, C. Scarchilli, K. Fujita, and P. Grigioni (2019), Influence of Summer Sublimation on δD, δ18O, and δ17O in Precipitation, East Antarctica, and Implications for Climate Reconstruction From Ice Cores, *Journal of Geophysical Research: Atmospheres*, *124*(13), 7339–7358, doi:10.1029/2018JD030218. 40

Paulson, C. A. (1970), The Mathematical Representation of Wind Speed and Temperature Profiles in the Unstable Atmospheric Surface Layer, *Journal of Applied Meteorology*, *9*(6), 857–861, doi:10.1175/1520-0450(1970)009<0857:TMROWS>2.0.CO;2. 22

Pedro, J. B., H. C. Bostock, C. M. Bitz, F. He, M. J. Vandergoes, E. J. Steig, B. M. Chase, C. E. Krause, S. O. Rasmussen, B. R. Markle, and G. Cortese (2016), The spatial extent and dynamics of the Antarctic Cold Reversal, *Nature Geoscience*, *9*(1), 51–55, doi:10.1038/ngeo2580. 1

Persson, A., P. L. Langen, P. Ditlevsen, and B. M. Vinther (2011), The influence of precipitation weighting on interannual variability of stable water isotopes in Greenland, *Journal of Geophysical Research*, *116*(D20), D20,120, doi:10.1029/2010JD015517. 3, 37

Pfahl, S., and H. Wernli (2008), Air parcel trajectory analysis of stable isotopes in water vapor in the eastern Mediterranean, *Journal of Geophysical Research Atmospheres*, *113*(20), 1–16, doi:10.1029/2008JD009839. 7, 8

Porter, S. E., and E. Mosley-Thompson (2014), Exploring seasonal accumulation bias in a west central Greenland ice core with observed and reanalyzed data, *Journal of Glaciology*, *60*(224), 1093–1100, doi:10.3189/2014JoG13J233. 16

Reynolds, O. (1894), On the Dynamical Theory of Incompressible Viscous Fluids and the Determination of the Criterion, *Phil. Trans. Roy. Soc. London*, *186*, 123–161. 23

Ricaud, P., E. Bazile, M. Del Guasta, C. Lanconelli, P. Grigioni, and A. Mahjoub (2017), Genesis of diamond dust, ice fog and thick cloud episodes observed and modelled above Dome C, Antarctica, *Atmospheric Chemistry and Physics*, *17*(8), 5221–5237, doi:10.5194/acp-17-5221-2017. 16

Risi, C., D. Noone, J. Worden, C. Frankenberg, G. Stiller, M. Kiefer, B. Funke, K. Walker, P. Bernath, M. Schneider, S. Bony, J. Lee, D. Brown, and C. Sturm (2012), Process-evaluation of tropospheric humidity simulated by general circulation models using water vapor isotopic observations: 2. Using isotopic diagnostics to understand the mid and upper tropospheric moist bias in the tropics and subtropics, *Journal of Geophysical Research Atmospheres*, *117*(5), 1–25, doi:10.1029/2011JD016623. 13

Ritter, F., H. Christian Steen-Larsen, M. Werner, V. Masson-Delmotte, A. Orsi, M. Behrens, G. Birnbaum, J. Freitag, C. Risi, and S. Kipfstuhl (2016), Isotopic exchange on the diurnal scale between near-surface snow and lower atmospheric water vapor at Kohnen station, East Antarctica, *The Cryosphere*, *10*(4), 1647–1663, doi:10.5194/tc-10-1647-2016. 3, 4

Schlosser, E., C. Reijmer, H. Oerter, and W. Graf (2004), The influence of precipitation origin on the δ18O-T relationship at Neumayer station, Ekströmisen, Antarctica, *Annals of Glaciology*, *39*, 41–48, doi:10.3189/172756404781814276. 2

Schlosser, E., K. W. Manning, J. G. Powers, M. G. Duda, G. Birnbaum, and K. Fujita (2010), Characteristics of high-precipitation events in Dronning Maud Land, Antarctica, *Journal of Geophysical Research Atmospheres*, *115*(14), doi:10.1029/2009JD013410. 39

Schlosser, E., B. Stenni, M. Valt, A. Cagnati, G. P. Jordan, W. M. Kevin, M. Raphael, and G. D. Michael (2016), Precipitation and synoptic regime in two extreme years 2009 and 2010 at Dome C, Antarctica-implications for ice core interpretation, *Atmospheric Chemistry and Physics*, *16*(8), 4757–4770, doi:10.5194/acp-16-4757-2016. 16

Schmidt, G. A., G. Hoffmann, D. T. Shindell, and Y. Hu (2005), Modeling atmospheric stable water isotopes and the potential for constraining cloud processes and stratosphere-troposphere water exchange, *Journal of Geophysical Research Atmospheres*, *110*(21), 1–15, doi:10.1029/2005JD005790. 13

Schmitt, F. G. (2017), La turbulence de 1870 à 1920: la naissance d'un nom et d'un concept, *Comptes Rendus - Mecanique*, *345*(9), 620–626, doi:10.1016/j.crme.2017.06.003. 21

Schneider, D. P., E. J. Steig, T. D. Van Ommen, D. A. Dixon, P. A. Mayewski, J. M. Jones, and C. M. Bitz (2006), Antarctic temperatures over the past two centuries from ice cores, *Geophysical Research Letters*, *33*(16), 1–5, doi:10.1029/2006GL027057. 1

Servettaz, A. P., A. J. Orsi, M. A. Curran, A. D. Moy, A. Landais, C. Agosta, V. H. L. Winton, A. Touzeau, J. R. McConnell, M. Werner, and M. Baroni (2020), Snowfall and Water Stable Isotope Variability in East Antarctica Controlled by Warm Synoptic Events, *Journal of Geophysical Research: Atmospheres*, *125*(17), 1–14, doi:10.1029/2020JD032863. 16

Sime, L. C., G. J. Marshall, R. Mulvaney, and E. R. Thomas (2009), Interpreting temperature information from ice cores along the Antarctic Peninsula: ERA40 analysis, *Geophysical Research Letters*, *36*(18), 1–5, doi:10.1029/2009GL038982. 3

Sodemann, H., V. Masson-Delmotte, C. Schwierz, B. M. Vinther, and H. Wernli (2008), Interannual variability of Greenland winter precipitation sources: 2. Effects of North Atlantic Oscillation variability on stable isotopes in precipitation, *Journal of Geophysical Research Atmospheres*, *113*(12), 1–21, doi:10.1029/2007JD009416. 37

Sorbjan, Z., and A. A. Grachev (2010), An evaluation of the flux-gradient relationship in the stable boundary layer, *Boundary-Layer Meteorology*, *135*(3), 385–405, doi:10.1007/s10546-010-9482-3. 22

Stearns, C. R., and G. A. Weidner (1993), Sensible and latent heat flux estimates in Antarctica, *Antarctic Research Series*, *61*, 109–138, doi:10.1029/AR061p0109. 41

Steen-Larsen, H. C. (2020), Snow surface accumulation measured using SSA stake measurents, EastGRIP camp Greenland, May 2018, doi:https://doi.org/10.1594/PANGAEA.921853. 27

Steen-Larsen, H. C., S. J. Johnsen, V. Masson-Delmotte, B. Stenni, C. Risi, H. Sodemann, D. Balslev-Clausen, T. Blunier, D. Dahl-Jensen, M. D. Ellehøj, S. Falourd, A. Grindsted,

V. Gkinis, J. Jouzel, T. Popp, S. Sheldon, S. B. Simonsen, J. Sjolte, J. P. Steffensen, P. Sperlich, A. E. Sveinbjörnsdóttir, B. M. Vinther, and J. W. C. White (2013), Continuous monitoring of summer surface water vapor isotopic composition above the Greenland Ice Sheet, *Atmospheric Chemistry and Physics*, *13*(9), 4815–4828, doi:10.5194/acp-13-4815-2013. 3, 14, 15, 20

Steen-Larsen, H. C., V. Masson-Delmotte, M. Hirabayashi, R. Winkler, K. Satow, F. Prié, N. Bayou, E. Brun, K. M. Cuffey, D. Dahl-Jensen, M. Dumont, M. Guillevic, S. Kipfstuhl, A. Landais, T. Popp, C. Risi, K. Steffen, B. Stenni, and A. E. Sveinbjörnsdottír (2014), What controls the isotopic composition of Greenland surface snow?, *Climate of the Past*, *10*(1), 377–392, doi:10.5194/cp-10-377-2014. 1, 4, 14

Steen-Larsen, H. C., C. Risi, M. Werner, K. Yoshimura, and V. Masson-Delmotte (2017), Evaluating the skills of isotope-enabled general circulation models against in situ atmospheric water vapor isotope observations, *Journal of Geophysical Research: Atmospheres*, *122*(1), 246–263, doi:10.1002/2016JD025443. 39

SteenLarsen, H. C., and S. Wahl (2021a), 2m wind speed, wind direction and air temperature at EastGRIP site on Greenland Ice Sheet, summer 2019, doi:10.1594/PANGAEA.925618. 27

SteenLarsen, H. C., and S. Wahl (2021b), 2m processed sensible and latent heat flux, friction velocity and stability at EastGRIP site on Greenland Ice Sheet, summer 2019, doi:10.1594/PANGAEA.928827. 27

SteenLarsen, H. C., and S. Wahl (2021c), Calibrated 2m stable water vapor isotope data from EastGRIP, Greenland Ice Sheet summer 2019, doi:10.1594/PANGAEA.928823. 27

Steig, E. J., V. Gkinis, A. J. Schauer, S. W. Schoenemann, K. Samek, J. Hoffnagle, K. J. Dennis, and S. M. Tan (2014), Calibrated high-precision 17O-excess measurements using cavity ring-down spectroscopy with laser-current-tuned cavity resonance, *Atmospheric Measurement Techniques*, *7*(8), 2421–2435, doi:10.5194/amt-7-2421-2014. 18

Stenni, B., C. Scarchilli, V. Masson-Delmotte, E. Schlosser, V. Ciardini, G. Dreossi, P. Grigioni, M. Bonazza, A. Cagnati, D. Karlicek, C. Risi, R. Udisti, and M. Valt (2016), Three-year monitoring of stable isotopes of precipitation at Concordia Station, East Antarctica, *The Cryosphere*, *10*(5), 2415–2428, doi:10.5194/tc-10-2415-2016. 16

Stichler, W., U. Schotterer, K. Fröhlich, P. Ginot, C. Kull, H. Gäggeler, and B. Pouyaud (2001), Influence of sublimation on stable isotope records recovered from high-altitude glaciers in the tropical Andes, *Journal of Geophysical Research: Atmospheres*, *106*(D19), 22,613–22,620, doi:10.1029/2001JD900179. 40

Stull, R. (1988), *An Introduction to Boundary Layer Meteorology*, Springer Netherlands, Dordrecht, doi:10.1007/978-94-009-3027-8. 21, 22

Sturm, C., Q. Zhang, and D. Noone (2010), An introduction to stable water isotopes in climate models: Benefits of forward proxy modelling for paleoclimatology, *Climate of the Past*, *6*(1), 115–129, doi:10.5194/cp-6-115-2010. 3, 13

Swinbank, W. C. (1951), THE MEASUREMENT OF VERTICAL TRANSFER OF HEAT AND WATER VAPOR BY EDDIES IN THE LOWER ATMOSPHERE, *Journal of Meteorology*, *8*(3), 135–145, doi:10.1175/1520-0469(1951)008<0135:TMOVTO>2.0.CO;2. 22

Taylor (1915), Eddy motion in the atmosphere, *Dynamical Meteorology*, pp. 12–53. 23

Thomas, E. R., J. Melchior Van Wessem, J. Roberts, E. Isaksson, E. Schlosser, T. J. Fudge, P. Vallelonga, B. Medley, J. Lenaerts, N. Bertler, M. R. Van Den Broeke, D. A. Dixon, M. Frezzotti, B. Stenni, M. Curran, and A. A. Ekaykin (2017), Regional Antarctic snow accumulation over the past 1000 years, *Climate of the Past*, *13*(11), 1491–1513, doi:10.5194/cp-13-1491-2017. 16

Touzeau, A., A. Landais, S. Morin, L. Arnaud, and G. Picard (2018), Numerical experiments on vapor diffusion in polar snow and firn and its impact on isotopes using the multi-layer energy balance model Crocus in SURFEX v8.0, *Geoscientific Model Development*, *11*(6), 2393–2418, doi:10.5194/gmd-11-2393-2018. 3

Town, M. S., S. G. Warren, V. P. Walden, and E. D. Waddington (2008), Effect of atmospheric water vapor on modification of stable isotopes in near-surface snow on ice sheets, *Journal of Geophysical Research*, *113*(D24), D24,303, doi:10.1029/2008JD009852. 3

Turner, J., G. J. Marshall, K. Clem, S. Colwell, T. Phillips, and H. Lu (2020), Antarctic temperature variability and change from station data, *International Journal of Climatology*, *40*(6), 2986–3007, doi:10.1002/joc.6378. 15

Uemura, R., V. Masson-Delmotte, J. Jouzel, A. Landais, H. Motoyama, and B. Stenni (2012), Ranges of moisture-source temperature estimated from Antarctic ice cores stable isotope records over glacial-interglacial cycles, *Climate of the Past*, *8*(3), 1109–1125, doi:10.5194/cp-8-1109-2012. 1

Van AS, D. (2011), Warming, glacier melt and surface energy budget from weather station observations in the Melville Bay region of northwest Greenland, *Journal of Glaciology*, *57*(202), 208–220, doi:10.3189/002214311796405898. 22

van As, D., M. van den Broeke, C. Reijmer, and R. van de Wal (2005), The summer surface energy balance of the high Antarctic plateau, *Boundary-Layer Meteorology*, *115*(2), 289–317, doi:10.1007/s10546-004-4631-1. 16

Van den Broeke, M., D. Van As, C. Reijmer, and R. Van de Wal (2005), Sensible heat exchange at the Antarctic snow surface: A study with automatic weather stations, *International Journal of Climatology*, *25*(8), 1081–1101, doi:10.1002/joc.1152. 16

van Geldern, R., and J. A. Barth (2012), Optimization of instrument setup and post-run corrections for oxygen and hydrogen stable isotope measurements of water by isotope ratio infrared spectroscopy (IRIS), *Limnology and Oceanography: Methods*, *10*(12), 1024–1036, doi:10.4319/lom.2012.10.1024. 19

Vinther, B. M., H. B. Clausen, D. A. Fisher, R. M. Koerner, S. J. Johnsen, K. K. Andersen, D. Dahl-Jensen, S. O. Rasmussen, J. P. Steffensen, and A. M. Svensson (2008), Synchronizing ice cores from the Renland and Agassiz ice caps to the Greenland Ice Core Chronology, *Journal of Geophysical Research Atmospheres*, *113*(8), 1–10, doi:10.1029/2007JD009143. 1

Vinther, B. M., S. L. Buchardt, H. B. Clausen, D. Dahl-Jensen, S. J. Johnsen, D. A. Fisher, R. M. Koerner, D. Raynaud, V. Lipenkov, K. K. Andersen, T. Blunier, S. O. Rasmussen, J. P. Steffensen, and A. M. Svensson (2009), Holocene thinning of the Greenland ice sheet, *Nature*, *461*, doi:10.1038/nature08355. 2

Vinther, B. M., P. D. Jones, K. R. Briffa, H. B. Clausen, K. K. Andersen, D. Dahl-Jensen, and S. J. Johnsen (2010), Climatic signals in multiple highly resolved stable isotope records from Greenland, *Quaternary Science Reviews*, *29*(3-4), 522–538, doi:10.1016/j.quascirev.2009.11.002. 1

Wahl, S., H. C. SteenLarsen, J. Reuder, and M. Hörhold (2021), Quantifying the Stable Water Isotopologue Exchange Between the Snow Surface and Lower Atmosphere by Direct Flux Measurements, *Journal of Geophysical Research: Atmospheres*, *126*(13), 1–24, doi:10.1029/2020JD034400. 29

Weng, Y., A. Touzeau, and H. Sodemann (2020), Correcting the impact of the isotope composition on the mixing ratio dependency of water vapour isotope measurements with cavity ring-down spectrometers, *Atmospheric Measurement Techniques*, *13*(6), 3167–3190, doi:10.5194/amt-13-3167-2020. 19

Werner, M., U. Mikolajewicz, M. Heimann, and G. Hoffmann (2000), Borehole versus isotope temperatures on Greenland: Seasonality does matter, *Geophysical Research Letters*, *27*(5), 723–726, doi:10.1029/1999GL006075. 13

Werner, M., M. Heimann, and G. Hoffmann (2001), Isotopic composition and origin of polar precipitation in present and glacial climate simulations, *Tellus, Series B: Chemical and Physical Meteorology*, *53*(1), 53–71, doi:10.3402/tellusb.v53i1.16539. 13

Werner, M., P. M. Langebroek, T. Carlsen, M. Herold, and G. Lohmann (2011), Stable water isotopes in the ECHAM5 general circulation model: Toward high-resolution isotope modeling on a global scale, *Journal of Geophysical Research Atmospheres*, *116*(15), 1–14, doi:10.1029/2011JD015681. 4, 14

White, J. W., R. B. Alley, J. Brigham-Grette, J. J. Fitzpatrick, A. E. Jennings, S. J. Johnsen, G. H. Miller, R. Steven Nerem, and L. Polyak (2010), Past rates of climate change in the Arctic, *Quaternary Science Reviews*, *29*(15-16), 1716–1727, doi:10.1016/j.quascirev.2010.04.025. 1

Winkler, R., A. Landais, H. Sodemann, L. Dümbgen, F. Prié, V. Masson-Delmotte, B. Stenni, and J. Jouzel (2012), Deglaciation records of17O-excess in East Antarctica: Reliable reconstruction of oceanic normalized relative humidity from coastal sites, *Climate of the Past*, *8*(1), 1–16, doi:10.5194/cp-8-1-2012. 1

Xi, X. (2014), A Review of Water Isotopes in Atmospheric General Circulation Models: Recent Advances and Future Prospects, *International Journal of Atmospheric Sciences*, *2014*(1), 1–16, doi:10.1155/2014/250920. 13

Zuhr, A. M., T. Münch, H. C. Steen-Larsen, M. Hörhold, and T. Laepple (2021), Local-scale deposition of surface snow on the Greenland Ice Sheet, *The Cryosphere*, *15*(10), 4873–4900, doi:10.5194/tc-15-4873-2021. 3